

RUHR-UNIVERSITÄT BOCHUM

**Mapping urban surface materials with
imaging spectroscopy data on
different spatial scales**

D i s s e r t a t i o n
zur Erlangung des akademischen Grades
d o c t o r r e r u m n a t u r a l i u m (Dr. rer.nat.)

eingereicht von
Marianne Kathrin Jilge

Fakultät für Geowissenschaften
Geographisches Institut

März 2019

GUTACHTER:

Prof. Dr. Carsten Jürgens (Ruhr-Universität Bochum)

Prof. Dr. Ben Somers (Katholieke Universiteit Leuven, Belgien)

Acknowledgements

At this point I would like to thank everyone who contributed to the success of my dissertation.

First of all, I would like to thank Prof. Dr. Carsten Jürgens in particular for the dedicated support, the competent advice and the always motivating words that have contributed significantly to the success of this work. My grateful thanks also go to Prof. Dr. Ben Somers for the technical discussions and for taking over the second supervision.

Many thanks to all my colleagues of the team “Spectroscopy and Land degradation” from the German Aerospace Center (DLR) in Oberpfaffenhofen for their valuable comments and help in all aspects of my work. Here my special thanks go to Dr. Uta Heiden for the professional support, the inspiring discussions and her consistent support, especially in the difficult phases of this work. Many thanks also to Martin Habermeyer for his always honest words and particularly his support in learning IDL.

I would also like to thank Prof. Dr. Hannes Feilhauer for his inexhaustible patience and his ability to explain complex aspects very simply and vividly. Further thanks go to Dr. Carsten Neumann for the technical discussions and his support, which contributed significantly to my third paper.

Special thanks go to my family and friends for the persistent support, patience and encouragement through all phases of this PhD. My parents Birgit und Gerhard Jilge, who consistently supported me at all times and made this career path possible for me. My sister Regina Jilge, who took care of a lasting balance from work and thus contributed to many new thoughts. Matthias Würsching, who has shown me a lot of patience, encouragement and understanding from the beginning of my studies to my doctoral thesis and beyond.

Finally, I would like to thank the Project Management Agency of the German Aerospace Center (DLR) and the Ministry of Economics and Technology (BMW), Germany for funding the project EnFusionMAP (50EE1343).

Curriculum Vitae

Personal information

Name	Marianne Kathrin Jilge
Date of birth	16 April 1988
Place of birth	Munich, Germany

Academic

10/2016 – 03/2019	PhD student in Geography, Ruhr-University Bochum, Germany.
10/2014 – 03/2015	Bachelor study in Physics with minor in meteorology, Ludwig Maximilians University, Munich, Germany.
10/2012 – 09/2014	Master study in Applied Geoinformatics, Paris Lodron University of Salzburg, Austria. <i>Graduation: Master of Science (M. Sc.), Sept. 2014</i>
04/2009 – 09/2012	Bachelor study in Cartography and Geomedia, University of Applied Sciences Munich (HM), Germany. <i>Graduation: Bachelor of Engineering (B. Eng.), Sept. 2012</i>
10/2008 – 03/2009	Bachelor study in Geotelematics and Navigation, University of Applied Sciences Munich (HM), Germany.

School

09/2006 – 07/2008	Fachoberschule, Wasserburg am Inn, Germany. <i>Graduation: Fachabitur (Sozialwesen), July 2008</i>
09/2000 – 07/2004	Realschule, Trostberg, Germany. <i>Graduation: Mittlere Reife (Betriebswirtschaft), July 2004</i>

Work

since 03/2018	Research Associate, German Remote Sensing Data Center (DFD), Land surface dynamics, Oberpfaffenhofen, Germany.
01/2015 – 02/2018	Research Associate, AG Geomatik, Geographical Institute, Ruhr-University Bochum, Germany. Place of Work: German Aerospace Centre (DLR), Oberpfaffenhofen, Germany.
02/2014 – 08/2014	Master thesis, German Remote Sensing Data Center (DFD), Geo-Risks and Civil Security, Oberpfaffenhofen, Germany.

06/2012 – 08/2012	Bachelor thesis, German Remote Sensing Data Center (DFD), Geo-Risks and Civil Security, Oberpfaffenhofen, Germany.
02/2012 – 06/2012	Internship, German Remote Sensing Data Center (DFD), Geo-Risks and Civil Security, Oberpfaffenhofen, Germany.
04/2011 – 07/2011	Student assistant, University of Applied Sciences Munich (HM), Department of Geoinformatics, Munich, Germany.
12/2010 – 01/2012	Working Student, GeoGraphicProduction GmbH, Munich, Germany.
08/2004 – 07/2006	Vocational education as office clerk, Autohaus Manfred Knappe GmbH & Co.KG, Traunstein, Germany. <i>Graduation: July 2008</i>

Publications

Jilge, M., Heiden, U., Neumann, C., Feilhauer, H. (2019). Gradients in urban material composition: A new concept to map cities with spaceborne imaging spectroscopy data. *Remote Sensing of Environment*, 223(2019), pp. 179-193.

Jilge, M., Heiden, U., Habermeyer, M., Mende, A., Jürgens, C. (2017) Detecting unknown artificial urban surface materials based on spectral dissimilarity analysis. *Sensors*, 17(1826), pp. 1-20.

Jilge, M., Heiden, U., Habermeyer, M., Mende, A., Jürgens, C. (2016) Identifying pure urban image spectra using a learning urban Image spectral archive (LUISA). *Proceedings of SPIE Remote Sensing*, 2016, 10008(100080J), *Remote Sensing Technologies and Applications in Urban Environments*, pp. 1-14.

Geiß, C., Jilge, M., Lakes, T., Taubenböck, H. (2016). Estimation of seismic vulnerability levels of urban structures with multisensor remote sensing. *IEEE Journal of selected topics in applied earth observations and remote sensing*, 9(5), pp. 1913-1936.

Contreras, D., Blaschke, T., Tiede, D., Jilge, M. (2015). Monitoring recovery after earthquakes through the integration of remote sensing, GIS and ground observation: The case of L'Aquila (Italy). *Cartography and Geographic Information Science*, 43(2), pp. 115-133.

Jilge, Marianne (2014) Seismic vulnerability assessment of large urban areas using the TanDEM-X Mission and RapidEye data. Master thesis, Paris Lodron University of Salzburg, Austria.

Jilge, M. (2012) Ableitung von Tag-/Nachtkarten aus Fernerkundungsdaten und zusätzlichen Geoinformationen. Bachelor thesis, University of Applied Sciences Munich (HM), Department of Geoinformatics, Munich, Germany.

Declaration of Authorship

Hiermit versichere ich, MARIANNE JILGE, GEB. 16.04.1988 IN MÜNCHEN, an Eides statt, dass ich die vorgelegte Dissertation mit dem Titel „*Mapping urban surface materials with imaging spectroscopy data on different spatial scales*“ selbständig und ohne unzulässige fremde Hilfe verfasst habe. Ich habe alle Hilfsmittel und sonstigen Hilfen angegeben und an den jeweiligen Stellen, die ich wörtlich oder dem Sinne nach aus anderen Veröffentlichungen entnommen habe, kenntlich gemacht.

Außerdem versichere ich, dass ich die Dissertation weder in der vorliegenden noch einer ähnlichen Form zu keinem früheren Zeitpunkt an der Ruhr-Universität Bochum oder einer anderen in- oder ausländischen Hochschule als Dissertation eingereicht habe. Die elektronische Version stimmt mit der schriftlichen Version der Dissertation überein.



Germering, 25. März 2019

Unterschrift

Abstract

Urban environments are subject to numerous processes that directly influence the human life. The knowledge of the current state of urban habitats is of fundamental importance for its recording, analysis, prevention, and forecast. Surface materials are one of the basic indicators for a large number of these urban processes and therefore a comprehensive mapping of urban surface materials is demanded. Imaging spectroscopy data allows the identification of the reflected light from urban surface materials based on their characteristic spectral signature acquired in continuous narrow spectral bands. The spectral diversity of urban surface materials and typically small-scaled urban objects lead to spectral mixtures, where the quantity depends on the spatial resolution of the monitoring system. However, methods used for a detailed mapping of urban surface materials with imaging spectroscopy data require the prior knowledge of spectrally pure signatures of all surface materials occurring in the investigated area. Hence, the spatial resolution of the sensor system is decisive for the level of detail when mapping urban surface materials.

This work focuses on the development of methods for mapping urban surface materials by means of imaging spectroscopy data with different spatial resolution. High spatial resolution imaging spectroscopy data from airborne platforms were used for the development of a method for the automated determination of spectrally pure surface material signatures as a basic prerequisite for the subsequent use of image analysis methods to obtain detailed urban surface material maps. In this context, it deals with the main limitations of the transferability of an urban image spectral library for the determination of spectrally pure material pixels. Subsequently generated maps of detailed surface materials enabled the determination of interpretable gradual material transitions for the analysis of the dominated material occurrences in a given test site. The relation with very complex spectral mixtures resulting from 30 m spatial resolution simulated spaceborne imaging spectroscopy data allows the determination and analysis of typical material compositions within certain administrative units.

General findings from this work represent a sensor- and site-independent framework for the automated extraction of spectrally pure pixels using an urban image spectral library while coping with its potential incompleteness. The results reveal an important step towards the development of a generic urban spectral library. Results using 30 m imaging

spectroscopy data show an improved ability to analyse material compositions at a finer level of detail compared to previous studies using such kind of data. Potentials of spaceborne imaging spectroscopy data for regular area-wide mapping of urban surface materials is complemented by the fact that the used method does not require any prior determination of spectrally pure signatures of urban surface materials.

Zusammenfassung

Unsere Städte rufen eine Vielzahl unterschiedlicher urbaner Prozesse hervor, die einen direkten Einfluss auf unser Leben haben. Für die Erfassung, Analyse, Prävention und Vorhersage dieser Prozesse ist der aktuelle Zustand der Städte von grundlegender Bedeutung und erfordert daher deren Kenntnis. Einer der grundlegenden Indikatoren für viele urbane Prozesse ist auf das Vorkommen von Oberflächenmaterialien zurückzuführen, wodurch eine umfassende Kartierung dieser unumgänglich ist. Die abbildende Spektroskopie ermöglicht aufgrund der zahlreichen kontinuierlichen Spektralbänder die Analyse erfasster Reflektanzen hinsichtlich charakteristischer spektraler Signaturen zur Kartierung urbaner Oberflächenmaterialien. Die spektrale Vielfalt urbaner Oberflächenmaterialien sowie die typischerweise kleinräumigen urbanen Objekte sind für die Entstehung spektraler Mischungen verantwortlich. Die Anzahl der spektralen Mischungen steht daher auch in direktem Zusammenhang mit der räumlichen Auflösung des Aufnahmesystems. Eine detaillierte Kartierung der städtischen Oberflächenmaterialien mit den Methoden der abbildenden Spektroskopie bedürfen jedoch der vorherigen Kenntnis spektral reiner Signaturen aller im Untersuchungsgebiet vorkommenden Oberflächenmaterialien. Demzufolge ist die räumliche Auflösung des Sensorsystems für die Kartierung von urbanen Oberflächenmaterialien entscheidend.

Im Fokus dieser Arbeit stand die Entwicklung von Methoden zur Kartierung urbaner Oberflächenmaterialien mittels abbildender Spektroskopiedaten unterschiedlicher räumlicher Auflösung. Hochauflösende abbildende Spektroskopiedaten flugzeuggetragener Plattformen wurden für die Entwicklung eines Verfahrens zur automatisierten Extraktion spektral reiner Oberflächenmaterialsignaturen als Grundvoraussetzung für den späteren Einsatz von Bildanalyseverfahren zur Gewinnung detaillierter Kartierungen von urbanen Oberflächenmaterialien verwendet. In diesem Zusammenhang werden die grundlegenden Einschränkungen bei der Übertragbarkeit einer urbanen Bildspektralbibliothek für die Erfassung von spektral reinen Pixeln bewältigt. Anschließend generierte Karten von detaillierten Oberflächenmaterialien erlauben die Interpretation von Materialgradienten sowie die Analyse des dominierenden Materialvorkommens im Untersuchungsgebiet. Im Zusammenhang stehende komplexe Spektralmischungen, die sich aus der räumlichen Auflösung simulierter Hyperspektraldaten mit 30 m ergeben, manifestieren das

Vorkommen typischer Materialzusammensetzungen, die innerhalb abgrenzbarer Verwaltungseinheiten analysierbar sind. Allgemeine Erkenntnisse aus dieser Arbeit zeigen die Entwicklung eines sensor- und ortsunabhängigen Konzepts für die automatisierte Extraktion spektral reiner Pixel unter Verwendung einer urbanen Bildspektralbibliothek und der Berücksichtigung deren möglichen Unvollständigkeit. Im Allgemeinen stellen die Ergebnisse einen weiteren Schritt zur Entwicklung einer generisch nutzbaren urbanen Spektralbibliothek für räumlich hochauflösende Hyperspektraldaten dar.

Ergebnisse unter Verwendung von Spektroskopiedaten mit 30 m räumlicher Auflösung ermöglichen eine detailliertere Analyse von Materialzusammensetzungen im Vergleich zu vorangehenden Studien bei der Nutzung von Daten mit selbiger räumlicher Auflösung. Die Potenziale der zukünftigen Hyperspektralsatelliten für die regelmäßige flächendeckende Kartierung urbaner Oberflächenmaterialien wird dabei durch die Tatsache ergänzt, dass die angewandte Methode keine vorherige Bestimmung spektral reiner Signaturen von urbanen Oberflächenmaterialien erfordert.

Contents

Acknowledgements	I
Curriculum Vitae.....	II
Declaration of Authorship	VI
Abstract	VIII
Zusammenfassung	X
Contents.....	XIII
List of figures	XV
List of tables	XVIII
Abbreviations	XIX
Introduction	1
1.1 Human settlements and urbanization	3
1.2 Earth observation in urban areas and the implications of different spatial resolutions	5
1.3 Urban surface materials and mapping	8
1.3.1 Urban surface materials and their influence on urban processes.....	9
1.3.2 Surface material mapping with imaging spectroscopy data	11
1.4 Research objectives.....	16
1.5 Thesis organization	17
1.6 Author's contribution to individual chapters	21
Identifying pure urban image spectra using a learning urban image spectral archive (LUISA)	23
Detecting unknown artificial urban surface materials based on spectral dissimilarity analysis.....	49
Gradients in urban material composition: A new concept to map cities with spaceborne imaging spectroscopy data.....	81
Synthesis	123
5.1 Overall discussion.....	125
5.2 Main conclusion and prospects for urban surface material mapping with imaging spectroscopy.....	133
References	139

List of figures

CHAPTER I

- Fig. 1:** Development and trend of the world's urban and rural population from 1950-2050. (Source: Own illustration based on UN (2018a)). 4
- Fig. 2:** Exemplary illustration of varying spatial resolution for an image with 4 x 4 m (left; e.g. HyMap) and 30 x 30 m (right; e.g. EnMAP) pixel size and its influence on the occurrence of mixed pixels (yellow and green outlined pixels) in urban areas (Source: Own illustration with background image from GoogleEarth®). 8
- Fig. 3:** Spectral variability of clay roofing tiles (left) and asphalt (right) acquired from HyMap data in Munich, Dresden, and Potsdam, Germany. 10
- Fig. 4:** Overview of the peer-reviewed publications (corresponding chapters are marked with Roman numerals) of this thesis and their relation to map urban surface materials. 19

CHAPTER II

- Fig.1:** Concept of LUISA 29
- Fig. 2:** Study area: District Ludwigsburg west and Pflugfelde, Germany. 36
- Fig. 3:** Post-classification using maximum likelihood classifier on the basis of extracted pure pixels from LUISA-T. 39

CHAPTER III

- Fig. 1:** Basic concept of a spectral dissimilarity analysis to detect unknown urban surface materials in high-resolution airborne imaging spectroscopy data. 55
- Fig. 2:** Study area and imaging spectroscopy (HyMap) data for the four test sites A, B, C, and D in Munich, Germany ($R = 1652 \text{ nm}$, $G = 719 \text{ nm}$, $B = 543 \text{ nm}$). 56
- Fig. 3:** Validation data for test sites (A–D) in Munich, Germany. 64

Fig. 4: Masking steps to determine unknown artificial pixels for (a) a subset of test site D using the BSL without tiles by (b) separating artificial pixels from pre-classification results; (c) extracting dissimilar artificial pixels based on a 1% dissimilarity threshold; (d) enhancing the mask by a second similarity analysis to include outliers; (e) removing single pixels and (f) removing border pixels based on the von-Neumann criteria for eliminating mixed pixels. 66

Fig. 5: Remaining unknown artificial pixels after single and border pixel removal. 67

Fig. 6: Extraction of unknown artificial material classes from the (a) mask of unknown artificial pixels determined from the (b) image data of test site D with a BSL setting without roofing tiles and a dissimilarity threshold of 1%. Unknown artificial pixels are subject to (c) spatial and spectral clustering to identify spectral mixtures from (d) mean unknown class reflectance, accompanied by (e) post-processing to delete unknown material classes of remaining mixed pixels to result in an (f) scene-specific spectral library of unknown artificial material classes. 69

Fig. 7: Impact of an increasing dissimilarity threshold on the number of detected unknown artificial material classes elucidated for test site C with a BSL without tiles. 70

Fig. 8: Percentage of spatial agreement by validating all pixels of an unknown material class (columns) detected for different library setups in the four test sites (A-D). Validation results are composed of a spatial match (black) of unknown pixels with validation pixels of material classes zinc or dark roofing tiles, visual inspections (hatched) by visual comparisons of mean spectra due to missing validation data, and (grey) misclassifications or missing data for an unknown material class. 71

CHAPTER IV

Fig. 1: a) Plant species show a maximum occurrence probability on environmental gradients (such as temperature, water, light, and nutrient availability) where the environmental conditions meet their ecological demand. However, they are able to subsist outside this optimum setting, resulting in a unimodal occurrence probability on the environmental gradient. b) Similarly, urban materials (here M1 – M7) are assumed to show a unimodal trend in their cover fractions along a non-spatial gradient in the material feature space. Co-occurrences in these distributions result in characteristic material mixtures that form gradual transitions and may be mapped with spectral data. 89

Fig. 2: Detailed urban surface material map determined from HyMap data with a systematic sampling scheme (section 5.1) in which circles represent the sample size and position in the Munich study site.	93
Fig. 3: Simulated EnMAP data for the Munich study site based on HyMap data.	95
Fig.4: Flowchart of gradient analysis for analysing material compositions in urban environments.	96
Fig. 5: Material-specific DCA-spaces facilitate the visualization of varying cover fractions in the samples to determine maximum occurrences of individual material classes. The position of a circle centre defines the position of a sample and its material composition in the DCA-space, while the circle diameter visualizes the material-specific cover fractions in each sample. The samples are coloured as a result of the transformation of the DCA-space into a colour space (see Fig. 9b). Accumulated samples indicate the maximum occurrence of this material in the gradient space.	101
Fig. 6: Biplot scaling of the main material groups a) minerals, b) hydrocarbons, c) metals, d) vegetation, and e) the remaining material classes, composed of soil, water, and railway tracks (see Table 1), to visualise the maximum occurrences of individual material classes in the DCA-space (represented by the position of material names in the DCA-space).	102
Fig. 7: Model fits of the PLS regression analysis for a) the first and b) the second gradient.	103
Fig. 8: Mapping of predicted DCA scores for simulated EnMAP pixels in the study site in Munich for a) the first and b) the second gradient.	103
Fig. 9: a) Prediction map of DCA scores for composed gradient models for the study site in Munich, with a selection of samples from the sampling scheme (Fig. 2) that represent distinct USTs (I-VIII) - for historical high-resolution GoogleEarth® orthophotos - to support the identification of b) the colour scheme (legend) with regard to the delimitation of USTs (solid and dashed lines) based on characteristic material compositions.	105
Fig. 10: Proportions (in %) of the two most commonly co-occurring material cover fractions (minimum material fraction has to be at least 5%) in the four main material groups for a selection of averaged samples per UST (Fig. 9a.I-VIII). The class 'others' comprises the remaining materials of the four main material groups as well as soil, water, and railway tracks.	107

List of tables

CHAPTER II

<i>Table 1: Generic class hierarchy for LUISA-A</i>	31
<i>Table 2: Confusion matrix for post-classification of known material class using validation polygons.</i>	40

CHAPTER III

<i>Table 1: Airborne imaging spectroscopy data used for the extraction of reference spectra for the BSL.</i>	57
<i>Table 2: Class hierarchy to separate BSL spectra of material classes (their occurrence is in brackets) into artificial and natural surface material groups.</i>	58
<i>Table 3: Pre-classification accuracies for the test sites (column 1) using the full BSL setting comprise grouped producer and user accuracies within natural (columns 2–3) and within artificial material classes (columns 4–5) demonstrating the general separation of the broad classes natural and artificial. Overall accuracies (column 6) and kappa statistics (column 7) reveal the general pre-classification accuracies of single material classes.</i>	65

CHAPTER IV

<i>Table 1: Categorisation of urban surface materials (with material abbreviations) into material groups, including total and sampled cover fractions per surface material in the Munich study site.</i>	94
--	----

Abbreviations

AMEE	Automated morphological endmember extraction
ATCOR	Atmospheric and topographic correction
BRDF	Bidirectional reflectance distribution function
BSL	Basic spectral library
DCA	Detrended correspondence analysis
DLR	German aerospace center
EAGLE	EIONET (Environmental Information and Observation Network) Action Group on land monitoring in Europe
EM	Endmember
EnMAP	Environmental mapping and analysis program
EO	Earth Observation
FusingSAF	Fusing shape and amplitude features
GSD	Ground sampling distance
GV	Gradient values
HRSC	High Resolution Stereo Camera
HyMap	Australian airborne hyperspectral imaging sensor
IAS	Iterative adaptive smoothing filter
IEA	Iterative error analysis
ID	Identifier
IS	Imaging spectroscopy
ISODATA	Iterative self-organizing data analysis technique
JMD	Jeffries-Matusita distance
LCZ	Local climate zone
LUISA	Learning urban image spectral archive
LUISA-A	Learning urban image spectral archive - Archive
LUISA-T	Learning urban image spectral archive – Tools
MESMA	Multiple endmember spectral mixture analysis
NIR	Near infrared
OSP	orthogonal subspace projection
PLSR	Partial least square regression

PVC	Polyvinylchloride
RMSE	Root mean square error
SAM	Spectral angle mapper
SCA	Spectral correlation angle
SCM	Spectral correlation measure
SD	Standard deviation
SID	Spectral information divergence
SMA	Spectral mixture analysis
SPECCHIO	Spectral information system
SRTM	Shuttle Radar Topography Mission
SSEE	spatial-spectral endmember extraction tool
SWIR	Short wavelength infrared
UN	United Nations
UST	Urban structure type
UTM	Universal Transverse Mercator
V-I-S	Vegetation-impervious-soil
VNIR	Visible and near-infrared
WA	Weighted Average
WGS 84	World Geodetic System 1984

CHAPTER I

Introduction

1.1 Human settlements and urbanization

Century of the City as [Seto et al. \(2010\)](#) designated the present century – associated with the rapid progress of urbanization and the continuous growth of the world population – gives a first impression of the demands on the population and the transformation processes inside and outside the cities. The world population was doubled from 3 billion in 1959 to 6 billion in 1999 and is estimated to might reach the mark of 10 billion people in 2055 ([UN, 2017](#)) with an annual global population growth of around 1.16% ([The World Bank, 2018](#)). Already in the Middle Ages the city was considered as a place of wealth and prosperity, resulting to a migration of the rural population to the city. The perspective of people migrating to the city has shifted mainly due to better education and job opportunities, globalization, economic, cultural and socio-political reasons (e.g. due to working places, quality of life, transportation, friends etc.). The trend continues, so that nowadays the majority of the world's population is residing in urban environments. In this context, more than half of the world's population was registered to settle in urban areas in 2007, with an upward trend (Fig. 1; [UN, 2018a](#)). This trend, also known as urbanization, leads to a fast growing and dynamically changing urban landscape ([Bell et al., 2010](#); [Malheiros and Vala, 2004](#); [Sánchez-Rodríguez et al., 2005](#)) with a dense agglomeration also in peri-urban areas. Thus, urbanization can be seen as a result from population increase, economic expansion and the need for space ([Ravetz et al., 2013](#)). In recent years, more and more cities have developed into so-called megacities, which result from a population of more than 10 million inhabitants. In 2018, 33 cities around the world were recognized as megacities, and within the next 12 years it is estimated that another 10 cities will be added to this list ([UN, 2018b](#)). This globally densification of cities in terms of population, formation of new and altering constructions, and the expansion of infrastructure is accompanied by a continuous change in the cityscape.

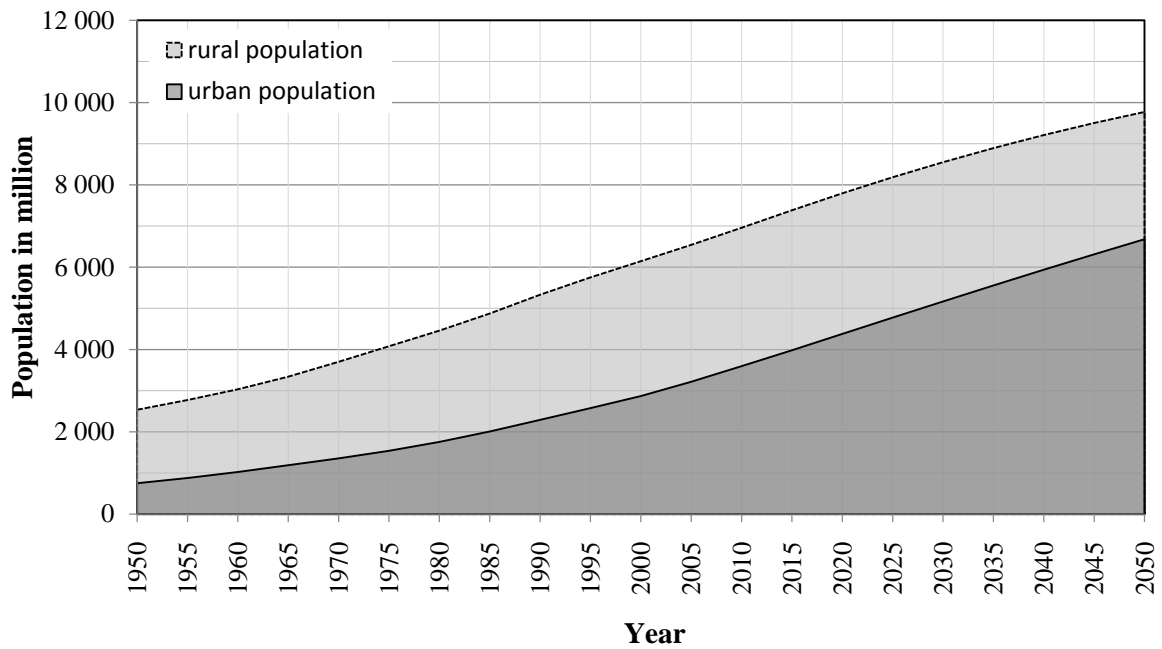


Fig. 1: Development and trend of the world's urban and rural population from 1950-2050. (Source: Own illustration based on UN (2018a)).

Although these changes take place in rather small spatial units on the earth's surface, it has far-reaching effects on the global economy, society, and especially on the climate and pollution in the urban and non-urban ecosystems (Grimm et al., 2008). Several population-induced effects are associated with physical and socio-economic impacts on individuals, as well as on a global level. For instance, an increasing imperviousness affects the hydrological processes in the city which is related to a reduced surface runoff (Leopold, 1968; Weng, 2001; Cuo et al., 2008; Ampe et al., 2012; Wirion et al., 2017) that aggravates the risk of extreme flood events. The associated reduction of vegetation and urban green spaces is also a key factor that is decisive for the urban climate by reducing CO₂ and greenhouse gases (Yang et al., 2003; Hoek et al., 2008; Kennedy et al., 2009) and temperature regulation in the city (Middel et al., 2014). Thus, urban surfaces and structures are responsible for microclimatic effects in the city (Arnfield, 2003). While the effects of the city on the climate were already recognized in the early years of the 19th century (Howard, 1833), in recent years the phenomenon of the so called urban heat island (Oke, 1973; Grimmond, 2007) is probably the most commonly studied aspect in climatic studies of urban environments. In order to investigate such effects caused by urban growth, a regular monitoring of the city is demanded to enable a fast response for decision makers and urban planners regarding sustainability and development.

1.2 Earth observation in urban areas and the implications of different spatial resolutions

„Earth observation is the gathering of information about planet earth’s physical, chemical and biological systems. It involves monitoring and assessing the status of, and changes in, the natural and man-made environment.“ (Group on Earth observations, 2019).

Ongoing processes of urbanization around the world are accompanied by continuous changes in the land cover - in, around and beyond the city (section 1.1). A regular monitoring of urban areas facilitates the assessment and estimation of urban processes and their direct and indirect impacts on humans, nature and the climate. Gathered information from water-, land-, air- or space-based platforms is therefore a substantial source for decision-makers and planners (National Research Council, 2007). The acquisition of data to monitor, detect and assess changes on the earth is known as earth observation (EO; Group on Earth Observation, 2019).

Since decades, a comprehensive spatiotemporal monitoring of these rapid changes and its effects has been studied by means of EO. Data taken from remote sensing systems are a major component of EO that can provide a comprehensive and up-to-date monitoring of the rapidly changing urban environment. The monitoring of urban areas with remote sensing enables the mapping of land cover and the derivation of information on its land use (Roberts and Herold, 2004) for large areas. In general, such information might be gathered by different remote sensing techniques (active or passive) which are based on in-situ measurements, airborne (aircraft and unmanned aerial vehicles) or spaceborne platforms. The enormous temporal and spatial changes resulting from new constructions for housing, workplaces, leisure facilities and infrastructure lead to a constantly changing city scape and hamper the monitoring of changes in land cover and land use in the field. Airborne and spaceborne remote sensing systems aim to provide extensively detailed information about the earth’s surface for different research priorities. They are associated with different spatial, spectral, radiometric and temporal conditions (Jensen and Cowen, 1999). For a detailed introduction on remote sensing and the principle functioning of the different technologies it is referred to Hildebrandt (1996), Schowengerdt (1997), Richards and Jia (1999), Lillesand and Kiefer (2000), Mather (2004), and Albertz (2009). The different remote sensing technologies are very briefly introduced in this section.

Passive remote sensing systems (optical remote sensing systems) record the incoming sunlight that is reflected from the objects on the earth surface. While active sensor systems (radar remote sensing systems) emit a radar beam and record its incoming backscatter from an object on the earth's surface. Active remote sensing systems are able to record weather-independent data during day- and night-time. While passive remote sensing systems are dependent on the sunlight and mainly on cloud free conditions to provide useful information from the earth's surface. The numerous vertical objects such as facades are challenging for radar systems and result in effects such as layover ([Dong et al., 1997](#)) and occlusions of objects due to radar shadow ([Soergel, 2010](#)). However, due to the recording technology of radar systems the characterisation of built-up areas using these sensor systems is ideally suitable for analysing information of object structure and texture. [Soergel \(2010\)](#) gives a comprehensive overview on radar remote sensing in urban areas.

Optical sensors are acquiring spectral information on the surface cover of urban objects in photograph-like images in the wavelength regions within 300 and 3000 nm. Based on the spectral detail that can be monitored, optical sensors are further separated in multispectral and hyperspectral systems. Multispectral systems are measuring the reflected sunlight in a few spectral bands from the electromagnetic spectrum with a rather broad bandwidth. There are numerous mainly spaceborne multispectral missions with different settings for spectral data acquisition, varying temporal and spatial resolutions ranging from sub-meters up to 1 km (e.g. WorldView, Quickbird, Spot, RapidEye, Sentinel, Landsat etc.).

Very detailed spectral information of objects are recordable from hyperspectral sensor systems. Hyperspectral remote sensing is also often referred to as imaging spectroscopy ([Schaepman et al., 2009](#)). Such data enables a detailed differentiation, concerning the occurrence of surface materials (section 1.3.1) in impervious patterns and built-up areas, that cannot be differentiated with multispectral remote sensing sensors ([Small, 2005](#); [Jensen and Cowen, 1999](#); [Herold et al., 2003](#); [Gamba and Dell'Acqua, 2007](#)). Hyperspectral sensors are characterised by the fact that they acquire spectral information through a large number of very narrow, contiguous spectral bands. Commonly very high spectral and spatial information are recorded from imaging spectrometers mounted on airborne platforms (e.g. AVIRIS, [Green et al., 1998](#); HyMap, [Cocks et al., 1998](#); HySpex, [NEO, 1995](#); and APEX [Jehle et al., 2010](#)). The analysis of shape and absorption features from the spectral signature of the reflected irradiance allows a detailed differentiation of the spectral response function of urban surfaces (e.g. [Ben-Dor et al., 2001](#); [Segl et al., 2003](#); [Herold et al., 2004](#); [Heiden et al., 2007](#); [Heiden et al., 2012](#)). The need for regular

monitoring of the spectral properties of the earth's surface is becoming increasingly important in order to infer more detailed information on the material composition of impervious and built-up surfaces for investigating urban processes (sections 1.3.1 and 1.3.2). However, flight campaigns carrying imaging spectrometers are limited in the temporal resolution, as it is often difficult to obtain a permission to fly over populated areas, and the costs of a revisiting data acquisition is often prohibitive. Thus, imaging spectroscopy data from space are advantageous for regular and area-wide mapping purposes due to their temporal resolution that cannot be realized with airborne systems. In the past years and nowadays the availability of spaceborne imaging spectroscopy systems is still quite limited (e.g. Hyperion, [Pearlman et al., 2003](#); CHRIS-PROBA, [Duca and Del Frate, 2008](#); DESIS, [Mueller et al., 2017](#)). However, with the launch of EnMAP ([Guanter et al., 2015](#)), HypSIRI ([Abrams and Hook, 2013](#)), PRISMA ([Guarini et al., 2017](#)), HISUI ([Matsunaga et al., 2014](#)) in the next months and years, spaceborne data with high spectral and temporal resolution will be available. Nevertheless, the possibilities of acquiring thematically very detailed spectral information of urban areas will be hampered by a characteristic spatial resolution of 20 to 30 m (section 1.3.2).

Different airborne and spaceborne remote sensing systems are associated with different spatial resolution capabilities for monitoring the earth's surface. The spatial resolution is defined by a consistent areal size of the observation area on the earth's surface which is represented by an image element (pixel). Pixels can be composed of only one urban object that is covered by one surface materials or by different urban objects covered by different surface materials (Fig. 2). These so called mixed pixels result from a jointly recording of objects that are smaller than the spatial resolution of the sensor system ([Jensen and Cowen, 1999](#)). The spectral signature of these mixed pixels is therefore a combination of the spectral characteristics of the corresponding surface materials (section 1.3.1) and their cover fractions. Thus the heterogeneity of the observed environment coupled with the characteristic spatial resolution of the monitoring sensor system is responsible for the number and mixing ratio of spectrally mixed pixels ([Small and Lu, 2006](#)). That means a decreasing spatial resolution of the sensor system leads to a continuously increasing number of mixed pixels in the image (Fig. 2). While at the same time, with coarser spatial resolution, the number of spectrally pure pixels, which represent only one urban object covered by one surface material (section 1.3.2), decreases.

Very high spatial, spectral and temporal resolution would be the ideal case for monitoring urban environments but are not available yet. When using airborne or spaceborne

hyperspectral data, a compromise of spatial or temporal constraints must therefore always be made.

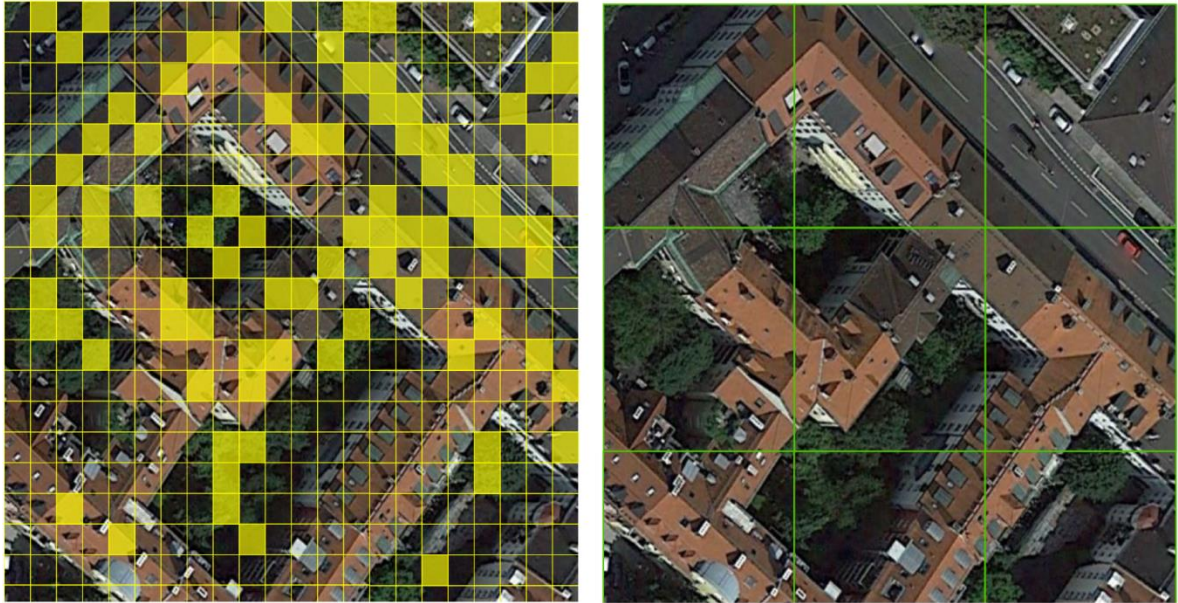


Fig. 2: Exemplary illustration of varying spatial resolution for an image with 4 x 4 m (left; e.g. HyMap) and 30 x 30 m (right; e.g. EnMAP) pixel size and its influence on the occurrence of mixed pixels (yellow and green outlined pixels) in urban areas (Source: Own illustration with background image from GoogleEarth®).

1.3 Urban surface materials and mapping

Ongoing urbanization processes paired with continuous population growth result in the formation of new housing and working facilities. Consequently, this is associated with a rapidly and continuously changing urban landscape with far-reaching impacts on the population and the environment worldwide (section 1.1). A detailed monitoring can be conducted by using remote sensing systems (section 1.2) that provide ideal conditions and image analysis techniques for a regular observation of such highly dynamic landscapes. This section outlines the relevance of this thesis to highlight the context of the innovative research parts (sections 2, 3 and 4) of this work that is related to the research needs of mapping urban surface materials.

1.3.1 Urban surface materials and their influence on urban processes

Historical, structural and functional influences of the composition of abiotic and biotic components constitute urban areas as a distinct ecosystem (Sukopp and Weiler, 1998; Wittig et al., 1998; Niemela, 1999). The occurrences of urban surface materials varies due to geographical conditions (e.g. climate, trends) that are characteristic for certain regions. For instance, roofing tiles are commonly used in residential areas of European cities while in Northern American cities slates are typically used as roofing materials on smaller single and multi-family houses. Surface materials of mineral, hydrocarbon-based, metallic, opaque or biotic origin are used on different urban objects, while structural and chemical compositions of these materials vary from manufacturer to manufacturer. Processes such as the firing or drying of roofing tiles or different coatings lead to a huge material variability. Measurements with imaging spectroscopy systems (sections 1.2 and 1.3.2) demonstrate the variations of chemical, physical and structural compositions of surface materials in their spectral signatures. Degradation processes caused by the sun, wind, and rain are a further influencing factor on the spectral diversity of urban surface materials. Variations in the illumination (incident sunlight), orientation of objects (shaded roof side), object structure (texture), and the inclination angle (roofing inclination) towards the sensor are also affecting the spectral variability of an urban surface material due to so called bidirectional reflectance distribution function (BRDF) effects (Schott, 1997; Lucht et al., 2000; Lacherade et al., 2005; Schaepman-Strub et al., 2006). Thus, urban areas are highly complex environments with an enormous spatially and spectrally variability of urban objects and their surface covering materials within and between the material classes. The spectral diversity within a material class (e.g. due to weathering and minor differences in coating) and towards spectrally similar materials (e.g. asphalt and concrete; Herold et al., 2004; Heiden et al., 2007) is known as spectral intra- and inter-class variability. In figure 3 the spectral variability of clay roofing tiles and asphalt is exemplarily illustrated. The spectra were acquired from HyMap sensor in three German cities.

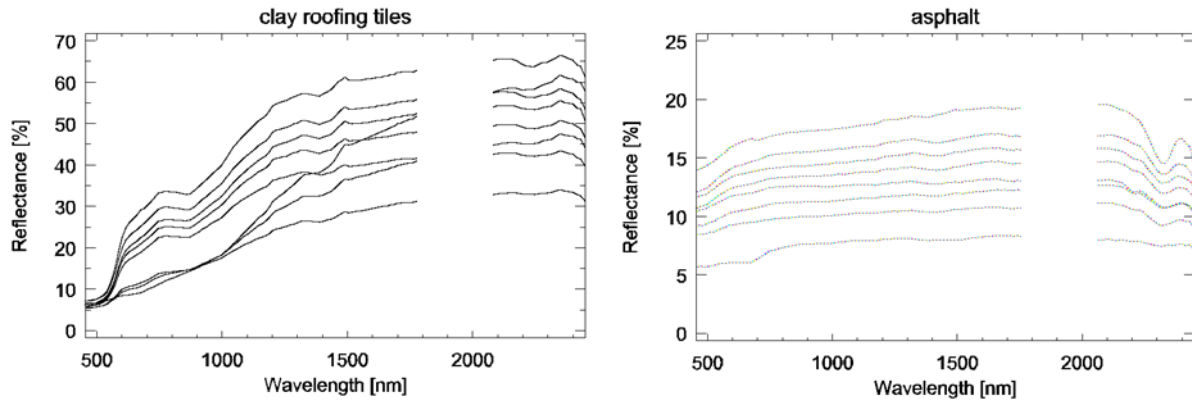


Fig. 3: Spectral variability of clay roofing tiles (left) and asphalt (right) acquired from HyMap data in Munich, Dresden, and Potsdam, Germany.

Detailed information on urban surface materials serve as a basic source of information for a variety of analysis for understanding urban processes. In [Heldens et al. \(2011\)](#) a comprehensive overview of the relevance of material information for applications related to urban development and planning, evaluation of urban growth, risk and vulnerability assessment, urban climate or for methodological research in the field of mapping urban land cover or for algorithms in spectral analysis is given. In such studies it is demonstrated that, among several human- and object-related characteristics (e.g. human activities, size, location, and orientation of urban objects), the physical and chemical properties of the covering materials such as reflection properties (albedo) have an influence on the urban climate ([Hoyano et al., 1999](#)). For example, temperature differences in cities can be traced back to occurring surface materials, which are linked to different surface temperatures due to the material-specific reflection and absorption degrees of the incident sunlight. The analysis of varying temperatures over urban areas is a key factor for the determination of the urban heat island ([Wilby, 2003](#); [Wilby, 2007](#)) and is further decisive for other urban climatic processes such as wind speed, humidity and even air quality ([Heldens, 2010](#)). Another urban application, based on a detailed material mapping, can serve to calculate hydrological models ([Carlson and Arthur, 2000](#); [Ampe et al., 2012](#); [Wirion et al., 2017](#)) to evaluate the city's water balance and its surface runoff ([Weng, 2001](#)) due to rain masses in cities on the basis of their material-specific characteristics of water permeability ([Gill et al., 2007](#); [Alberti et al., 2007](#); [Carle et al., 2005](#)). Surface material maps are therefore frequently requested as an important source of information for several risk and vulnerability assessments as well.

1.3.2 Surface material mapping with imaging spectroscopy data

Beside time- and cost-intensive restrictions, surface material mapping in the field can be almost not conducted for large-scale applications. Thus, remote sensing has been proven as an ideal tool for monitoring urban areas (section 1.2). Specifically hyperspectral remote sensing data are best suited for an area-wide mapping of urban surface materials due to the high spectral sensitivity of the sensors.

The number of spectrally mixed pixels is directly related to the rather small-scaled urban objects, the spectral complexity of urban surfaces, and the spatial resolution of the acquisition system (sections 1.2 and 1.3.1). For the detailed mapping of urban surface materials high spatial and spectral resolution properties, available from airborne imaging spectroscopy data, are required (Jensen and Cowen, 1999; Gamba and Dell'Acqua, 2006). An overview on the specific requirements for mapping urban surface materials with imaging spectroscopy data is given in Herold et al. (2003). However, the spatial resolution of remote sensing systems cannot overcome the effects of illumination, shadowing and object displacements of vertical structures that hampers the analysis of urban areas (van der Linden and Hostert, 2009; Adeline et al., 2013; Yang et al., 2015; van der Linden et al., 2018). Nevertheless, a high spectral resolution enables the differentiation of spectral ambiguities resulting from spectral inter- and intra-class variabilities of urban surface materials (Small, 2003; Herold et al., 2004; van der Linden et al., 2007). While a high spatial resolution reduces the number of highly complex mixed pixels (section 1.2) that needs to be deconvolved for a detailed mapping of urban surface materials. The more materials contributing to the spectral signature of a mixed pixel the higher is the uncertainty of the deconvolution (Winter et al., 2003). To give an impression on the number of mixed pixels related to the spatial resolution, Heldens et al. (2017) identified more than half of the pixels as mixed pixels using a 4 m spatial resolution data set. Thus, deconvolution of mixed pixels to map urban surface materials is still challenging even with high spatial and spectral resolution data sets.

Over the last decades, detailed urban surface material maps and the determination of material-related information have been already proven and highlight the potentials of using airborne imaging spectroscopy (e.g. Ben-Dor, 2001; Roessner et al., 2001; Herold, et al., 2003; Segl et al., 2003; Herold et al., 2004; Heiden et al., 2007; Franke et al., 2009; Heiden et al., 2012; Demarchi et al., 2014; Priem and Canters, 2016; Chen et al., 2017; Degerickx

et al., 2019 etc.). In these research studies a variety of methods were developed for tackling the heterogeneity of urban environments due to their spatial and spectral complexity. Thus, for example, Roessner et al. (2001) developed an spatial and spectral region growing approach that considers spectral variations of determined endmembers for an automated differentiation of urban surface materials. Benediktsson et al. (2005) determines morphological profiles for classifying urban environments, where Gamba et al. (2007) identified object boundaries for mapping purposes and Heiden et al. (2007) differentiate urban surface materials by determining material-specific spectral features in the spectral signature. In van der Linden et al. (2007) machine learning techniques were proposed for classifying urban land cover, while Franke et al. (2009) developed and a hierarchical MESMA approach (Multiple Endmember Spectral Mixture Analysis; Roberts et al., 1998) for extracting endmembers in urban environments.

Endmembers (EMs) are defined as the “spectral signatures, the radiance or reflectance values over hundreds of contiguous spectral bands, of the pure, constituent materials in a hyperspectral scene” (Zare and Ho, 2014, pp. 95). The endmember terminology does not incorporate spectral variabilities of a material class e.g. due to differences in the illumination, degradation or chemical properties (section 1.3.1). However, the variability of EMs (also known as bundles of EMs) is important for an accurate estimation of material fractions in mixed pixels (Somers et al., 2011; Zare and Ho, 2014). Especially in urban areas where some material classes are spectrally very similar (e.g. asphalt, concrete, soil) automated EM determination (see below) is often incomplete. The high spectral- inter- and intra-class variability of urban surface materials (Fig. 3) needs to be considered for detailed and accurate surface urban material mapping. For this reason, this work avoids using the term EM, since the spectral variability of material classes is fundamental for an accurate mapping of urban surface materials. Further it should be noted that if the term EM is used in the context of urban surface materials, it corresponds to the meaning of spectrally pure urban surface materials (or spectrally pure pixels), including the spectral inter- and intra-class variability for a thematically namable material.

Most recently spectral unmixing techniques are used for deconvolving mixed pixels to determine urban surface materials on a sub-pixel scale. From a methodological point of view the imaging spectroscopy community has placed great emphasis on the development of linear and non-linear spectral mixture analysis techniques (Keshava, 2003; Keshava and Mustard, 2002; Adams and Gillespie, 2006; Shimabukuro et al., 1991). Spectral unmixing techniques were used for decomposing mixed pixels from various natural and urban

environments (e.g. [Adams and Smith, 1986](#); [Asner and Lobell, 2000](#); [Okin et al., 2001](#); [Asner and Heidebrecht, 2002](#); [Neville et al., 2003](#); [Roth et al., 2012](#); [Roberts et al., 2017](#)). Such unmixing techniques strive on the determination of the corresponding material fractions so called abundances ([Keshava and Mustard, 2002](#)) of pure material spectra (that are also known as EM), in spectrally mixed pixels ([Adams et al., 1993](#); [Settle and Drake, 1993](#)) independently of the spatial, spectral or radiometric resolution of the imagery.

The decomposition of mixed pixels in their material abundances requires prior knowledge of all spectrally pure signatures (EM) of material components existing in the study area. Prior determination of spectrally pure pixels plays a key role for spectral unmixing techniques but they are also relevant for other methodological approaches such as for training purposes in image classification ([Clark et al., 2003](#); [van der Linden et al., 2007](#); [Plaza et al., 2009](#)), or simply for data mining reasons ([Okujeni et al., 2017](#)) e.g. to archive spectral references. Therefore, the determination of spectrally pure pixels delineates a fundamental step in most of the approaches of mapping urban environments while using imaging spectroscopy data. Spectral references of pure urban surface materials, can be obtained by spectroscopic measurements in the field (e.g. [Ben-Dor et al., 2001](#); [Herold et al., 2004](#); [Roberts et al., 2004](#)), in the laboratory (e.g. [Roberts et al., 1993](#)), determined from image data (e.g. [Bateson et al., 2000](#); [Plaza et al., 2002](#); [Dennison and Roberts, 2003](#)) or by simulations (e.g. [Dennison et al., 2006](#); [Eckmann et al., 2008](#); [Sonnentag et al., 2007](#)).

The importance of selecting EMs for a subsequent mapping of “spatial distribution, associations and abundances” ([Martínez et al., 2006](#); pp. 93) has led to the development of a variety of semi- and fully automated methods for the extraction of EMs from imaging spectroscopy data (e.g. Pixel Purity Index, [Boardman et al., 1995](#); N-FINDR, [Winter, 1999](#); Iterative Error Analysis, [Plaza et al., 2004](#)). [Somers et al. \(2016\)](#) give an overview on EM extraction methods from image data. Such techniques are extensively studied (e.g. [Martínez et al., 2006](#); [Plaza et al., 2004](#)) and yield to overcome major drawbacks of time- and cost-intensive fieldwork. These methods allow one EM per material class to be extracted from an image ([Zare and Ho, 2014](#); [Iordache et al., 2014](#)). However, advanced EM extraction tools such as MESMA ([Roberts et al., 1998](#)) further focus on the selection of EMs in terms of type and number and also take into account the spectral inter- and intra-class variability of EMs ([Zhang et al., 2006](#)). The knowledge of the full spectral inter- and intra-class variability of EMs that characterizes the study area is of great importance and is known to influence the successful use of spectral unmixing models ([Smith et al., 1994](#);

Bateson et al., 2000; Roth et al., 2012). Somers et al. (2011) discussed in detail the influence of EM variability to spectral mixture analysis.

EMs and spectrally pure pixels are commonly assembled in a so-called spectral library that serve as data container for storing previously labelled spectral signatures of extracted or measured spectrally pure materials as reference spectra. Spectral libraries are therefore the basis for most of the unmixing or classification methods to determine information on urban surface materials. For a successful use of spectral libraries the spectral characteristics of the study area needs to be fully described by the reference spectra in the spectral library. There are a few urban spectral libraries containing spectral signatures of selected artificial surface materials developed from field and laboratory measurements as well as from image determination (e.g. Ben-Dor et al., 2001; Herold et al., 2004; Clark et al., 2007; Heiden et al., 2007; Okujeni et al., 2013; Kotthaus et al., 2014). The use of image spectral libraries have the advantage that determined spectrally pure pixels from the image data themselves contain beside the site-specific spectral signatures also the variations from temporal (e.g. illumination, orientation, atmosphere) and sensor specifications (e.g. bandwidth, spectral bands, field of view, flight direction). Reference spectra of spectral libraries, needs to be identified and labelled manually even when using (semi-) automated endmember extraction algorithms. This requires a profound spectral, spatial and temporal expertise of the acquired urban surface materials and is therefore still a challenging task. The comprehensive mapping of urban surface materials using spectral libraries is directly influenced by the available and the spectral intra- and inter-class variability of reference spectra. Any incompleteness in the used spectral library with regard to missing spectrally pure materials and an incomplete representation of inter- and intra-class variabilities of the materials occurring in the study area leads to disregarding these spectrally pure pixels in the further mapping of urban surfaces. This hampers the transferability of urban spectral libraries to a new urban area, but the demand for a universal use of an urban spectral library is still ongoing. First advances towards a generic application of an urban spectral library were tested in Okujeni et al. (2017), Wetherley et al. (2017) and Dudley et al. (2015) where reference spectra were combined with different spectral, spatial and temporal resolutions. However, the incompleteness of an urban spectral library will still persist as it will be impossible to establish an urban spectral library containing the spectral variability of all surface materials of cities around the world. The use of an urban spectral library for a detailed analysis of urban surface materials is still limited to urban areas whose spectral diversity can be explained by the corresponding urban spectral library.

A further issue arises while analysing urban areas using spaceborne imaging spectrometers. Although upcoming spaceborne imaging spectrometers will offer a high temporal resolution, enabling regular and area-wide mapping of urban areas, the spatial resolution of 20 to 30 m will lead to an image dominated by highly complex spectrally mixed pixels (section 1.2, Fig. 2). Hence, the spectral complexity of mixed pixels cannot be sufficiently expressed by available spectrally pure pixels and therefore requires advanced techniques to quantify the occurrence of urban surface materials. There are only a couple of studies using spaceborne imaging spectroscopy data due to the limited number of former or operating sensor systems in space (section 1.2; e.g. [Xu and Gong, 2007](#); [Cavalli et al., 2008](#); [Duca and Del Frate, 2008](#); [Weng et al., 2008](#); [Licciardi and Del Frate, 2011](#); [Demarchi et al., 2012a](#); [Demarchi et al., 2012b](#); [Fan and Deng, 2014](#); [Zhang, 2016](#)). However, in the next years new hyperspectral satellites will be launched (see section 1.2) which will enhance the data availability and provide new opportunities for a regular monitoring of urban areas. First studies are already using simulated imageries to investigate the potentials of these new sensor systems for urban applications (e.g. [Roberts et al., 2012](#); [Okujeni et al., 2015](#); [Rosentreter et al., 2017](#)). The issue of deconvolving highly complex spectral mixtures led in all studies to the determination of generalized material classes in broader land cover classes. For instance, [Weng et al., 2008](#) extended the well-known VIS-model (vegetation, impervious and soil; [Ridd, 1995](#)) by further differencing between high and low albedo classes. While [Okujeni et al., 2015](#) distinguishes into the classes roof, pavements, low vegetation (such as grassland and shrubs) and trees. A more detailed mapping of urban surface materials with spaceborne imaging spectroscopy data could not yet be implemented. An overview on recent progress using imaging spectroscopy data – airborne and spaceborne – for mapping urban areas is given in [van der Linden et al. \(2018\)](#).

The main challenges associated with the potentials and limitations of the use of airborne and spaceborne imaging spectroscopy data for monitoring urban areas are related to:

- Spatial resolution
- Spectrally mixed pixels
- Prior determination of spectrally pure pixels (EM)
- Prerequisite spectral expertise on urban surface materials
- Temporal resolution and revisit time
- Huge spectral diversity of urban surface materials

1.4 Research objectives

The high spectral variability of urban surface materials often on small scaled urban objects leads to spectral mixtures when monitoring them with remote sensing systems. A detailed mapping of urban surface materials using classification or spectral unmixing techniques still requires the spectral knowledge of occurring surface materials in the investigation area. The spatial scale is therefore a leading factor to map urban surface materials with imaging spectroscopy. The use of spectral libraries overcomes the challenging task of manual identification (labelling) of pure material spectra in spatial high resolution data sets. However, the use of spectral libraries has been so far limited to sensor and site specifications such as sensor and illumination properties. In addition, it requires a complete collection of all occurring surface materials and their spectral variations in the study site in order to achieve the most accurate mapping result of urban surface materials (section 1.3.2). Thus, the transferability of spectral libraries to a new test site is so far limited. This thesis addresses the site and sensor limitations when using a spectral library for mapping urban surface materials.

With upcoming spaceborne imaging spectrometers a higher temporal but a coarser spatial resolution of up to 30 m will be available that open up the possibility of a regular area-wide monitoring of the rapidly changing urban environments. However, spectrally pure pixels in such data are rare or completely absent, so that the mapping of urban surface materials on the same level of detail as with airborne data is not possible. Hence, broader categories of material groups were analysed in recent research studies (e.g. [Weng et al., 2008](#); [Okujeni et al., 2015](#); [Rosentreter et al., 2017](#); [Okujeni et al., 2017](#)). However, the changing perspective to the spatial unit of urban neighbourhoods demonstrates similar compositional and structural characteristics. Neighbourhood specific compositions of urban surface materials were still found in high resolution data sets (e.g. [Heiden et al., 2003, 2012](#); [Heldens, 2010](#); [Bochow et al., 2007](#)). Therefore, this work also focuses on the investigation of material compositions related to certain neighbourhoods in order to analyse complex spectral mixtures on a more detailed level.

This rather methodically oriented work aims on the development of methods for mapping urban surface materials with imaging spectroscopy data with different spatial resolutions. In particular, it focused on the applicability to overcome the limitations in the use of urban spectral libraries for automated determination of spectrally pure pixels from airborne

imaging spectroscopy data. In addition, the possibilities in the analysis of very complex spectral mixtures are investigated in order to analyse urban material compositions in more detail. The following three research objectives for mapping urban surface materials with imaging spectroscopy data on different spatial resolution data sets are addressed:

- Can an initial urban spectral library be used to automatically extract and identify sensor- and site-independent, scene-based endmembers from high spatial resolution imaging spectroscopy data that are required for further mapping techniques?
- Can an image-based spectral library be used to determine spectrally pure pixels in urban areas despite a potential incompleteness of the spectral library, so that it can be transferred to an unknown urban area?
- Do complex urban spectral mixtures of spaceborne imaging spectroscopy data with a spatial resolution of 30 m form gradual material transitions and can they be mapped and analysed?

1.5 Thesis organization

The main research objectives of this thesis, outlined in section 1.4, are individually addressed in chapter II-IV. These chapters are structured as stand-alone manuscripts published in international peer-reviewed journals (chapter III and IV) or as reviewed conference proceedings in a prestigious digital online library (chapter II). For a consistent presentation of this thesis only formatting changes in chapter II, III, and IV were made.

The mapping of urban surface materials using imaging spectroscopy data is strongly dependent on the spatial resolution of the data set. The use of spectral unmixing algorithms and classification approaches has one thing in common: they require the prior determination of spectrally pure pixels for all occurring surface materials in order to enable a detailed mapping of urban surface materials per pixel. Consequently, the determination of spectrally pure pixels is a major task prior spectral unmixing or classification techniques can be conducted. Thus, in chapter II a new framework, called LUISA (Learning urban image spectral archive) using an image-based spectral library for the automated determination and identification of spectrally pure pixels in urban environments was developed. The transferability of a spectral library to a new study site is usually associated with the incompleteness of the spectral library. In this concept, this limitation is taken into account by an approach that also identifies unknown spectrally pure pixels that are missing

in the spectral library (chapter III). This approach facilitates a framework towards the generation of a generic spectral library. In chapter II the LUISA framework is outlined, while chapter III focuses on the automated determination of unknown artificial spectrally pure pixels using an initial spectral library. LUISA was developed for the use of airborne imaging spectroscopy data that are associated with a high spatial resolution.

However, a decreasing spatial resolution of imaging spectrometers is directly associated with the increasing occurrence of spectral mixtures in the pixels and simultaneously reduces the number of spectrally pure pixels in the investigation area. Future spaceborne imaging spectrometers will achieve a spatial resolution of around 30 m, which will reduce the occurrence of spectrally pure pixels in urban areas to a minimum or even lead to a complete loss of it. This hinders the mapping of urban surface materials with common methods and requires a new strategy that allows such an analysis of complex spectral mixtures without the need for spectrally pure pixels. Thus, in chapter IV a method originated from vegetation ecology was adapted that assumes the environment as a fuzzy continuum of itself. Spectral mixtures are analysed based on the composition of surface materials that form interpretable urban surface material gradients. Gradients were determined on the basis of a detailed map of urban surface materials that could be generated using extracted pure pixels from the LUISA framework. Subsequent mapping of urban surface material gradients were linked to administrative planning units and could be analysed for their commonly co-occurrence of urban surface materials.

The relation and context of mapping urban surface materials on different spatial scales from this work is outlined in Fig. 4. The mapping of urban surface materials with air- and spaceborne imaging spectroscopy data and their specifically addressed research developments are exemplified by separate case studies as follows.

Chapter II – *Identifying pure urban image spectra using a learning urban image spectral archive (LUISA)* – conceptualized a framework of a learning urban image spectral archive that is designed to automatically extract predominantly pure urban image spectra that can be used for further spectral analysing techniques such as spectral unmixing or classification methods. The framework is designed for generic use in any urban environment acquired by an airborne imaging spectrometer with high spatial resolution.

Chapter III – *Detecting unknown artificial urban surface materials based on spectral dissimilarity analysis* – aims on the development of a method to overcome the limitations of an incomplete urban spectral library. Therefore, a concept was developed that extracts

predominantly unknown pure material spectra by spectral similarity and dissimilarity analysis in high-resolution imaging spectroscopy data and categorizes them in unique material classes using spectral and spatial cluster analysis.

Chapter IV – *Gradients in urban material compositions: A new concept to map cities with spaceborne imaging spectroscopy data* – examines the highly complex spectrally mixed pixels from spaceborne imaging spectroscopy data with a spatial resolution of 30 m for the composition of urban surface materials. In this study, characteristic material compositions are analysed and utilized as an indicator for the delineation of certain types of urban structures.

In chapter V the findings are synthesised from a more general perspective and outlines prospective research directions.

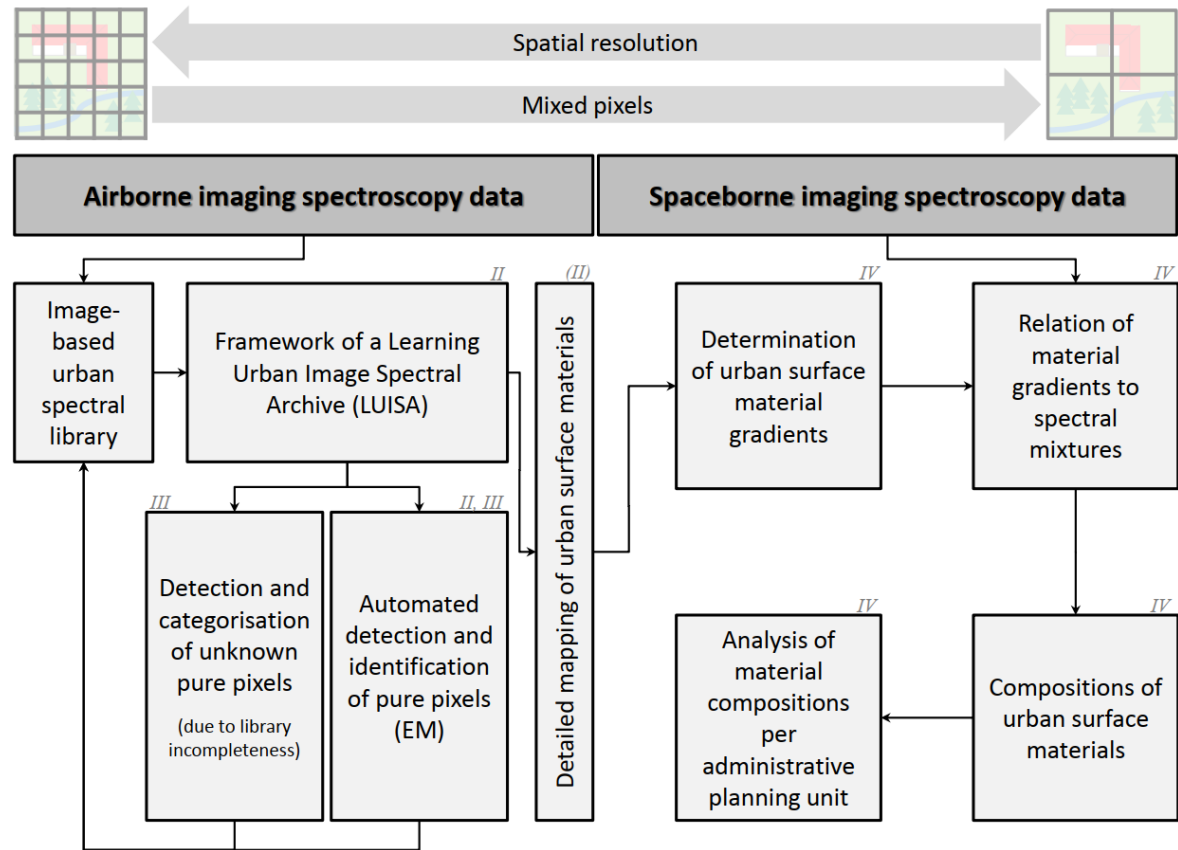


Fig. 4: Overview of the peer-reviewed publications (corresponding chapters are marked with Roman numerals) of this thesis and their relation to map urban surface materials.

1.6 Author's contribution to individual chapters

Chapter II

Marianne Jilge conceived the experiments, designed and performed the analysis, collected the data and wrote the paper. Uta Heiden helped to conceive the experiments, contributed to the design of the paper, provided the initial spectral library and revised the paper. Martin Habermeyer helped with software development and revised the paper. André Mende contributed with preliminary tests of the concept by developing a classifier to automatically map urban surface materials from HyMap data. Carsten Jürgens contributed on a conceptual level and revised the paper.

Chapter III

Marianne Jilge conceived and designed the analysis, collected data and prepared data, developed the analysis tools, performed the analysis and wrote the paper. Uta Heiden contributed to the design of the experiments and helped with writing and revised the paper. Martin Habermeyer helped with software development and revised the paper. André Mende contributed with preliminary tests of the concept by developing a classifier to automatically map urban surface materials from HyMap data. Carsten Jürgens contributed on a conceptual level and revised the paper.

Chapter IV

The concept and design of the analysis in the paper was jointly conceived and designed by Marianne Jilge, Uta Heiden and Hannes Feilhauer. Marianne Jilge performed all analyses and wrote the paper. Uta Heiden provided advice regarding the data (surface material map), contributed to the interpretation of the results (gradients) and partly wrote and revised the paper. Carsten Neumann contributed to preliminary tests and first data analysis and revised the paper. Hannes Feilhauer further contributed with the provision of gradient analysis tools and partly wrote and revised the paper.

CHAPTER II

Identifying pure urban image spectra using a learning urban image spectral archive (LUISA)

*Proceedings of SPIE Remote Sensing, 2016, 10008(100080J),
Remote Sensing Technologies and Applications in Urban
Environments*

Marianne Jilge, Uta Heiden, Martin Habermeyer, André Mende and
Carsten Jürgens

© Society of Photo-Optical Instrumentation Engineers (SPIE), 2016
Proceedings of SPIE
doi: 10.1117/12.2241370

Abstract

In this study a learning urban image spectral archive (LUISA) has been developed, that overcomes the issue of an incomplete spectral library and can be used to derive scene-specific pure material spectra. It consists of a well described starting spectral library (LUISA-A) and a tool to derive scene-based pure surface material spectra (LUISA-T). The concept is based on a three-stage approach: (1) Comparing hyperspectral image spectra with LUISA-A spectra to identify scene-specific pure materials, (2) extracting unknown pure spectra based on spatial and spectral metrics and (3) provides the framework to implement new surface material spectra into LUISA-A. The spectral comparison is based on several similarity measures, followed by an object- and spectral-based ruleset to optimize and categorize potentially new pure spectra.

The results show that the majority of pure surface materials could be identified using LUISA-A. Unknown spectra are composed of mixed pixels and real pure surface materials which could be distinguished by LUISA-T.

Keywords: spectral archive, pure pixels, urban areas, hyperspectral remote sensing

1. Introduction

Urban areas are complex in their structure and are frequently characterized by a large variety of diverse surface materials [1]. The cityscape is influenced by an ever-increasing number of dwellings, and a congestion of housing and places of work due to the worldwide detectable ongoing urbanization processes. Continuously, newly developed construction materials or modified material compositions are edging into the market. The material appearance is also governed by coating and degradation processes. However, geographical, cultural, and climatic trends can be observed in the material occurrence of a city.

Urban surface materials are biasing a number of urban processes such as surface runoff [2], [3] and urban climate [4], [5], [6]) in various ways due to their physical characteristics. In [7] the dominant urban applications necessitating knowledge about urban surface materials are specified. Therefore, the awareness of occurring urban surface materials is of high interest. In relation to the rapid urban changes a field-based assessment of surface materials is almost impossible due to time and costs, especially when analyzing large urban areas. Urban monitoring with remote sensing data has been extensively proven. However, the high diversity of urban surface materials associated with a typically high spectral variability, including high variations within a material class (intra-class variability) and between material classes (inter- class variability), and the spatial object heterogeneity necessitates the potentials of high resolution hyperspectral sensor systems. Due to the complexity of urban areas only a small number of studies have already applied hyperspectral remote sensing data to detect urban surface materials (e.g. [8], [9], [10], [11]). Automated endmember extraction methods have been developed and successfully applied, however, for labelling the extracted endmembers expert knowledge is required. Furthermore, the theory behind automated endmember extraction methods representing spectral extrema of materials is not valid for all urban surface materials. Some urban surface materials are not characterized by strong absorption bands and are basically differentiable by their reflectance (e.g. roofing tiles and roofing bitumen). Therefore, adapted endmember extraction methods have been developed (e.g. SSEE [12], OSP [13]). The spectral variability of a material class in a given test site is represented by appropriate pure material pixels. Thus we used the term ‘pure pixels or pure material spectra’ for the various instances of endmember sets.

Libraries containing image spectra are commonly used to identify pure material spectra as training data for further analysis such as spectral unmixing or classification. Hence, no

expert knowledge for the pixel labeling is required. Scene- based spectral libraries are very useful since they contain identical conditions such as illumination or status of degradation. In the domain of hyperspectral remote sensing of urban areas [8] developed a spectral library for investigating the city of Tel-Aviv, Israel, [14], [10] and [1] make use of library spectra derived from airborne data and in situ measurements for studying urban material appearance in Dresden and Potsdam, Germany, and [9] determine Santa Barbara, USA with library spectra acquired by in situ measurements. Pure pixels from an urban imagery can be extracted by a spectral comparison of image spectra with reference spectra using similarity measures [15], distance measures [9] or analyzing material-specific spectral features [16], [17], [10]. Accordingly, spectral libraries have to represent site-specific spectral variability of occurring surface material classes. A successful extraction of urban surface materials for any urban area would necessitate a complete and well described urban spectral library containing all material classes and their spectral variations. Such a spectral library is not existent due to the reasons given above. In this paper we present an approach to overcome this limitation. The objectives of this paper are:

- The development of a generic urban spectral archive which takes the incompleteness of a spectral library into account.
- A fully automated image based identification of urban surface materials using high resolution hyperspectral images.
- Utilization of extracted pure material spectra for further applications (such as spectral unmixing or supervised classification).

The paper describes the development of a generic approach of a learning urban image spectral archive (LUISA) to be used for the universal recognition of pure pixels in urban areas by tackling the issue of an incomplete spectral library. This work is structured by introducing the concept of LUISA (chapter 2.1) and their modules LUISA-A and LUISA-T (chapter 2.1.1 and 2.1.2). Chapter 2.2 outlines the study area and datasets used for the application of LUISA and the appropriate results (chapter 3) and discussion (chapter 4). A conclusion and an outlook are finally given in chapter 5.

2. Methods

2.1 LUISA

The major drawback of using spectral libraries to derive pure material spectra is that only pixels can be identified as pure if the library comprises all instances of material spectra which occur in the test site. That means that objects covered by a pure material which are not represented in a spectral library by a corresponding reference spectra or material instance, will be not identified as pure material spectra due to a low similarity between the image spectra and the reference spectra. Thus, pure pixels with missing reference spectra in a spectral library are in a sense unknown (‘unknown pure pixels’) and are not taken into account as pure pixels by traditional spectral similarity analysis.

The learning urban image spectral archive (LUISA) is conceptualized to extract and identify image-based pure urban material spectra, even the unknown pure pixels, and is composed of modules: 1) LUISA-A and 2) LUISA-T. LUISA-A is basically the ‘archive’ of the entire concept of LUISA. It represents a comprehensive universally structured spectral archive tailored for urban areas and is accurately described in chapter 2.1.1. The second LUISA module is depicted by LUISA-T, in the proper senses the ‘tools’ of LUISA for an automatically image-based identification of urban surface materials on the basis of a high resolution hyperspectral image. LUISA-T can be generally divided in the two target-aimed components for a) identifying pure material spectra by a spectral comparison of image pixels with LUISA-A spectra, followed by b) analyzing spectral dissimilarities in combination with spatial and spectral metrics for extracting unknown pure material spectra due to a certain incompleteness of LUISA-A and provide the prerequisites for an expansion of LUISA-A with identified pure pixels. Resulting image based pure urban material classes are usable for instance for a material based classification of the image (chapter 2.3 and 3.1) or for spectral unmixing such as MESMA [18] to derive material abundances. Furthermore, derived pure material spectra can be implemented as new reference spectra in LUISA-A to learn and expand the archive for further analysis. The accuracy of the extracted surface material classes can be tested by applying a post-classification on the image and validate it by comparing the result with validation data (chapter 2.3). In Figure 1 the generic concept of LUISA is outlined as well LUISA-A and LUISA-T are explained in detail in chapter 2.1.1 and 2.1.2. LUISA was applied and validated for a test-site in Germany (chapter 3 and 3.1) for which no location-based

spectral reference data were implemented in LUISA-A to test the generic usability of the archive.

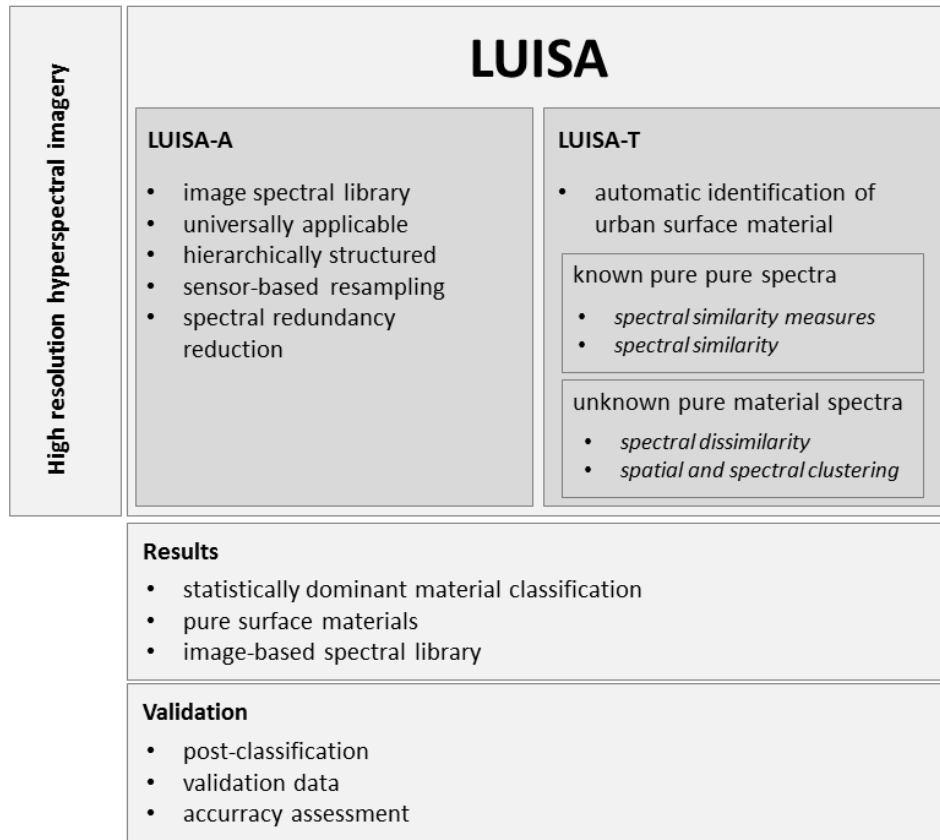


Fig. 1: Concept of LUISA

2.1.1 LUISA-A

Spectral libraries are commonly used for a spectral comparison with image data. At that pixels with the highest similarity to reference spectra or by a certain probability threshold are labeled automatically to their appropriate material class. For an accurately and complete identification of pure pixels the composed reference spectra in the spectral library should feature the intra-class variability of the study area. That implies a spectral library with composed reference spectra specifically acquired from the study area to cover all occurring material variations. Library spectra acquired from the image itself implicate equivalent conditions and thus are optimally representing the test-site specific spectral characteristics. A comprehensive starting spectral library of pure urban surface materials derived from three German cities (Munich, Dresden, and Potsdam) was built. Therefore, more than 5,200 reflectance spectra were extracted from HyMap scenes acquired in

different years and pre-processing schemes to consider spectral variations of recorded materials [10]. Wavelengths containing water vapor bands and noisy bands were removed to avoid random errors in the pixel-based similarity analysis (chapter 2.1.2). Thus, the starting spectral archive consists of 113 spectral bands ranging from 455 nm to 2,449 nm and is composed of 22 natural and manmade material classes and reference spectra for shadowed areas. The reference spectra are organized in a spectral archive and generically structured in an advanced class hierarchy to ensure a universal application. This categorized spectral archive represents the collection of distinct spectral variations of pure urban material spectra and forms LUISA-A. For structuring LUISA-A spectra we developed an enhanced universal class hierarchy on the basis of the hierarchical concept of EAGLE which is composed of land cover and land characteristics [19]. The LUISA hierarchy is developed with main focus on urban surface materials. Nevertheless, it enables a continuous extension of hierarchical class instances as well as the integration of new derived pure material spectra into LUISA-A. In table 1 the utilized class hierarchy is exemplarily introduced to organize reference spectra in LUISA-A.

Table 1: Generic class hierarchy for LUISA-A

Types of ecosystems	Land cover component	Land cover types	Land cover elements	Bio-geo-chemical types	Material classes	Spectral variations	
Abiotic	Natural Surfaces	Unconsolidated	Exposed soil	Non-contaminated	Soil	[instances]	
					Sand		
				Contaminated			
			Gravel				
		Consolidated	Rocks				
	Artificial surfaces	Impervious and partially pervious	Overbuilt	Mineral	Clay tiles		
					Concrete		
				Metallic	Copper		
					Aluminum		
					Zinc		
				Hydrocarbon	Polyethylene		
					Bitumen		
					Tar paper		
					Polyvinylchloride		
				Biomass			
				Opaque			
				Non-overbuilt (other constructions)	Mineral		Concrete
		Cobblestone					
		Lose chippings					
		Hydrocarbon	Tartan				
			Synthetic turf				
			Asphalt				
Pervious (not partially pervious)	Waste materials						
	Other artificial surfaces						
Biotic	Woody vegetation	Trees	Broadleaf	Deciduous tree	[instances]		
			Coniferous	Coniferous tree			
			Palm trees				
		Bushes/ shrubs					
	Herbaceous	Graminaceous					
	Succulents/ others						
	Lichen/ Mosses						
Water	Liquid	Inland	Lake/ Ponds		[instances]		
			Rivers				
			Pools				
		Coastal					
		Open sea					
	Solid	Snow/ Glacier					

Incidentally LUISA is conceptualized to cope with an incomplete spectral archive that means in addition that spectra structured on the basis of the class hierarchy are not necessarily subdivided in seven hierarchical levels. Primarily reference spectra related to ecosystem type ‘water’ or ‘biotic’ are not arranged in seven hierarchical levels due to a lower study interest. The lowest distinguishable hierarchical level, containing spectral instances for most of those ecosystem types are constituted by level four or five. Even so, the class hierarchy is at any time extendable to guarantee a universal application and structured reference spectra in LUISA-A. Reference spectra are addressed by numeric class codes signifying corresponding class level instances. The class codes can additionally be

used for organizing and identifying LUISA-A spectra in a spectral information system (chapter 5) such as SPECCHIO [20].

There are still a large number of redundant reference spectra (extremely high intra-class variability) in LUISA-A due to the combination of different site-specific spectral libraries or by implementing new reference spectra extracted by LUISA (chapter 2.1.2). LUISA-A, as a centerpiece of LUISA provides the option to reduce spectral redundant reference data mainly for computational reasons but also for ensuring a certain inter-class variability to avoid errors in the similarity analysis (chapter 2.1.2). For the purpose of reducing spectral redundant data from LUISA-A the frequently used unsupervised clustering technique ISODATA [21], [22] was applied to determine appropriate material instances which are considering the spectral variability of a material class. Therefore, each material class of the spectral archive is investigated by the ISODATA algorithm to cluster similar spectra by an automatically defined threshold. The mean spectra of each cluster optimally represents a material instance and remains as reference spectra in LUISA-A. Furthermore, an automatically spectral resampling of LUISA-A spectra provides a generic use, independent of the recording sensor system and sensor calibration of the study area, because image spectra are characterizing the spectral sensor properties with which the spectra were recorded. To ensure the per-pixel based spectral comparison (chapter 2.1.2) of image data with LUISA-A reference spectra to identify pure pixels, LUISA-A spectra were automatically adjusted to the spectral characteristics of the input hyperspectral image. Therefore, a spectral resampling of LUISA-A spectra with a bandwidth of 1 nm and a subsequent upscaling to the appropriate sensor characteristics of the underlying hyperspectral image enables sensor-independent applications.

2.1.2 LUISA-T

LUISA-T forms the second module of LUISA and contains a number of tools for identifying image based pure material spectra using a well-organized and comprehensive spectral archive (LUISA-A) regardless missing reference spectra. It is separated into two leading components to a) identify known pure material spectra using a similarity analysis and an automatic thresholding technique with the assistance of reference spectra archived in LUISA-A (chapter 2.1.1) and b) to derive and categorize unknown pure pixels due to the incompleteness of the spectral archive (LUISA-A) by means of a spatial and spectral

cluster analysis. Pure pixels of an image are discernible by a certain spectral conformity compared to tagged reference spectra. The similarity determination between two spectra (image and reference spectra) is the assigned task of a similarity analysis. Therefore, similarity measures are aiming to mathematically describe spectral signatures in an n-dimensional hyperspace and subsequently evaluate their congruence numerically. The numerical evaluation of two spectra is commonly represented by a normalized range between 0 and 1, where a similarity value of 0 means congruent (high similarity values) and a value of 1 stands for completely different (low similarity values). LUISA provides a selection of commonly used and proposed similarity measures such as Spectral Angle Mapper (SAM [15]), Spectral Information Divergence (SID [23]), the hybrid mixed measure SID-SAM [24], Spectral Correlation Measure (SCM [25]), Spectral Correlation Angle (SCA [26]), an hybrid measure SID-SCA [27], Jeffries-Matusita Distance (JMD [28]), and the hybrid measure JMD-SAM [29] for the similarity analysis. In the similarity analysis image spectra are evaluated and linked to corresponding material classes by their highest similarity or the statistically dominant similarity class by a pixel-wise comparison with LUISA-A spectra. To extract appreciable similarity values LUISA-A reference spectra were ranked in descending order (from high similarity values to low similarity values). The first ten similarity values of the ranking were used for defining the statistically dominant similarity class by using the highest similarity value of the material class which occurs most often in the ranking. This target class is used due to the simple reason of a higher probability that this pixel was more frequently found to be represented by this material class.

For the subsequent automated pure pixel thresholding separated pixel masks containing abiotic or biotic pixels, derived from the image pre-classification (classification based on similarity values), were used. The automated pure pixel thresholding relies on histogram statistics of similarity values. The region with the highest change in the occurrence of similarity values represents the thresholding point to delimit known pure pixels from the pre-classified image by the optimal tradeoff between similarity and dissimilarity. This point can be easily found by deriving the local maxima in this region of the histogram's second derivative function. As a preprocessing step, a simple median filter to remove noise from the histogram is proposed. The known pure pixel thresholding approach is suggested to be applied on abiotic and biotic pixels individually to ensure the typical differences in spectral variations of abiotic and biotic material classes.

Different material classes are constituted by distinct spectral signatures and differ from reference spectra in LUISA-A. Potentially pure unknown material spectra were therefore delimited based on pixels with low similarity values. This extraction of potentially pure unknown material spectra uses the dissimilarity analysis proposed in [30]. There is no fixed number of remaining pure unknown pixels, even so, at least 1% of the image. Correspondingly, 1% of the pixels with the lowest similarity values detected from the ranking of the statistical dominant material class were derived as potentially pure unknown pixels. Remaining unknown pure pixels are incorporated as second similarity analysis of the image where the extracted potentially pure unknown pixels act as temporary spectral library. Resulting similarity values are compared with the similarity values of the first similarity analysis and assigned to the mask of potentially pure unknown pixels, if the similarity is higher to the temporary spectral library spectra. Again a separation into biotic and abiotic material classes is proposed. The masks of potentially pure unknown pixels also implicate mixed pixels. Mixed pixels typically occur along object borders due to material mixtures with adjacent objects. In addition single pixels frequently do not represent pure material spectra regarding the spectral scale of objects and the spatial resolution of the sensor. Therefore, pixels in the mask of potentially pure unknown pixels are spatially clustered to remove mixed pixels from object borders by means of a moving window. This process uses the von Neumann neighborhood [31] to investigate direct pixel neighbors for the same type (mask element) and removes pixels from the mask if a mask pixel has not at least four adjacent mask pixels. Especially in urban areas which are composed of different sized object (e.g. storage halls, detached houses, streets etc.), the removal of object borders may be critically and should be treated ad hoc.

Remaining mask pixels are considered as unknown pure pixels of unknown affiliation to a material class. In the spatial and spectral cluster analysis unknown pure pixels are categorized to unknown material classes. For this purpose pure pixels were again spatially clustered and a cluster ID is assigned to each pixel aggregation. Subsequently, based on a user defined SAM threshold each cluster is analyzed for its spectral intra-class homogeneity. Cluster elements are detached if spectral intra-class homogeneity is exceeded. This analysis considers different materials on one object. The same material can be used on different objects, therefore the spectral inter-class of objects is analyzed and objects are linked if a user defined SAM threshold of cluster elements is not reached. Determined clusters are representing the spectral intra- class variability of a new unknown material class. A combination of known and unknown pure material spectra may be used

as endmember sets for a spectral unmixing or as training data in supervised classification methods (chapter 2.3). Extracted pure pixel spectra may be further used to integrate them in LUISA-A as new material instances or new material classes.

2.2 Study Area and Hyperspectral Image Data

For evaluating the universality of LUISA, it was applied on a test site where no site specific reference spectra were implemented into LUISA-A. As study area the medium-sized town Ludwigsburg located in the federal state of Baden- Wuerttemberg in Germany was used. The city founded in the Baroque is located approximately 12 km in the north of Stuttgart on the plateau of the river Neckar basin between the fort Hohenasperg in the west and the Neckar valley in the east (approximately 48.9°N, 9.2°E). Ludwigsburg is structured in the central city (center, north, east, south, and west) and seven further districts. In 2010 the city was characterized by 78.50% residential areas and 21.50% commercial and industrial areas [32] covering large halls predominantly used for automotive industry and machine engineering. For this study we selected a snippet from the south-western part of the city (Ludwigsburg West and the district Pflugfelde). The extent illustrated in figure 2 represents the typical complexity of urban areas. It is composed of a wide range of urban surface materials occurring in differently sized and dense industrial areas mainly in the upper part and residential buildings in the southern part of the region. The outer region is composed of agricultural fields and individually wooded areas.

To extract pure material spectra with LUISA-T for the test site a hyperspectral image from an air campaign with the HyMap sensor was carried out in August 4, 2010 by the German Aerospace Center (DLR). Six flight lines over Ludwigsburg were flown. The whiskbroom sensor recorded the test site in a spectral range from 450 nm to 2500 nm with 128 spectral bands and a spatial resolution of 4 meters. More information about the characteristics of the HyMap sensor can be found in [33]. The data were pre-processed to Level 2A. That includes the removal of three bad band as well as the removal of the same spectral bands removed from LUISA-A to enable an adequate spectral similarity analysis. The remaining 110 spectral bands were corrected for atmospheric effects and converted to reflectance data within the atmospheric correction software ATCOR [34]. Additionally, the image was corrected for radiometric effects and geometric distortion and finally georeferenced to the

UTM WGS 84 coordinate system. In figure 2 a subset of the first flight line, covering the previously described Ludwigsburg study area is illustrated. The used data set is not a perfect example due to the systematically detectable low reflectance values which are resulting from the relatively high noise level of the data.

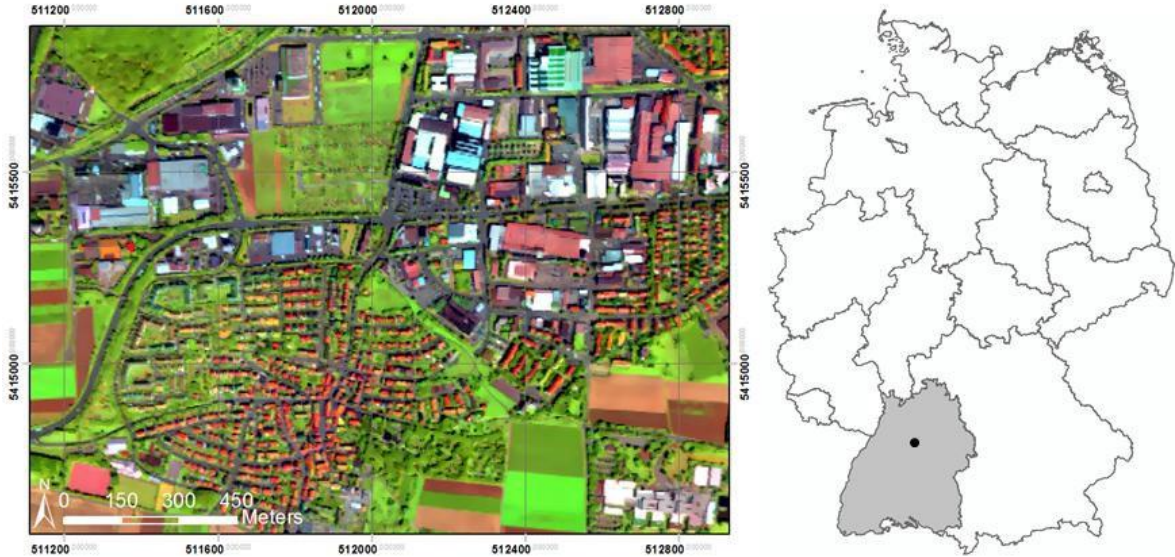


Fig. 2: Study area: District Ludwigsburg west and Pflugfelde, Germany.

Furthermore, the typically high intra-class variability of urban objects was reduced by utilizing the iterative adaptive smoothing filter (IAS) [35]. The IAS algorithm based on the SAM and root mean square error to reduce noise and intra- class variability, while spatially and spectrally detectable object borders remain. Thus, the typically high intra-class variability of urban areas [36], [37] for instance due to a high diversification especially in roofing materials [10] mainly caused by coating and aging will persist. Intra-class variability can lead to undetected spectral differences of spectrally similar material classes [35] and can hamper the differentiation of classes.

2.3 Validation

For evaluating the usability of extracted pure pixels by LUISA-T a supervised post-classification by using the derived pure pixels as training data was used. The maximum likelihood classifier is the most commonly used supervised classification algorithm in the field of remote sensing [38]. The algorithm assigns pixels with the highest probability to a class based on a statistical heuristic of the probability density. A specified probability

threshold [39] for each material class can be defined to only classify the image by the respective material class if the probability threshold is retained.

For evaluating the accuracy of the post-classification by a confusion matrix and Cohen's kappa coefficient [40] validation data are required. Therefore, abiotic and biotic objects were assessed by ground truth inventories, photographs, Google Earth® images and spectral expert knowledge were used as validation data. For this purpose, small areas of objects were digitalized and allocated by the respective material class. Entire object outlines as validation data are avoided due to the issue of a high probability to represent mixed pixels along object borders (chapter 2.1.2) and due to small scaled objects of different material types allocated on the object itself (e.g. dormers). Thus, also spectral variations in an object due to differing roofing orientations are well avoided.

3. Results

For applying LUISA on the test site in Ludwigsburg, Germany (chapter 2.2) a spectral resampling of LUISA-A (chapter 2.1.1) to the spectral calibration characteristics of the underlying HyMap scene was carried out. In addition, redundant reference spectra of material classes were reduced by ISODATA clustering (chapter 2.1.1) individually for each material class. At that too similar spectral variations to the determined material class instances were eliminated. The final archive (LUISA-A) was consisting of 151 reference spectra categorized to the LUISA class hierarchy outlined in chapter 2.1.1.

As similarity measure for the similarity analysis to extract known pure material spectra the SID-SCA (chapter 2.1.2) which promises higher accuracies [27] for the pre-classification was used. The pre-classification result of the statistical dominant material class was applied to build abiotic and biotic pixel masks which are individually used for the known pure pixel thresholding. A known pure pixel threshold of 0.000378329 was extracted for abiotic materials and a threshold of 0.000055524 for biotic materials using the median filtered histogram statistics of the respective statistical dominant material classes to identify the tradeoff between similarity and dissimilarity (chapter 2.1.2). By using the automated thresholding approach to identify pure pixels 11.8% of the abiotic pixel mask and 17.2% of the biotic pixel mask were recognized as pure material spectra.

For extracting remaining unknown pure pixels, 1% of the pixels with the lowest detectable similarity values of the statistical dominant material class were derived as potentially pure

unknown pixels. These pixels were used as reference signatures (temporary spectral library) in a second similarity analysis of the hyperspectral image. Subsequently, a case analysis of the newly derived similarity values with the similarity values of previous similarity analysis is carried out. Pixels with a higher similarity value (values closer to 0) achieved by the second analysis were added to the mask of potentially pure unknown pixels. This includes outliers of potentially unknown pure pixels to the mask. The mask of potentially pure unknown pixels was again separated by abiotic and biotic material classes for a more precise categorization of unknown pure pixels in the end. Hence, the removal of mixed pixels by eliminating single pixels and the deletion of border pixels along objects due to a higher probability to be express mixed pixels was individually applied on the abiotic and biotic pixels. Pixels pre-classified as shadowed areas were not further considered. Remaining pixels are considered as unknown pure pixels. For discriminating their affiliation of material classes pure unknown pixels were subject of spatial clustering and spectral homogeneity analysis. For that, unknown pure pixels with adjacent unknown pure pixels (using the von Neumann neighborhood) were spatially clustered and a unique cluster ID was assigned. The spectral homogeneity analysis based on an empirically defined SAM threshold of 0.1 for the spectra intra-class homogeneity and the inter-class homogeneity. As a result, spatial clusters were separated if the spectral similarity of pixels exceeded the intra-class homogeneity by the given threshold, or spatial clusters were linked if the spectral similarity of cluster pixels were within the allowed inter-class homogeneity. Achieved clusters of unknown pure material spectra are representing the spectral variations of a new unknown material class. For biotic pure pixels one unknown material class and for abiotic pure pixels nine unknown material classes were encountered. Extracted unknown pure material spectra may be used for learning LUISA-A with new reference spectra after identifying the descriptive material.

3.1 Validation of LUISA results

For validating the usability of extracted pure material spectra by LUISA-T a maximum likelihood classification using the identified material classes as training data was applied. However, not all extracted material classes could be entered as training data class for the classification due to not sufficiently covered training pixels of a represented class. There were not enough pure pixels representing the class sand, coniferous tree, tartan, roofing

paper and zinc. Unfortunately, also six of the newly detected unknown abiotic material classes were not adequately indicated by pure pixels for using them as training data in the maximum likelihood classification. However, in this study the main focus lies on urban surface materials. Therefore, and due to unavailable particularized ground truth data of land cover elements for biotic classes (i.e. differentiation of coniferous trees and deciduous trees), a combination of vegetated classes (trees and grassland) were used as training data class ‘vegetation’. Thus, we applied the maximum likelihood classifier on the class vegetation, asphalt, paving concrete, roofing concrete, partially red loose chippings, aluminum, roofing bitumen, polyethylene, PVC, roofing clay tiles, one biotic unknown class, and three abiotic unknown material classes. Furthermore, a probability threshold of 95% for each material class for classifying the image was set. Hence not the entire image was assigned to a material class. Unclassified areas were indicated by a lower probability to represent a certain material class. Therefore, these unclassified areas may represent unknown surface materials due to the missing training data of some material classes (e.g. the mentioned material classes above) or mixed pixels. Figure 3 illustrates the post-classification of the study area using the maximum likelihood algorithm by applying the extracted pure material classes from LUISA-T.

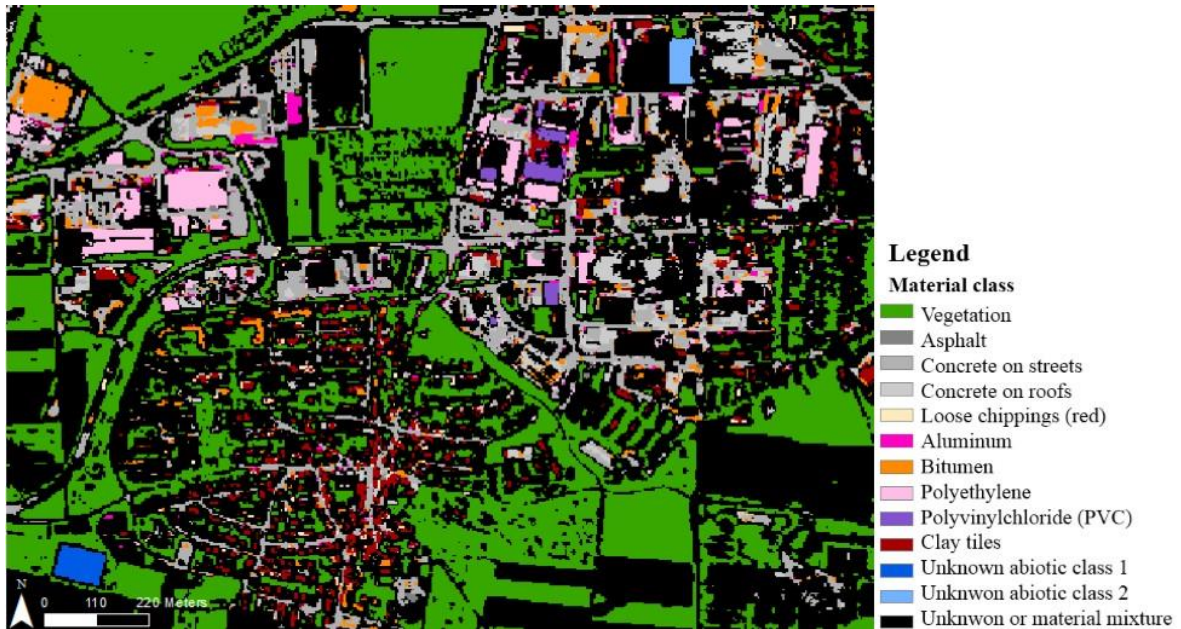


Fig. 3: Post-classification using maximum likelihood classifier on the basis of extracted pure pixels from LUISA-T.

3.2 Accuracy assessment of post-classification

The post-classification accuracy is determined by calculating a confusion matrix [41] for the known material classes on the basis of the validation polygons introduced in chapter 2.3. Concrete appearance as roofing material or paving material is not just discriminable by its spectral material characteristic, therefore ancillary information such as a building mask is required. Accordingly material classes of roofing and paving concrete were merged for evaluating the post-classification accuracies of known material classes. The confusion matrix in table 2 is based on reference polygons. Due to the setup of validation data a utilization of validation pixels would not provide meaningful results.

Table 2: Confusion matrix for post-classification of known material class using validation polygons.

	REFERENCE								sum [classification]
	vegetation	asphalt	concrete	aluminum	bitumen	polyethylene	PVC	clay tiles	
vegetation	16	0	0	0	0	0	0	0	16
asphalt	0	2	0	0	0	0	0	0	2
concrete	0	13	4	0	3	0	0	0	20
aluminum	0	0	0	1	0	0	0	0	1
bitumen	0	0	0	0	10	0	1	0	11
polyethylene	0	1	0	0	0	18	1	0	20
PVC	0	0	0	0	0	0	4	0	4
clay tiles	0	0	0	0	0	0	0	20	20
sum [reference]	16	16	4	1	13	18	6	20	94

An overall accuracy of 79.8% and a kappa of 0.76 were achieved for known material classes. Classified areas as unknown abiotic material classes were evaluated manually. The abiotic object classified in dark blue in the lower left corner of the post-classification (figure 3) is representing a sports area covered by a greenish surface. Based on the spectral characteristics this material class could be identified as ‘green tartan’ which is often found as surface material on sports areas. This class was found as unknown abiotic material class because the tartan reference spectra in LUISA-A just provide material instances of red tartan. So this area was correctly identified as unknown material class and was used to learn LUISA-A by new material instances for the tartan class.

The second detectable object covered by another unknown abiotic material class was found in the north-east of the image (depicted in light blue; figure 3) as roofing material of a large hall. During the field work this rooftop was recognized as rusty corrugated sheet for which also no reference spectra existed in LUISA-A, and was therefore correctly found as new material class.

4. Discussion

Although the used hyperspectral images do not provide perfect conditions due to a relatively high level of noise (chapter 2.2), several known and unknown pure material spectra were found. Particularly the accuracy assessment of known material classes used as training data for the post-classification provides a kappa of 0.76. This result shows the suitability of extracted pure material spectra by LUISA for further urban applications to analyze urban surfaces. The displayed confusion matrix (table 2) exemplifies the accuracy of the known material classes. It can be observed that especially material classes with strong absorption features were almost accurately found. Also the manual inspection of accuracies of unknown material classes found by LUISA-T (chapter 2.1.2) achieved promising outcomes to learn LUISA-A with new material spectra or material instances. The findings show that LUISA enables to universally extract pure material spectra of urban areas using by an incomplete but well described spectral archive (LUISA-A).

However, there are still some limitations which are influencing the results. The extraction of pure pixels by means of a similarity analysis does not sufficiently differentiate between the classes asphalt and concrete. This is a commonly emerging issue using similarity measures [9]. Asphalt and concrete spectra are relatively similar in their spectral shape. The reflection intensity (albedo) is the best criteria for differencing between these two spectra [10]. Our results show that SID as part of the underlying hybrid similarity measure does not sufficiently consider the albedo differences between two spectra. So far, in our knowledge there is no similarity measure available which does sufficiently consider the albedo differences between two spectra. However, for a reliable differentiation of asphalt and concrete spectra the consideration of the albedo is crucial and has to be taken into account. One possibility would be considering the mean albedo of each spectral signature and define a threshold to assign the spectra to the class asphalt or concrete. Furthermore, uncultivated fields were not found as pure pixels despite soil reference spectra consist in LUISA-A. As a consequence not enough pixels were found to build sufficiently represented training data for the post-classification. That's because of too little spectral variations of existing reference soil spectra which are included in LUISA-A. This issue is also observable in the pre-classification of the statistical dominant similarity values where most uncultivated fields exhibit a higher probability to be concrete or tartan. This lead to the issue that these areas were incorrectly integrated to the mask of abiotic material classes for extracting pure pixels. In addition these areas were not found as pure unknown pixels

due to the simple fact that the dissimilarity between soil and concrete was too low to be integrated in the mask of potentially pure pixels. New instances of soil spectra were not found in the derivation of unknown pure material spectra due to the fact that the extraction of unknown pure material classes by LUISA-T is based on the dissimilarity analysis mentioned in chapter 2.1.2. Therefore, only unknown materials with a certain dissimilarity to reference spectra of LUISA-A can be derived. This issue was found on some rooftops covered by fiber cement, which is a missing material class in LUISA-A. However, its material composition and therefore the spectral shape is too similar to existing roofing concrete spectra so that fiber cement was not found as new (unknown) material class. Therefore, a manual updating of new material classes such as fiber cement to LUISA-A would promise higher accuracies in the allocation of spectral similar material classes. In addition, it was found that one of the determined abiotic unknown material classes is rather a class of remaining unknown pure pixels where the respective spectra do not correspond between each other. This results by the defined SAM threshold for the inter- and intra-class homogeneity analysis to separate or link similar unknown pure material classes. However, a refined threshold overestimates spectral cluster similarities and excessively separates material classes. So it seems that some material mixtures are still remaining in the unknown pure material classes. Hence, a further improvement of the mask of potentially unknown pure pixels would cope with this issue.

5. Conclusion and Outlook

Spectral libraries for identifying surface materials in a certain area are easy to use and do not require expert knowledge about spectral characteristics. Pixels can be automatically identified as a component of a given material class by means of similarity measures. These include also the extraction and automatic labeling of pure material spectra (bundles of endmembers) for further analysis such as usual classifications of surface materials or spectral unmixing for assessing the abundances of material classes. Previous approaches using spectral libraries to derive pure material spectra necessitate complete spectral libraries containing reference spectra acquired from the certain study area. However, urban areas are very complex in their spatial and spectral characteristic. Continuously changes in material composition and appearance are common and differ in geographic regions, cultures and traditions. An extraction of pure material spectra by a similarity analysis

between image spectra and reference spectra required therefore a complete spectral library covering the spectral complexity of the study area. Universally applicable spectral libraries covering all spectral variations of occurring surface materials in urban areas do not exist and will never be feasible. The concept of LUISA provides a framework for a universally applicable spectral archive to extract pure material spectra in spite of incomplete reference spectra for high resolution hyperspectral remote sensing data of urban areas. A similarity analysis provides the basis of extracting initially known pure pixels for which reference spectra exist in the spectral archive (LUISA-A) by an automated thresholding technique. Remaining unknown pure pixels are extracted and categorized by spatial and spectral metrics. Good classification accuracies with a kappa of 0.76 verifies the usability of LUISA for urban areas without integrated site-specific reference spectra in LUISA-A.

We are currently working on a framework to automatically integrate extracted pure material spectra as new reference spectra in LUISA-A to enhance the incompleteness for further urban studies. An improvement of the classification accuracy by a better consideration of albedo variations (e.g. [42]) especially for spectrally similar shaped material classes (such as asphalt and concrete) is intended. Additionally, derived unknown pure material classes have to be investigated for remaining mixed pixels by for instance analyzing the miscibility to further improve the classification accuracy and therefore the usability of extracted pure pixels for further analysis.

Acknowledgements: This work was supported by the German Aerospace Center (DLR) - Project Management Agency and Ministry of Economics and Technology (BMWi), Germany, under the project EnFusionMap (50 EE 1343).

References

- [1] Roessner, S., Segl, K., Heiden, U. and Kaufmann, H., “Automated differentiation of urban surfaces based on airborne hyperspectral imagery,” *IEEE Transactions on Geoscience and Remote Sensing* 39 (7), 1525-1532, (2001).
- [2] Fletcher, T.D., Andrieu, H. and Hamel, P., “Understanding, management and modelling of urban hydrology and its consequences for receiving waters; a state of the art review,” *Advances in Water Resources* 51, 261–279, (2013).
- [3] Miller, J. D., Kim, H., Kjeldsen, T. R., Packman, J., Grebby, S. and Dearden, R., “Assessing the impact on urbanization on storm runoff in peri-urban catchment using historical change in impervious cover,” *Journal of Hydrology* 515, 59-70, (2014).
- [4] Taha, H., “Urban climates and heat islands: albedo, evapotranspiration, and anthropogenic heat,” *Energy and Buildings* 25, 99-103, (1997).
- [5] Heldens, W., Heiden, U., Esch, T. and Dech, S., “Potential of hyperspectral data for urban micro climate analysis,” *Proc. Hyperspectral Workshop*, (2010).
- [6] Stewart, I.D. and Oke, T.R., “Local Climate Zones for Urban Temperature Studies,” *BAMS American Meteorological Society* 93 (12), 1879–1900, (2012).
- [7] Heldens, W., Heiden, U., Esch, T., Stein, E. and Mueller, A., “Can the future EnMAP Mission contribute to urban applications? A literature survey,” *Remote Sensing* 3, 1817-1846, (2011).
- [8] Ben-Dor, E., Levin, N. and Saaroni, H., “A spectral based recognition of the urban environment using the visible and near-infrared spectral region (0.4-1.1 μm). A case study over Tel-Aviv, Israel,” *International Journal of Remote Sensing* 22 (11), 2193-2218, (2001).
- [9] Herold, M., Roberts, D. A., Gardner, M. E. and Dennison, P. E., “Spectrometry for urban area remote sensing – development and analysis of a spectral library from 350 to 2400 nm,” *Remote Sensing of Environment* 91, 304- 319, (2004).
- [10] Heiden, U., Segl, K., Roessner, S. and Kaufmann, H., “Determination of robust spectral features for identification of urban surface materials in hyperspectral remote sensing data,” *Remote Sensing of Environment* 111, 537-552, (2007).
- [11] Franke, J., Roberts, D. A., Halligan, K. and Menz, G., “Hierarchical Multiple Endmember Spectral Mixture Analysis (MESMA) of hyperspectral imagery for urban environments,” *Remote Sensing of Environment* 113, 1712-1723, (2009).
- [12] Rogge, D., Rivard, B., Zhang, J., Sanchez, A., Harris, J. and Feng, J., “Integration of spatial-spectral information for the improved extraction of endmembers,” *Remote Sensing of Environment* 110, 287-303, (2007).
- [13] Harsanyi, J. C. and Chang, C-I., “Hyperspectral image classification and dimensionality reduction: An orthogonal subspace projection approach,” *IEEE Transaction on Geoscience and Remote Sensing* 32, 779-785, (1994).
- [14] Heiden, U., Roessner, S., Segl, K. and Kaufmann, H., “Analysis of spectral signatures of urban surfaces for their identification using hyperspectral HyMap data,” *Remote Sensing and Data Fusion over Urban Areas, IEEE/ISPRS Joint Workshop*, 173-177, (2001).
- [15] Kruse, F.A., Lefkoff, A.B., Boardman, J.W., Heidebrecht, K.B., Shapiro, A.T., Barloon, P.J. and Goetz, A.F.H., “The spectral image processing system (SIPS)—interactive visualization and analysis of imaging spectrometer data,” *Remote Sensing of Environment* 44, 145–163, (1993).
- [16] Clark, R.N. and Swayze, G.A., “Mapping Minerals, Amorphous Materials, Environmental Materials, Vegetation, Water, Ice and Snow, and Other Materials: The USGS Tricorder Algorithm,” *Summaries of the Fifth Annual JPL Airborne Earth Science Workshop, JPL Publication* 95 (1), 39-40, (1995).

- [17] Clark, R. N., Swayze G. A., Livo K. E., Kokaly R. F., Sutley S. J., Dalton J. B., McDougal R. R. and Gent C. A., "Imaging spectroscopy: Earth and planetary remote sensing with the USGS Tetracorder and expert systems," *Journal of Geophysical Research* 108(E12), (2003).
- [18] Roberts, D. A., Gardner, M., Church, R., Ustin, S., Scheer, G. and Green, R. O., "Mapping chaparral in the Santa Monica Mountains using multiple endmember spectral mixture models," *Remote Sensing of Environment* 65, 267-279, (1998).
- [19] Arnold, S., Kosztra, B., Banko, G., Smith, G., Hazeu, G., Bock, M. and Valcarcel-Sanz, N. "The EAGLE concept – a version of a future European Land monitoring framework," *Proc. EARSeL Symposium "Towards Horizon 2020"*, 551-568, (2013).
- [20] Hueni, A., Malthus, T., Kneubuehler, M. and Schaepman, M., "Data exchange between distributed spectral databases," *Computers & Geosciences* 37 (7), 861-873, (2011).
- [21] Geoffrey, H., Ball, David, J., and Hall, "ISODATA, a novel method of data analysis and pattern classification," *Technical Report, Stanford Research Institute, California, USA*, (1965).
- [22] Memarsadeghi, N., Netanyahu, N.S. and LeMoigne, J., "A Fast Implementation of the ISODATA Clustering Algorithm," *International Journal of Computational Geometry and Applications* 17 (1), 71-103, (2006).
- [23] Chang, C.I., "An information theoretic-based approach to spectral variability, similarity and discriminability for hyperspectral image analysis," *IEEE Transaction on Information Theory* 46 (5), 1927–1932, (2000).
- [24] Du, Y., Chang, C. I., Ren, H., Chang, C.C., Jensen, J. O. and D'Amico, F. M., "New hyperspectral discrimination measure for spectral characterization," *Opt. Eng.* 43 (8), 1777-1786, (2004).
- [25] Van der Meer, F. and Bakker, W., "CCSM: Cross correlogram spectral matching," *International Journal of Remote Sensing* 18 (5), 1197-1201, (1997).
- [26] Bajwa, S. G., Bajcsy, P., Groves, P. and Tian, L. F., "Hyperspectral image data mining for band selection in agricultural application," *Transaction of the ASAE* 43, 895-907, (2004).
- [27] Naresh Kumar, M., Seshasai, M. V. R., Vara Prasad, K. S., Kamala, V., Ramana, K. V., Dwivedi, R. S. and Roy, P. S., "A new hybrid spectral similarity measure for discrimination among Vigna species," *International Journal of Remote Sensing* 32 (14), 4041-4053, (2011).
- [28] Swain, P. H. and King, R. C., "Two effective feature selection criteria for multispectral remote sensing," *LARS Technical Reports, Purdue University, USA*, (1973).
- [29] Padma, S. and Sanjeevi, S., "Jeffries Matusita based mixed-measure for improved spectral matching in hyperspectral image analysis," *International Journal of Applied Earth Observation and Geoinformation* 32, 138- 151, (2014).
- [30] Mende, A., Heiden, U., Bachmann, M., Hoja, D. and Buchroithner, M., "Development of a new spectral library classifier for airborne hyperspectral images on heterogeneous environments," *Proceedings of the 7th EARSeL Workshop of the Special Interest Group in Imaging Spectroscopy*, 1-9, (2011).
- [31] Toffoli, T. and Margolus, N., "Cellular Automata Machines: A New Environment for Modeling," *MIT Press, Massachusetts Institute of Technology*, 60, (1987).
- [32] Statistisches Landesamt Baden-Wuerttemberg, „Flaeche seit 1988 nach tatsaechlicher Nutzung“, 31 December 2010, <https://www.statistik-bw.de/BevoelkGebiet/GebietFlaeche/01515221.tab?R=GS118048>, (10. August 2016).
- [33] Cocks, T., Jenssen, A., Stewart, A., Wilson, I. and Shields, T., "The HyMap airborne hyperspectral sensor: the system, calibration and performance," *Proc. of the 1st EARSeL Workshop on Imaging Spectroscopy*, 1-6, (1998).
- [34] Richter, R. and Schlaepfer, D., "Atmospheric/ Topographic Correction for Satellite Imagery (ATCOR-2/3 User Guide", Version 9.0.2, (2016).

- [35] Rogge, D. and Rivard, B., "Iterative spatial filtering for reducing intra-class spectral variability and noise," *Proc. Hyperspectral Image and Signal Processing: Evolution in Remote Sensing (WHISPERS)*, 1-4, (2010).
- [36] Heiden, U., Segl, K., Roessner, S. and Kaufmann, H., "Determination and verification of robust spectral features for an automated classification of sealed urban surfaces," *Proc. Of 4th EARSeL Workshop on Imaging Spectroscopy, New quality in environmental studies*, 165-174, (2005).
- [37] Lacherade, S., Miesch, C., Briottet, X. and Le Men, H., "Spectral variability and bidirectional reflectance behavior of urban materials at a 20 cm spatial resolution in the visible and near-infrared wavelength. A case study over Toulouse (France)," *International Journal of Remote Sensing* 26 (17), 3859-3866, (2005).
- [38] Richards, J. A., "Remote Sensing Digital Image Analysis – An Introduction," Springer-Verlag, Berlin & Heidelberg, (2013).
- [39] Lillesand, T.M., Kiefer, R.W. and Chipman, J.W., "Remote Sensing and Image Interpretation," John Wiley & Sons, Hoboken, USA, (2004).
- [40] Cohen, J., "A coefficient of agreement for nominal scales," *Educational and Psychological Measurement* 20 (1), 37-46, (1960).
- [41] Congalton, R. G., "A review of assessing the accuracy of classifications of remotely sensed data", *Remote Sensing of Environment* 37, 35-46, (1991).
- [42] Ding, J. G., Li, X. B. and Huang, L. Q., "A novel method for spectral similarity measure by fusing shape and amplitude features," *Journal of Engineering Science and Technology Review* 8 (5), 172-179, (2015).

CHAPTER III

Detecting unknown artificial urban surface materials based on spectral dissimilarity analysis

Sensors 2017, 17(8), 1826, 1-20

Marianne Jilge, Uta Heiden, Martin Habermeyer, André Mende and Carsten Jürgens

© by the authors. Licensee MDPI, Basel, Switzerland. 2017

doi: 10.3390/s17081826

Received 31 May 2017; revised 4 August 2017; accepted 6 August 2017.

Abstract

High resolution imaging spectroscopy data have been recognised as a valuable data resource for augmenting detailed material inventories that serve as input for various urban applications. Image-specific urban spectral libraries are successfully used in urban imaging spectroscopy studies. However, the regional- and sensor-specific transferability of such libraries is limited due to the wide range of different surface materials. With the developed methodology, incomplete urban spectral libraries can be utilised by assuming that unknown surface material spectra are dissimilar to the known spectra in a basic spectral library (BSL). The similarity measure SID-SCA (Spectral Information Divergence-Spectral Correlation Angle) is applied to detect image-specific unknown urban surfaces while avoiding spectral mixtures. These detected unknown materials are categorised into distinct and identifiable material classes based on their spectral and spatial metrics. Experimental results demonstrate a successful redetection of material classes that had been previously erased in order to simulate an incomplete BSL. Additionally, completely new materials e.g., solar panels were identified in the data. It is further shown that the level of incompleteness of the BSL and the defined dissimilarity threshold are decisive for the detection of unknown material classes and the degree of spectral intra-class variability. A detailed accuracy assessment of the pre-classification results, aiming to separate natural and artificial materials, demonstrates spectral confusions between spectrally similar materials utilizing SID-SCA. However, most spectral confusions occur between natural or artificial materials which are not affecting the overall aim. The dissimilarity analysis overcomes the limitations of working with incomplete urban spectral libraries and enables the generation of image-specific training databases.

Keywords: imaging spectroscopy; urban areas; spectral library; dissimilarity; unknown surface materials

1. Introduction

Accurate differentiation and identification of urban surface materials is an important requirement for area-wide land cover mapping, and thus for subsequent derivation of further urban data products. Due to their high spectral and spatial information content [1], very-high resolution airborne imaging spectroscopy data have been recognised as a valuable data resource for augmenting surface material inventories [2,3]. Surface material inventories serve as input for various applications, such as urban planning, imperviousness mapping [4–6], hydrological modelling [7,8], urban green structure analysis [9,10], and urban climate modelling [11–16].

For successful and reliable surface material mapping using very-high resolution airborne imaging spectroscopy data, spectral mixture analysis has been frequently used. Such analysis requires the detection of endmembers that represent the spectrally diverse surface materials and their intra-class variabilities [17–19] in a given scene. The correct endmember detection is essential for the subsequent spectral unmixing analysis [20,21]. However, endmember can also be used for classification [22–24], or any other data mining methodology [25]. To date, most success has been achieved with image-specific endmembers since they comprise all scene-based structural and compositional information, sensor artefacts, and acquisition-based data characteristics [26].

Manual development of a suitable endmember set is challenging, since urban areas are spectrally very diverse [27–29]. Therefore, emphasis has been put on semi-automated empirical approaches, such as the well-known Pixel-Purity-Index method [30]. Fully automated endmember detection algorithms fit a simplex to the point cloud of the data set in the feature space. Examples of these model-based approaches are Minimum Volume Transforms [31] and the N-FINDR. Optimization techniques have been integrated in methods such as Iterative Error Analysis (IEA) or Automated Morphological Endmember Extraction (AMEE) (see [18]). Rogge et al. [32] made use of spatial sub-sampling via local endmember extraction to reduce the size of the original data set. However, the resulting endmembers of these automated algorithms still have to be labelled.

Urban spectral libraries are expert knowledge databases containing the spectral reflectance characteristics of selected artificial surfaces. They have been developed and used across all scales—laboratory [33,34], field [35], and image spectral libraries [36–38]. Image spectral libraries used for urban surface material mapping have been demonstrated for Santa Barbara, USA [39], Brussels, Belgium [40], and German cities such as Munich [41] and

Dresden [42]. In all cases, more than 20 spectrally different surfaces were detected, comprising biotic and artificial materials. Different colours, coatings, and degradation processes [43] of the materials result in various degrees of spectral intra-class variability. Further variability is introduced by the varying illumination effects [44] resulting from different inclinations of the sensor and the sunlight, and the urban object itself (roof pitch). Intra-class variabilities increase the number of spectrally distinct urban surfaces in very-high resolution airborne imaging spectroscopic data.

The need for image-specific urban spectral libraries is still very high and requires expert knowledge of the characteristics of spectral urban surfaces. In recent years, more attention has been paid to the development and utilization of universal image spectral libraries where a wide range of known urban surface material spectra are generated and stored [25,39]. This progress has evolved owing to the need for area-wide material mappings in diverse geographic regions. That means the inclusion of urban surface materials that characterise regional and cultural trends. Additionally, new urban materials continuously enter the market and their new spectral variations have to be taken into account. The spatial and temporal applicability of existing image spectral libraries is therefore limited.

Based on these observations, it is concluded that it will be impossible to create and maintain a complete and globally applicable spectral library. Imaging spectroscopy techniques are needed that are able to handle the incompleteness of spectral libraries when applied to unknown scenes, and that are also designed to cope with regional-, sensor-, or acquisition-specific characteristics. In this study, a spectral dissimilarity analysis has been developed to aim for a fully automated detection of unknown urban surface materials in high-resolution airborne imaging spectroscopy data using an extensive image library of urban materials. The specific objectives are to:

- Determine unknown scene-based surface material spectra using an incomplete spectral library
- Focus on the detection of pure spectra and avoid detection of spectral mixtures
- Categorise detected unknown surface materials based on spatial and spectral characteristics to support future material-specific identification

Basically, unknown surface materials are identified based on their spectral dissimilarity compared to known library spectra by means of an iterative similarity analysis (Sections 2.3.1 and 2.3.2). For the spectral dissimilarity analysis, a basic spectral library (BSL) is

used that comprises an extensive collection of urban surface materials occurring in Germany. The proposed methodology is suitable for detecting urban surface materials in imaging spectroscopy data that are not yet included in the BSL.

2. Methods

Initially, three data sets are needed for the dissimilarity analysis, (I) a very-high resolution image (Section 2.1); (II) a basic spectral library (Section 2.2); and (III) a class hierarchy that groups the surface materials in the BSL. The detection of unknown surface materials is based on (1) measuring the similarity between image spectra and library spectra by using a spectral similarity measure (Section 2.3.1); (2) masking pixels with the lowest similarities (high dissimilarities) as potentially unknown surface materials (Section 2.3.2); and (3) categorising the unknown surface materials by a spatial-spectral clustering approach (Section 2.3.3). The procedure also includes two steps to remove mixed pixels from the masks of unknown surface materials. The final result is a scene-specific spectral library with categorised spectrally homogeneous unknown material classes that can serve as a basis for precise labelling of the materials, e.g., by field surveys (Figure 1). The future material-specific identification of detected unknown surface materials is not in the scope of this paper. However, the resulting unknown material classes are spectrally homogeneous and represent predominantly pure image spectra. This means that only one surface material has contributed to the spectral signal of the respective pixel. Thus, the classes can serve as input for further unmixing or data mining techniques, and the detected material classes can be integrated as newly flagged reference spectra into the universal spectral library. Except for the final labelling step, this process is fully automated.

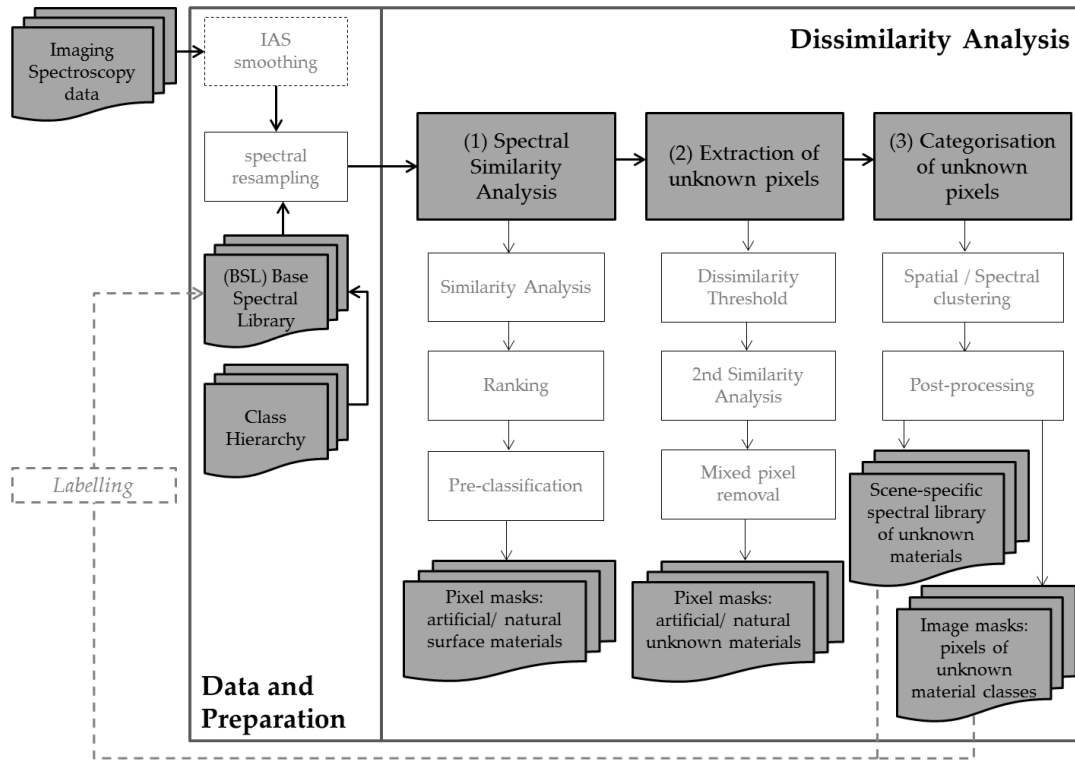


Fig. 1. Basic concept of a spectral dissimilarity analysis to detect unknown urban surface materials in high-resolution airborne imaging spectroscopy data.

2.1. Study Area and Imaging Spectroscopy Data

The city of Munich, Germany, was chosen as the study area to demonstrate the functionality of the developed approach. Four municipal areas characterised by diverse urban structures were selected as test sites (Figure 2). The test sites range in function from residential to commercial to industrial to leisure exploitation, and thus include a large variety of surface material classes accompanied by high inter-class variability.

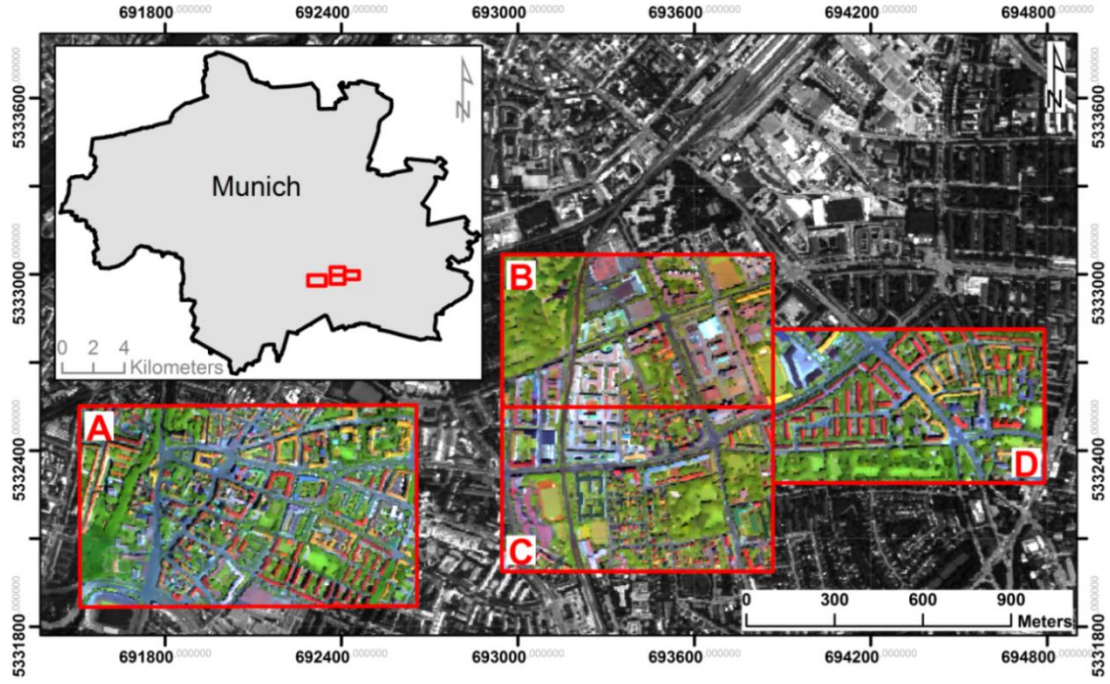


Fig. 2. Study area and imaging spectroscopy (HyMap) data for the four test sites A, B, C, and D in Munich, Germany ($R = 1652 \text{ nm}$, $G = 719 \text{ nm}$, $B = 543 \text{ nm}$).

The study area was recorded during the HyEurope2007 campaign on 17 and 25 July using the airborne imaging spectrometer HyMap operated by the German Aerospace Center (DLR) in Oberpfaffenhofen. This sensor records data in 128 contiguous spectral bands between 450 nm and 2500 nm. The flight altitude of about 2000 m resulted in a ground sampling distance (GSD) of 4 m and a swath width ranging from 2 to 2.5 km. A detailed description of the sensor characteristics can be found in [45].

Pre-processing of the data [41] includes correction for radiometric effects according to [45] and the removal of three noisy bands (bands number 1, 33, and 34). The remaining 125 spectral bands were subject to conversion from radiance to surface reflectance values and nadir-normalization by the ATCOR-4 software [46] due to recognition of a brightness gradient. Geometric correction and referencing to the UTM WGS-84 coordinate system was carried out with ORTHO software [47]. Orthorectification was based on the digital terrain model derived from SRTM (Shuttle Radar Topography Mission) data [48]. Mean geometric accuracy was calculated and resulted in 0.8 pixels for the entire data set. For a precise similarity analysis (Section 2.3.1), 12 more spectral bands (from the wavelength ranges 1788 to 2067 nm and 2465 to 2496 nm) were removed due to remaining noise and the presence of atmospheric effects. The final imaging spectroscopic data set contained 113 spectral bands.

2.2. Spectral Library Development

For the spectral dissimilarity analysis, an initial spectral library is needed. For setting up the BSL, image spectra were extracted from high resolution imaging spectroscopy data (HyMap) acquired over the German cities of Dresden, Potsdam [37], and Munich (Table 1).

Table 1: Airborne imaging spectroscopy data used for the extraction of reference spectra for the BSL.

Acquisition Date (DD-MM-YYYY)	Test Site	Pixel Size	No. of Bands
18-05-1999	Dresden	7.7 m	128
18-05-1999	Potsdam	4.0 m	128
01-08-2000	Dresden	3.3 m	126
20-07-2003	Dresden	3.5 m	126
17-06-2007	Munich	4.0 m	125
25-06-2007	Munich	4.0 m	125

Based on these diverse data sets, spectral variations resulting from different illumination and observation conditions [44], regional characteristics, and data processing are considered. Accordingly, the BSL contains all the surface materials occurring in the test sites to the best of the authors' knowledge, with special emphasis on artificial materials. However, due to phenological variations, different vegetation types and soils are underrepresented in the BSL.

Image spectra per material class were selected based on the hierarchical categorisation scheme introduced in [37]. Therefore, spectra for each surface material class were determined by defining regions of interest in the images (Table 1) based on field investigations, spectral expert knowledge, infrared aerial imagery, and Google image products. In order to use image spectra as reference spectra, spectral purity was ensured by selecting homogeneous areas while excluding boundaries and small urban objects. Finally, the library was manually inspected and reduced by eliminating any potentially remaining mixed material spectra, resulting in almost 5200 BSL spectra organised in 23 surface material classes that are further divided in 8 natural, 14 artificial, and one class of shadow. The shadow class is determined by image pixels collected over shaded natural and artificial surfaces. This class is used for excluding shaded regions in the dissimilarity analysis. An overview of included reference spectra per surface material class is given in Table 2.

Table 2: Class hierarchy to separate BSL spectra of material classes (their occurrence is in brackets) into artificial and natural surface material groups.

Artificial		Natural
Paving and Open Space Materials	Roofing Materials	
	roofing aluminium (181)	sand (31)
	roofing bitumen (400)	soil (96)
asphalt (339)	roofing concrete (352)	coniferous tree (248)
synthetic turf (264)	roofing copper (164)	deciduous tree (277)
tartan (75)	roofing polyethylene (358)	lawn (434)
paving concrete (167)	roofing polyvinyl chloride (PVC) (231)	pond (183)
red loose chippings (161)	roofing tar (15)	pool (34)
	roofing tiles (589)	river (354)
	roofing zinc (143)	

Additional 97 reference spectra of shadow have been integrated in order to avoid shaded areas in the artificial and natural pixel mask (Sections 2.3.1 and 2.3.2).

2.3. Dissimilarity Analysis

The dissimilarity analysis comprises three main processing steps that are outlined in Section 2. Further, as illustrated in the concept (Figure 1), two pre-processing steps, IAS smoothing and spectral resampling, are included. The first pre-processing step is optional and accounts for the high spectral intra-class variability of urban surfaces that can be referred to spectral variations, as described in Section 1, and image noise. The iterative adaptive smoothing (IAS) filter [49] reduces the image noise while retaining the object edges. The second pre-processing step incorporates a spectral resampling of the BSL to the spectral resolution of the imaging spectroscopy data used, in order to make processing independent of the relevant characteristic in the image data. The spectral resampling of the BSL is based on interpolating the spectra to the wavelength information of the input imaging spectroscopy data.

2.3.1. Spectral Similarity Analysis (1)

The spectral dissimilarity analysis starts with a quantitative analysis of spectral similarities among all image spectra (Section 2.1) and all available BSL spectra. Over the past decades a wide range of similarity measures have been developed to numerically evaluate the match between two spectra. These include, for instance, the well-known Spectral Angle Measure (SAM) [50], Spectral Information Divergence (SID) [51], Spectral Correlation Angle (SCA) [52], and Spectral Correlation Measure (SCM) [53]. Most of

these measures evaluate the match based on the spectral shape while ignoring the amplitude of the spectra. Additionally, hybrid similarity measures have been developed to exploit the advantages or minimise the weaknesses, of two similarity measures. The Jeffries–Matusita-Spectral Angle (JM-SAM) is one such hybrid approach that was developed for mangrove applications [54]. Naresh Kumar et al. [55] developed and compared SID-SCA with SID-SAM [56] and found higher performance of the SID-SCA in the visible wavelength range targeted to a discrimination of vigna species using laboratory measurements. The efficiency of specific similarity measures was analysed in [55,57,58], with SID-SCA being considered the best performing. Accordingly, SID-SCA was selected as the most appropriate technique for the spectral similarity analysis in this study. However, to the authors' knowledge, none of the similarity measures are specifically adapted to urban surface discrimination.

For the quantitative analysis of spectral similarities using SID-SCA, each pixel spectrum is compared with each BSL spectrum, resulting in n similarity values, where n is the total number of BSL spectra. Similarity values are normalised and inverted to enable a logical interpretation, meaning that similar spectra have similarity values close to 1 and dissimilar spectra have similarity values close to 0.

In the next step, the n similarity values per pixel are ranked in descending order (similar to dissimilar). The best match is represented by the highest obtainable similarity value. However, in this study the ten highest ranked similarity values are used to define the statistically dominant class according to [59]. In this case, the material classes occurring in the ranking of the first ten similarity values are linearly weighted on the basis of the total number of representatives per material class (Table 2), in order to equally consider over- and under-representation of single material classes. Weights of material classes are multiplied by the number of materials classes represented in the ranking and summed up to determine the overall weight of an observed pixel. Finally, the statistically dominant class is represented by the highest percentage obtained for the material weight divided by the summed overall weights.

In summary, for each pixel a single similarity value was defined that enables its assignment to one respective surface material class (Table 2). That allows for a simple separation of the pixels into the coarse material groups artificial and natural surfaces (artificial and natural masks) and shadow. This ranking and pre-classification is crucial for the subsequent extraction and later categorisation of unknown, predominantly pure pixels (Sections 2.3.2 and 2.3.3).

2.3.2. Extraction of Unknown Pixels (2)

Extraction of unknown pixels is based on the idea that pixels with very low similarity values are not represented in the BSL. Such pixels commonly comprise spectral mixtures as well as predominantly pure unknown materials. A dissimilarity threshold was introduced to distinguish known from unknown pixels and expressed as a percentage of the total number of image pixels. The threshold is applied separately to the artificial and to the natural materials mask, while pixels pre-classified as shadow are neglected. The resulting potentially unknown pixels are stored in two masks, one for pixels with unknown artificial materials and one for those with unknown natural materials. The separation of artificial and natural pixels is important owing to the underrepresentation of natural material classes in the BSL, as described in Section 2.2. Without the separation, natural surfaces are more commonly detected as potentially unknown pixels. This study solely focused on the pixel mask for potentially unknown artificial materials.

In the first instance, a fixed dissimilarity threshold is used to separate unknown from known pixels. However, when using a fixed dissimilarity threshold, a hard boundary for separating similar from dissimilar pixel spectra is set. This results in ignoring dissimilar pixel spectra with low similarity values, but not low enough to be considered as potentially unknown. These outliers are considered in a second similarity analysis, where all image spectra are compared to each of the potentially unknown pixel spectra extracted with the dissimilarity threshold. This comparison follows the same procedure as described in Section 2.3.1. Pixels that are more similar to the potentially unknown pixel spectra than determined by the first similarity analysis are subsequently added to the mask of potentially unknown pixels. The influence of the dissimilarity threshold and the subsequent second similarity analysis are analysed in Sections 3.3 and 3.4.

Potentially unknown pixels may also comprise spectral mixtures that need to be removed. Single pixels and the border pixels of pixel clusters commonly consist of spectral mixtures. To remove them a 3×3 pixel moving window is applied following von-Neumann criteria [60] for analysing neighbourhood relationships. Pixels are considered to be a mixture if an observed mask pixel is not surrounded by at least four direct mask pixels. The remaining pixels represent the mask of unknown and predominantly pure artificial pixels.

2.3.3. Categorisation of Unknown Pixels (3)

In the third step of the dissimilarity analysis, the mask of unknown and predominantly pure artificial pixels is used to build spectrally homogeneous clusters to facilitate a future material based labelling of the unknown pixel spectra. Initially, spatial clusters are built using the von-Neumann criteria. Clusters are then spectrally re-organised based on their internal and external spectral homogeneity. For spectral homogeneity assessment, SAM [50] was used due to the easy interpretation of the results and the high level of experience with this approach in the scientific community. For analysing the internal spectral homogeneity of a spatial cluster, all pixels within this cluster are compared to each other. If inverted similarity values (see Section 2.3.1) exceed an internal homogeneity threshold of 0.9 (radian measure), which is specified according to an inverted threshold of 0.1 [59], a new subcluster is built. An external spectral homogeneity analysis between the newly generated spatial clusters first determines the mean reflectance spectra of each cluster and second, makes a spectral comparison between clusters. Accordingly, clusters are aggregated if the determined similarity values do not exceed a radian measure of 0.9 [59] analogous to the internal homogeneity threshold. Resulting spatially and spectrally homogeneous clusters are subsequently assumed to represent individual unknown surface material classes. However, empirical tests reveal that an additional step (post-processing) is required to ensure the spectral purity of the derived unknown surface material classes. For this purpose, spatially isolated pixels of a single unknown material class are removed according to the single pixel removal method described in Section 2.3.2. Additionally, clusters with fewer than four pixels are deleted, since it is very likely that they still contain spectral mixtures or do not sufficiently represent a new material class.

The remaining pixels represent the final unknown surface material classes detected in the image. The categorisation step results in a scene-specific spectral library of unknown material classes, tagged with respective geographic coordinates, and an image mask of unknown material classes (Figure 1). Extracted unknown material spectra can be labelled and subsequently included in the BSL.

2.4. Experimental Setup

The functionality and effectiveness of the described dissimilarity analysis (Section 2.3) were tested using HyMap data for Munich, Germany (Section 2.1). Basically, two setups were designed, a library setup and a dissimilarity threshold setup. For the library setup, specific surface material classes and their respective instances are removed from the universal spectral library to simulate its incompleteness. Subsequently, whether the removed material classes could be detected as unknown surface material classes is tested using the dissimilarity analysis described in Section 2.3. For this purpose, four different BSL cases have been defined:

- (1) the BSL is fully applied and assumed to be complete for the respective test sites (*full*)
- (2) all instances of the material class roofing tiles are removed (*without tiles*)
- (3) all instances of the material class roofing zinc are removed (*without zinc*)
- (4) all instances of the material classes roofing tiles and zinc are removed (*without zinc and tiles*)

In library setup (2) roofing tiles are removed since they are a frequently occurring roofing material in German cities and are also observable in other countries. The roofing tile class has numerous spectral signatures because of the huge variety of material characteristics (colour, coating, etc.). In setup (3) zinc is removed, which is relatively unique due to its characteristically wide and deep absorption feature at 1020 nm, which makes it easily distinguishable. Additionally, setup (4) tested how the methodology handles the removal of more than one material class by removing both roofing tiles and zinc.

For the dissimilarity threshold setup, different percentage values, 1%, 2%, 3%, and 5%, are used to determine the mask of potentially unknown surface materials (Section 2.3.2). The impact of the dissimilarity threshold should be analysed regarding (1) the number of detectable unknown surface material classes; (2) the amount of spectral mixtures handled in the analysis, and 3) the influence on the final unknown surface material classes. The different library and dissimilarity threshold setups are individually applied to the four test sites (Section 2.1), producing a variety of outcomes.

2.5. Validation

Validation was carried out of the pre-classification of artificial and natural masks and of the detected unknown surface materials. For validating the pre-classified images, the determined statistically dominant material classes and the validation data were pooled into two groups, natural surfaces and artificial surfaces, on the basis of the utilised class hierarchy (Section 2.2). Validation comprises kappa statistics [61], overall accuracies, and producer- and user-accuracies for summarised natural and artificial material classes resulting from test site specific confusion matrices.

The validation data is also used for evaluating detected unknown surface material classes (Section 2.3.3). The spatially and spectrally aggregated unknown material clusters are compared for their spatial agreement with the validation data. For this purpose, unknown surface material classes are labelled manually based on expert knowledge and previous studies [41]. Accuracy is determined by calculating the percentage share of detected clusters and validation clusters.

Validation data rest upon digitised building blocks that have been used and described in [41]. The building blocks were manually digitised by means of orthophotos. Surface material classes (Section 2.2) were identified and manually assigned with spectral expert knowledge and field surveys. The underlying orthophotos were simultaneously acquired with a 3K-camera during the hyperspectral flight campaign and had a spatial resolution of 50 cm [62]. At least one digitised building block is present in each of the four test sites. Validation data for the purpose of this study are enhanced by manual selection of single object pixels on the basis of spectral expert knowledge. When selecting pixels as validation data, the spectral intra-class variability of the material classes occurring in the test sites was taken into account as accurately as possible. Regarding the experimental results (see Sections 3 and 4), validation data for roofing tiles are divided into two colour categories (dark roofing tiles and red roofing tiles). Figure 3 shows the validation data for each of the four test sites.

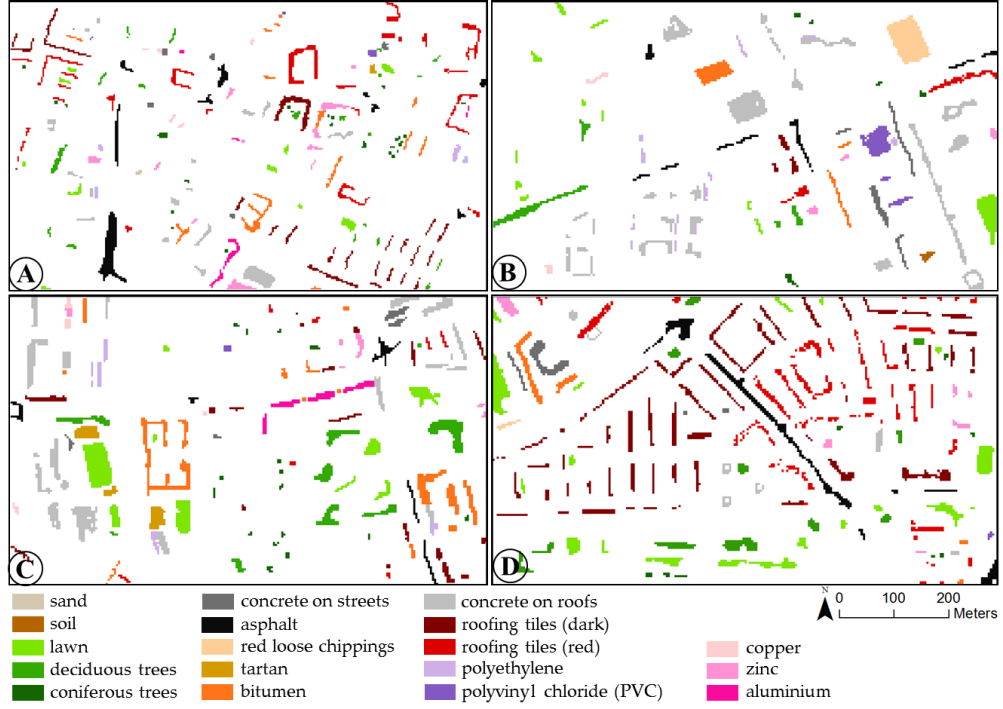


Fig. 3: Validation data for test sites (A–D) in Munich, Germany.

3. Results and Preliminary Assessment

The methodological steps described in Section 2.3 are individually applied to the four test sites (Section 2.1) according to the experimental setup (Section 2.4). The results of the three main steps, comprising pre-classification, masking of unknown predominantly pure pixels, categorising unknown material classes, and evaluating unknown material classes, is shown separately in Sections 3.1–3.4.

3.1. Pre-Classification (Step 1)

Pre-classification categorises image pixels into natural and artificial surfaces based on the statistically dominant surface material class (Section 2.3.1). The accuracy assessment was primarily done per surface material class (Table 2) to investigate potential confusion between single classes. Further, it has to be mentioned that validation of pre-classification results focusses on assessing the accuracies of predominantly pure surface materials, because the area-wide interpretation of spectral mixtures is not within the scope of this paper. The results of the accuracy assessment are listed in Table 3.

Table 3: Pre-classification accuracies for the test sites (column 1) using the full BSL setting comprise grouped producer and user accuracies within natural (columns 2–3) and within artificial material classes (columns 4–5) demonstrating the general separation of the broad classes natural and artificial. Overall accuracies (column 6) and kappa statistics (column 7) reveal the general pre-classification accuracies of single material classes.

Test Site	Producer Acc.-Natural	User Acc.-Natural	Producer Acc.-Artificial	User Acc.-Artificial	Overall Accuracy	Kappa Statistic
A	89.89%	83.98%	91.60%	90.92%	92.32%	0.91
B	93.15%	93.30%	86.95%	89.25%	83.14%	0.80
C	95.81%	90.63%	92.91%	93.13%	94.24%	0.93
D	93.07%	94.54%	78.83%	74.17%	86.22%	0.81

In general, kappa statistics show values between 0.80 and 0.93, with the best result for test site C. Overall accuracies range from 83.14 to 94.24%. The lowest user and producer accuracies were assessed for the artificial pixel mask of test site D. Accuracies are extensively analysed by inspecting confusion at the material level based on the respective confusion matrices. It reveals that confusion mainly occurs between materials within one of the two broad classes—natural and artificial surfaces. Confusion of spectrally similar material classes, such as asphalt and concrete (test site C), or between roofing tiles and red loose chippings, is well-known and documented by other studies [37]. Confusion among artificial and natural material classes is rare. An exception is bright sand that has been also identified as concrete. This is because sand (quartz) is one of the main components of concrete [37].

Results of the accuracy assessment demonstrate the suitability of the presented approach for distinguishing between the two broad classes (a) natural and (b) artificial surfaces. The following analysis focusses on artificial surfaces.

3.2. Mask of Unknown Artificial Pixels (Step 2)

In Figure 4 each single masking step to extract unknown predominantly pure artificial pixels, described in Sections 2.3.1 and 2.3.2, is graphically illustrated for a subset of test site D.

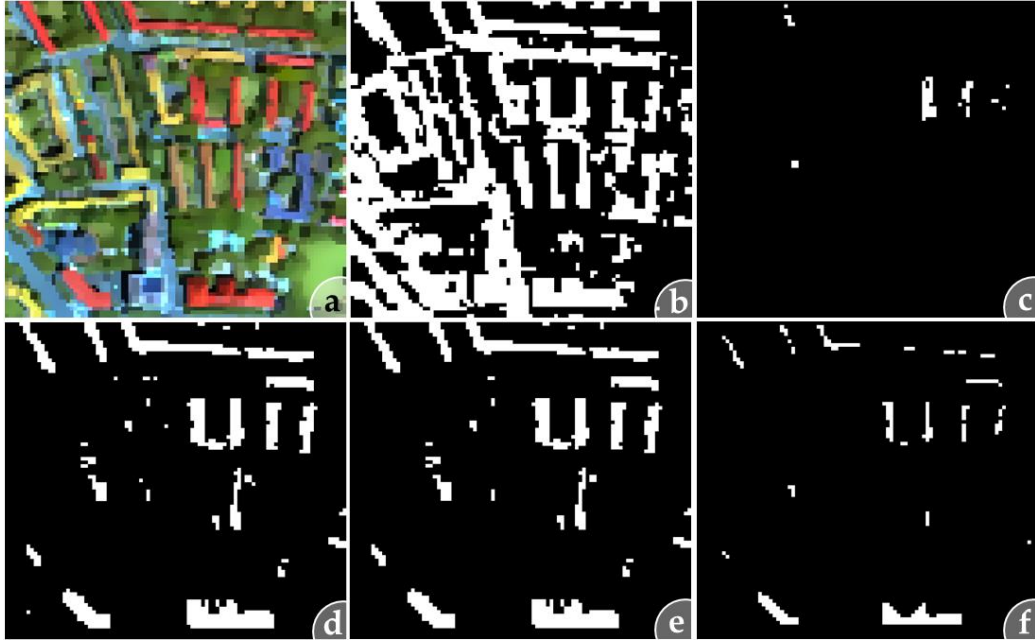


Fig. 4: Masking steps to determine unknown artificial pixels for (a) a subset of test site D using the BSL without tiles by (b) separating artificial pixels from pre-classification results; (c) extracting dissimilar artificial pixels based on a 1% dissimilarity threshold; (d) enhancing the mask by a second similarity analysis to include outliers; (e) removing single pixels and (f) removing border pixels based on the von-Neumann criteria for eliminating mixed pixels.

The results for all test sites are described in terms of the varying library setups and increased dissimilarity thresholds. First, the number of pre-classified artificial pixels is influenced by the library setup applied that imitates the level of incompleteness of the BSL. Artificial masks (Figure 4b) determined from libraries without tiles are generally smaller than masks resulting from libraries without zinc. This is reasonable, since the roofing tile class contains many more instances (589) than the zinc class (143) (see Table 2). Which library setup is used also influences the number and representation of the detected unknown surface material classes. The higher the incompleteness of the library with respect to a given test site, the more pixels are classified as unknown there (Figure 4f). This finding is demonstrated in Figure 4, which illustrates the application of the algorithm on the test site D subset. This test site is characterised by a large number of buildings covered with roofing tiles and shows a high number of detected unknown pixels for the library set “without tiles”. However, it also shows that some roofing tile pixels expected to be unknown are missing by comparing the artificial mask (Figure 4b) and validation data (Figure 3) with the resulting unknown pixel mask (Figure 4f).

Second, an increasing dissimilarity threshold causes an increase in detected potentially unknown pixels after the second similarity analysis. In general, the mask of potentially unknown pixels contains new unknown classes, more variability (instances) of these classes, and spectral mixtures. Especially the number of spectral mixtures needs to be monitored in more detail (Section 3.3). In all test sites and experimental settings mixed pixel removal (Section 2.3.2) results in a rather massive decrease of potentially unknown pixels and manifests the impact and importance of this step. It can be assumed that most of the spectral mixtures are excluded from the mask of unknown pixels except from those spectral mixtures that are unique (see Section 3.3). Further, a general slight increase of pixels detected as unknown can be observed with a rising dissimilarity threshold (Figure 5). Given a successful mixed pixel removal, it can be assumed that increasing dissimilarity thresholds integrate more spectral variability or instances of unknown materials.

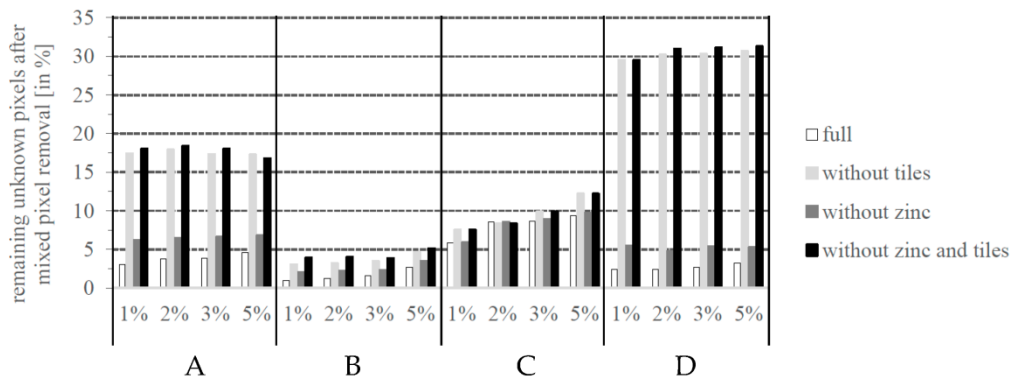


Fig. 5: Remaining unknown artificial pixels after single and border pixel removal.

3.3. Categorisation (Step 3)

Detected unknown pixels (Sections 2.3.3 and 3.2) are finally categorised based on spatial and spectral metrics to support subsequent labelling and integration into the BSL. This step also includes further revision regarding potentially remaining mixed pixels. In Figure 6 the functioning principle is shown in test site D for a spectral library setting without tiles and an applied dissimilarity threshold of 1%.

The mask of unknown artificial pixels (Figure 6a) shows homogeneous spatial clusters that correspond well with urban objects in the image data (Figure 6b). According to Section 2.3.3 clusters are re-organised in terms of spatial and spectral homogeneity (Figure 6c). Categorised clusters (unknown material classes) show a detailed separation and aggregation of distinct homogeneous urban objects (Figure 6c). The respective mean

reflectance spectra for each unknown material class are given in Figure 6d. Visual comparison of the mean reflectance spectra shows high similarity with mean spectra of roofing tiles in the validation data (Figure 3). However, visual comparisons of Figure 6a,c with the roofing tile classes of the validation data (Figure 3d) point out absent unknown mask pixels in the region of objects covered by red roofing tiles (Section 3.2). This accords with the known issue of spectral similarities between red roofing tiles and red loose chippings [37]. Accordingly, pixels representing red roofing tiles were not considered in the mask of potentially unknown pixels. In addition, five more unknown mean reflectance spectra (Figure 6d) do not correspond with the validation spectra. Visual inspection in combination with spectral expert knowledge revealed that amongst the identified roofing tile class spectral mixtures also remain (light green, dark green, yellow in Figure 6d). Their spatial appearance (Figure 6c) demonstrates that most of these spectra occur as single pixels without being attached to homogeneous clusters. Consequently, to ensure that only predominantly spectrally pure pixels are in the unknown material class, post-processing to remove the remaining mixed pixels from the mask of categorised pixels clusters was carried out. This results in three unknown material classes: the already identified unknown material class (roofing tiles), and two further unknown material classes (light and dark blue) that are displayed in Figure 6e. Corresponding mean reflectance spectra are given in Figure 6f. Despite the fact that the two remaining unknown material classes are characterised by a similar spectral shape, the main variations dominate the NIR and SWIR region in terms of amplitude differences, which is the decisive factor for separating the two classes. A visual inspection of the two unknown material classes with a very high-resolution image, e.g., image products from Google Earth, reveals that both classes feature solar panels. Although the BSL is an extensive collection of reference spectra, it so far lacks solar panels. First angular-dependent spectroscopic measurements (goniometer) have already shown that the spectral signature of solar panels is highly influenced by the observed azimuth. Consequently, a separation into two material classes is reasonable due either to a different construction type or to a varying inclination angle while acquiring spectral information. In addition to the detection of previously removed material classes (Section 2.4), two new unknown material classes identified as solar panels were found and confirm the efficiency of the method.

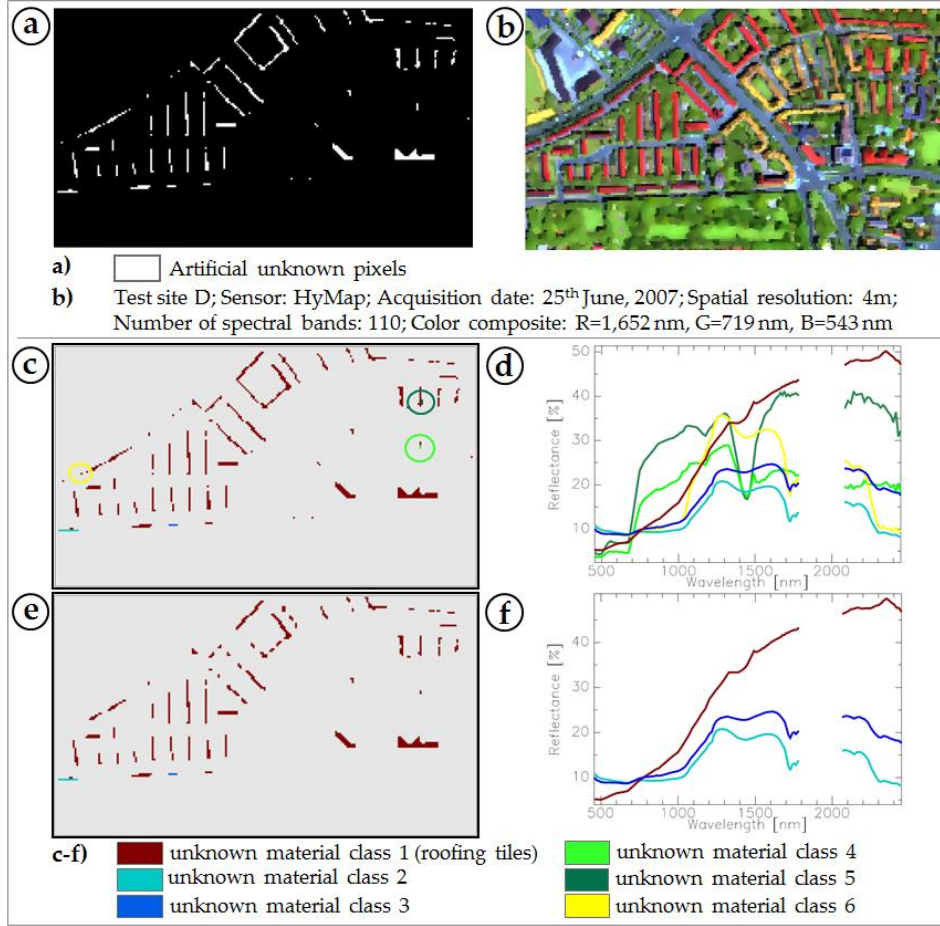


Fig. 6: Extraction of unknown artificial material classes from the (a) mask of unknown artificial pixels determined from the (b) image data of test site D with a BSL setting without roofing tiles and a dissimilarity threshold of 1%. Unknown artificial pixels are subject to (c) spatial and spectral clustering to identify spectral mixtures from (d) mean unknown class reflectance, accompanied by (e) post-processing to delete unknown material classes of remaining mixed pixels to result in an (f) scene-specific spectral library of unknown artificial material classes.

The sensitivity of the dissimilarity threshold regarding the number of detected and categorised unknown material classes is shown in Figure 7 for test site C. As described in Section 3.2, the increase in the dissimilarity threshold results in an increase in the mask of unknown pixels. Moreover, the number of spectrally homogeneous material classes and the number of pixels representing the classes both increase.

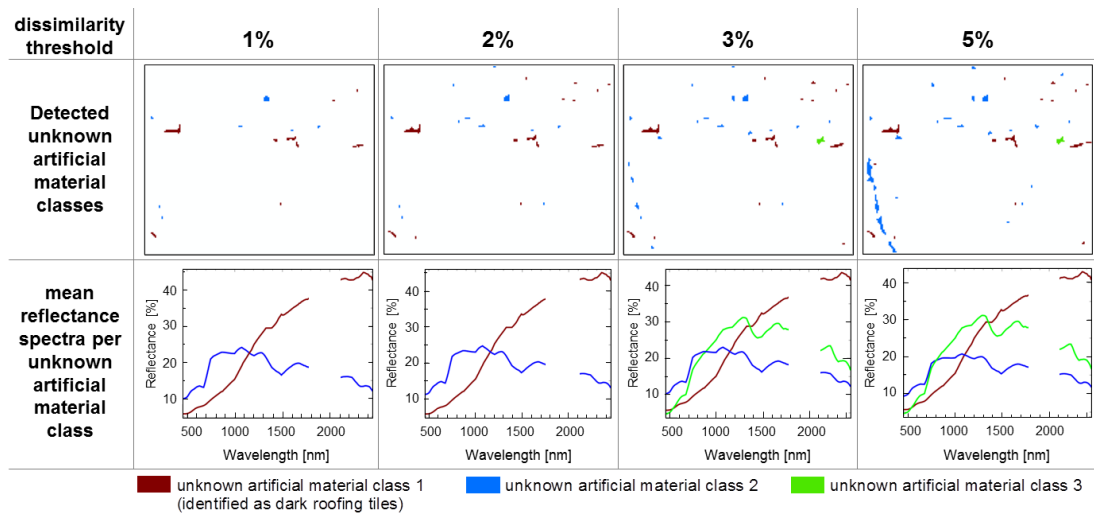


Fig. 7: Impact of an increasing dissimilarity threshold on the number of detected unknown artificial material classes elucidated for test site C with a BSL without tiles.

Visual inspection of the mean reflectance spectra and Google Earth images reveals that an unknown material class 1 (brown) could be identified as dark roofing tiles. Unknown material classes 2 (blue) and 3 (green) could be assigned as a greened roof (green) and parts of a partially greened tramline (blue). Both unknown material classes (green and blue) are not pure from a spectral point of view. The spectral signature of the greened roof is composed of photosynthetically active vegetation and the underlying substrate, whereas the tramline spectra results from a mixture of gravel, steel rails, and some vegetation fractions. Although the methods introduced in Sections 2.3.2 and 2.3.3 focus on removing mixed pixels, unknown mask pixels composed of spectral mixtures remain as long as they are spectrally unique and appear as large homogenous objects, such as large roofs or the track of a tramline. Also noticeable is the consistency of the spectral representation of the detected unknown material classes, which seems to be independent of the number of unknown material class pixels involved in the mean reflectance calculation.

3.4. Validation of Detected Roofing Tiles and Zinc Material Classes

The spectral and spatial representation of detected unknown materials that have been removed from the BSL (dark roofing tiles, zinc) are validated based on visual inspections and using reference data described in Section 2.5. Results of the quantitative accuracy assessment are summarised in Figure 8. The validation (Figure 8) is mainly based on a simple spatial match of pixels belonging to an unknown material class with validation

pixels of previously erased material classes. The mean spectra of the remaining unknown material class pixels were individually validated by visual comparisons (visual inspections) with the mean spectra of the respective validation class and by spectral expert knowledge. Accuracies determined by the two validation methods (match and visual inspection) are equally assessed. Consequently, the overall accuracy of detected unknown material class pixels is indicated by a combination of accuracies obtained from spatial match and visual inspection (Figure 8).

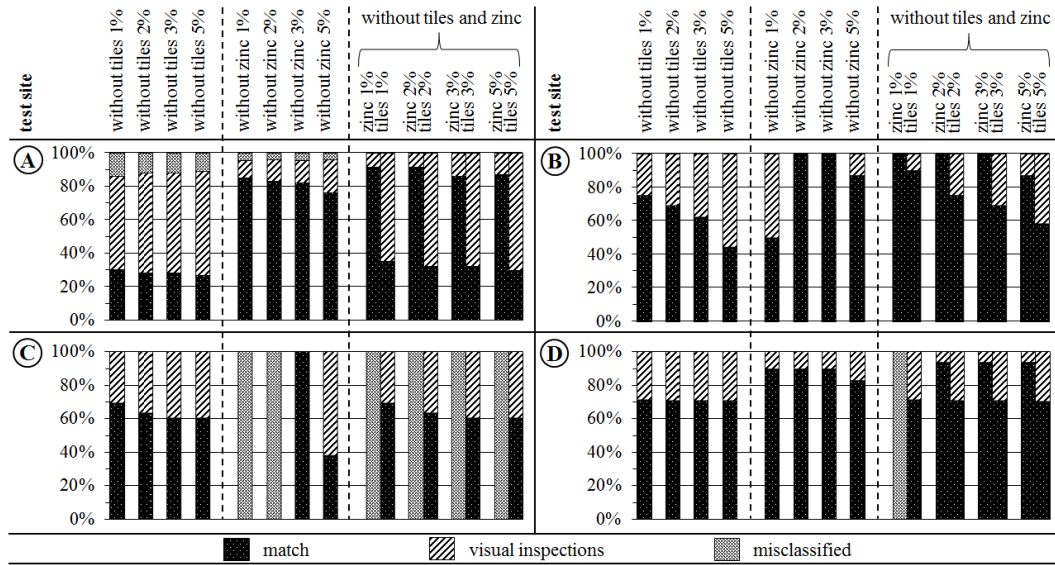


Fig. 8: Percentage of spatial agreement by validating all pixels of an unknown material class (columns) detected for different library setups in the four test sites (A-D). Validation results are composed of a spatial match (black) of unknown pixels with validation pixels of material classes zinc or dark roofing tiles, visual inspections (hatched) by visual comparisons of mean spectra due to missing validation data, and (grey) misclassifications or missing data for an unknown material class.

Generally, unknown material classes that were removed from the BSL could be re-detected as spatially and spectrally homogeneous pixel clusters. The agreement mainly varies with the test site and library setting. The number of misclassified unknown material classes is small except for test site C. Usually the match (black column) of the results with validation data slightly decreases with an increasing dissimilarity threshold. Hence, for determining the overall accuracy, the percentages of match and visual inspection need to be considered. A more precise inspection of Figure 8 demonstrates good (test site A) to very good matches (test sites B and D) for different library setups. However, in test site C zinc could not be detected by applying a dissimilarity threshold of 1% or 2%. Inspection of the results

reveals that zinc image spectra were spectrally not dissimilar enough to be added to the mask of potentially unknown pixels. In the pre-classification, urban objects covered by zinc are assigned to the material class aluminium. However, by increasing the dissimilarity threshold (3%, 5%) zinc was correctly detected.

Further, the results indicate that the more material classes missing in the spectral library, the more challenging their detection. Despite an increased level of library incompleteness, in general, the missing surface materials could be detected with the exception of test site C. Simultaneously, an increased level of library incompleteness results in less spectral variation per unknown material class because of the fixed percentage of image pixels that are flagged as unknown (dissimilarity threshold). Additionally, the detection of unknown material classes is also influenced by the number of pixels per material class in the test site image and the level of dissimilarity among distinct unknown classes. Underrepresented unknown material classes are not considered as potentially unknown if spectra of another unknown class are more dissimilar and the percentage amount (dissimilarity threshold) of dissimilar spectra is reached.

4. Discussion

Functioning, benefits, and drawbacks of spectral dissimilarity analysis (Section 2.3) are discussed in the following. The above results have confirmed the functioning of re-detection of previously removed material classes (Sections 3.3 and 3.4). Completely new surface materials (solar panels and tram rail tracks) could be detected and identified as discrete classes (Section 3.3). The developed methodology was extensively tested on four test sites with different settings for the BSL and varying dissimilarity thresholds (Section 2.4).

The findings reported in Sections 3.1 and 3.2 demonstrate the importance of the applied similarity measure SID-SCA. This measure is essential for the steps of pre-classifying the image, determining dissimilar pixel spectra for building a mask of potentially unknown pixels, and enhancing the potentially unknown pixel mask by means of a second similarity analysis. Pre-classification results are very promising as to the separation of natural and artificial pixels (Table 3). However, a detailed material-based accuracy assessment (Section 3.1) reveals the limits of the SID-SCA approach. Spectral confusion of different materials was observed, such as between zinc and aluminium. Both materials are

characterised by distinct broad absorption features, but their absorption maxima differ only slightly, by about 140 nm (Section 3.4). Based on SID-SCA, zinc pixels (test site C) are too similar to the aluminium class and thus are not added to the mask of potentially unknown pixels. Another example reveals the importance of considering amplitude as a spectral feature. Besides spectral absorption features, amplitude is the dominant spectral feature for differentiating asphalt and concrete. Previous studies [37,63] have already reported the importance of spectral features, the shape of a spectrum, and the amplitude for identifying urban surfaces. In [58] a hybrid similarity measure that fuses shape and amplitude features (Fusing SAF) was developed. The application of this measure (Fusing SAF) could provide enhanced results for material mapping of spectrally similar shaped material classes in urban areas. However, both cases of spectral confusion do not affect the aim of the important pre-classification step itself, since the confusion appears within the same material group (artificial or natural).

The pre-classification results are the basis for the subsequent extraction of potentially unknown predominantly pure pixels. The number of extracted potentially unknown pixels using a fixed dissimilarity threshold is increased by converting the dissimilarity threshold to a scene-based threshold and applying a second similarity analysis (Sections 2.3.2 and 3.3, Figure 4). This way, the fixed dissimilarity threshold is adapted to the characteristics of the image data used. In general, it was found that the number of potentially unknown pixels increases with an increasing dissimilarity threshold (Section 2.4). Findings from Section 3.2 indicate that unknown material spectra are already detectable with a dissimilarity threshold of 1%. A further increase in the dissimilarity threshold is typically associated with the formation of larger spatial clusters and usually results in more spectral variations of unknown material classes. Consequently, a larger dissimilarity threshold can be useful for a more incomplete spectral library. However, an increasing dissimilarity threshold is frequently associated with an increase in the number of finally remaining spectral mixtures (Section 3.2), which needs to be considered. On the other hand, spectral mixtures that build large spatial clusters such as vegetated roofs or tram rail tracks remain, despite the mixed pixel removal steps which are generally based on spatial constraints (single pixels, object border pixel).

The number of mixed pixels also correlates with the size of the urban objects and the associated GSD of the image. In this study, airborne imaging spectroscopy data with a GSD of about 4 m were used. By analysing different test sites characterised by different object sizes, we could observe how the performance of the approach declines for test site

C, which contains the smallest urban objects and thus fewer pure, surface material spectra. However, except for test site C, mixed pixel removal was successful. An additional test concerning the spectral purity of detected unknown surfaces, e.g., using iterative endmember selection [64] would be an important task for future studies. With the presented methodology, it will be up to the user to decide whether a predominantly pure material has been identified, or not.

5. Conclusions and Outlook

Image-specific urban spectral libraries are widely and successfully used in urban imaging spectroscopy studies. In this paper, a methodology is presented that can handle the incompleteness of spectral libraries. The proposed spectral dissimilarity analysis was developed to (1) detect image-specific unknown urban surface materials while (2) avoiding spectral mixtures, and to (3) categorise detected unknown surface materials, e.g., to support a material specific identification. The fundamental approach is based on the assumption that unknown surface materials are dissimilar to known spectra provided in the BSL. Dissimilar image spectra are extracted by means of a scene-based threshold applied on previously determined spectral similarity values resulting from SID-SCA analysis. Potentially unknown image spectra are separated from mixed pixels by spatial and spectral metrics. In a final step, the remaining dissimilar image spectra are categorised to build spectrally homogeneous material clusters.

The efficiency of the approach is demonstrated by applying it to different test sites, distinct dissimilarity thresholds, and to different cases of an incomplete spectral library. The incompleteness is simulated by removing material classes from an initial spectral library (BSL) with the aim to detect these classes again as unknown scene-based surface materials. In nearly all cases, the results indicate the successful re-detection of unknown surface materials using spectral dissimilarity analysis. Limitations are associated with the degree of incompleteness. It is shown that with a higher incompleteness of the BSL, unknown material classes are more reliably detected with a higher dissimilarity threshold. Beside the increase of spectral variabilities of detected unknown material classes, an increasing dissimilarity threshold is also associated with a gain in the number of remaining mixed pixels. It can be concluded that the dissimilarity threshold needs to be precisely adjusted based on the level of incompleteness of the BSL in order to detect unknown materials or

material instances, and to keep the number of remaining spectral mixtures down. Finally, it will be up to the user to find a trade-off between high spectral variability and a low number of remaining mixed pixels. However, even a small set of representative unknown predominantly pure pixels can be useful for applying any subsequent image analysis techniques. As an example, in [42] rare spectral representatives, seedlings, are used to further enhance the endmember set for area wide surface material identification in urban areas.

The suitability of the presented methodology is further underlined by the detection and identification of unique material classes such as solar panels, which were identified as a completely new surface material with respect to the BSL. Comparing the material classes represented in the initial BSL with other urban spectral libraries [34,35], it can be assumed that the application of this BSL to cities in the USA and Great Britain could be promising. However, it needs to be tested for other geographical regions, where more unknown surface materials can be expected. Another important aspect that should be addressed in future research on the applicability of the method is the GSD of the imaging spectroscopy data needed to obtain pure representatives of all surface materials of interest.

The high number of different surface materials and respective variations in urban areas hampers the use of spectral libraries and the transferability of library-based technologies for untested geographic regions. The developed methodology is a first step toward overcoming this limitation. It can be used to create image-specific training databases and it can also serve as a technology for enlarging urban spectral libraries to make possible their widespread utilisation. In the future, the technique will be enhanced in order to test the spectral purity of the unknown material classes and also to identify all spectrally pure surface materials in a high resolution imaging spectroscopy data set of an urban area.

Acknowledgments: This work was supported by the German Aerospace Center (DLR)—Project Management Agency and the Ministry of Economics and Technology (BMW), Germany, as part of the EnFusionMAP project (50 EE 1343). We thank Derek Rogge for his support with English editing.

Author Contributions: Marianne Jilge is the corresponding author who developed the concept, implemented and approved the methodology, performed the experiments, and wrote the paper. Uta Heiden defined the principle concept, initiated the research, and assisted in writing the paper. Martin Habermeyer helped with the programming to implement the idea. André Mende carried out first feasibility tests of the principle idea. Carsten Juergens reviewed the manuscript and gave advice concerning the principle concept.

References

1. Schaepman, M.E.; Ustin, S.L.; Plaza, A.J.; Painter, T.H.; Verrelst, J.; Liang, S. Earth system science related imaging spectroscopy—An assessment. *Remote Sens. Environ.* **2009**, *113*, S123–S137.
2. Aplin, P.; Atkinson, P.M.; Curran, P.J. Fine spatial resolution simulated satellite sensor imagery for land cover mapping in the United Kingdom. *Remote Sens. Environ.* **1999**, *68*, 206–216.
3. Herold, M.; Gardner, M.E.; Roberts, D.A. Spectral resolution requirements for mapping urban areas. *IEEE Trans. Geosci. Remote Sens.* **2003**, *41*, 1907–1919.
4. Van der Linden, S.; Hostert, P. The influence of urban surface structures on the accuracy of impervious area maps from airborne hyperspectral data. *Remote Sens. Environ.* **2009**, *113*, 2298–2305.
5. Behling, R.; Bochow, M.; Foerster, S.; Roessner, S.; Kaufmann, H. Automated GIS-based derivation of urbanecological indicators using hyperspectral remote sensing and height information. *Ecol. Indic.* **2015**, *48*, 218–234.
6. Lakes, T.; Kim, H.O. The urban environmental indicator “Biotope Area Ratio”—An enhanced approach to assess and manage the urban ecosystem services using high resolution remote-sensing. *Ecol. Indic.* **2012**, *13*, 93–103.
7. Ampe, E.M.; Vanhamel, I.; Salvatore, E.; Dams, J.; Bashir, I.; Demarchi, L.; Chan, J.C.-W.; Sahli, H.; Canters, F.; Batelaan, O. Impact of Urban Land-Cover Classification on Groundwater Recharge Uncertainty. *IEEE J. Sel. Top. Appl. Earth Obs. Remote Sens.* **2012**, *5*.
8. Wirion, C.; Bauwens, W.; Verbeiren, B. High resolution modeling of the urban hydrological response. In Proceedings of the 2017 Joint Urban Remote Sensing Event (JURSE), Dubai, UAE, 6–8 March 2017.
9. Alonzo, M.; McFadden, J.P.; Nowak, D.J.; Roberts, D.A. Mapping urban forest structure and function using hyperspectral imagery and lidar data. *Urban For. Urban Green.* **2016**, *17*, 135–147.
10. Laćan, I.; McBride, J.R. Pest Vulnerability Matrix (PVM): A graphic model for assessing the interaction between tree species diversity and urban forest susceptibility to insects and diseases. *Urban For. Urban Green.* **2008**, *7*, 291–300.
11. Heldens, W.; Heiden, U.; Esch, T.; Mueller, A.; Dech, S. Integration of remote sensing based surface information into a three-dimensional microclimate model. *ISPRS J. Photogramm. Remote Sens.* **2017**, *125*, 106–124.
12. He, T.; Liang, S.; Wang, D.; Shi, Q.; Goulden, M.L. Estimation of high-resolution land surface net shortwave radiation from AVIRIS data: Algorithm development and preliminary results. *Remote Sens. Environ.* **2015**, *167*, 20–30.
13. Liu, K.; Su, H.; Li, X. Estimating high-resolution urban surface temperature using a hyperspectral thermal mixing (HTM) approach. *IEEE J. Select. Top. Appl. Earth Obs. Remote Sens.* **2016**, *9*, 804–815.
14. Oltra-Carrió, R.; Sobrino, J.A.; Franch, B.; Nerry, F. Land surface emissivity retrieval from airborne sensor over urban areas. *Remote Sens. Environ.* **2012**, *123*, 298–305.
15. Sobrino, J.A.; Oltra-Carrió, R.; Sòria, G.; Bianchi, R.; Paganini, M. Impact of spatial resolution and satellite overpass time on evaluation of the surface urban heat island effects. *Remote Sens. Environ.* **2012**, *117*, 50–56.
16. Sobrino, J.A.; Oltra-Carrió, R.; Jiménez-Muñoz, J.C.; Julien, Y.; Sòria, G.; Franch, B.; Mattar, C. Emissivity mapping over urban areas using a classification-based approach: Application to the Dual-use European Security IR Experiment (DESIREX). *Int. J. Appl. Earth Obs. Geoinfor.* **2012**, *18*, 141–147.
17. Bateson, C.A.; Asner, G.P.; Wessman, C.A. Endmember bundles: A new approach to incorporating endmember variability into spectral mixture analysis. *IEEE Trans. Geosci. Remote Sens.* **2000**, *38*, 1083–1094.

18. Plaza, A.; Martínez, P.; Pérez, R.; Plaza, J. A quantitative and comparative analysis of endmember extraction algorithms from hyperspectral data. *IEEE Trans. Geosci. Remote Sens.* **2004**, *42*, 650–663.
19. Somers, B.; Asner, G.P.; Tits, L.; Coppin, P. Endmember variability in spectral mixture analysis: A review. *Remote Sens. Environ.* **2011**, *115*, 1603–1616.
20. Franke, J.; Roberts, D.A.; Halligan, K.; Menz, G. Hierarchical Multiple Endmember Spectral Mixture Analysis (MESMA) of Hyperspectral Imagery for Urban Environments. *Remote Sens. Environ.* **2009**, *113*, 1712–1723.
21. Theseira, M.A.; Thomas, G.; Taylor, J.C.; Gemmell, F.; Varjo, J. Sensitivity of mixture modelling to endmember selection. *Int. J. Remote Sens.* **2003**, *24*, 1559–1575.
22. Clark, R.N.; Swayze, G.A.; Livo, K.E.; Kokaly, R.F.; Sutley, S.J.; Dalton, J.B.; McDougal, R.R.; Gent, C.A. Imaging spectroscopy: Earth and planetary remote sensing with the USGS Tetracorder and expert systems. *J. Geophys. Res. Planets* **2003**, *108*.
23. Van der Linden, S.; Janz, A.; Waske, B.; Eiden, M.; Hostert, P. Classifying segmented hyperspectral data from a heterogeneous urban environment. *J. Appl. Remote Sens.* **2007**, *1*.
24. Plaza, A.; Benediktsson, J.A.; Boardman, J.W.; Brazile, J.; Bruzzone, L.; Camps-Valls, G.; Chanussot, J.; Fauvel, M.; Gamba, P.; Gualtieri, A.; et al. Recent advances in techniques for hyperspectral image processing. *Remote Sens. Environ.* **2009**, *113*, S110–S122.
25. Okujeni, A.; Van der Linden, S.; Suess, S.; Hostert, P. Ensemble Learning from synthetically mixed training data for quantifying urban land cover with support vector regression. *IEEE J. Sel. Top. Appl. Earth Obs. Remote Sens.* **2017**, *10*, 1640–1650.
26. Song, C.H. Spectral mixture analysis for subpixel vegetation fractions in the urban environment: How to incorporate endmember variability? *Remote Sens. Environ.* **2005**, *95*, 248–263.
27. Small, C. Estimation of urban vegetation abundance by spectral mixture analysis. *Int. J. Remote Sens.* **2001**, *22*, 1305–1334.
28. Small, C. A global analysis of urban reflectance. *Int. J. Remote Sens.* **2005**, *26*, 661–681.
29. Thompson, D.R.; Boardman, J.W.; Eastwood, M.L.; Green, R.O. A large airborne survey of Earth's visible-infrared spectral dimensionality. *Opt. Express* **2017**, *25*, 9186–9195.
30. Boardman, J.W.; Kruse, F.A.; Green, R.O. Mapping target signatures via partial unmixing of AVIRIS data. In Proceedings of the Fifth JPL Airborne Earth Science Workshop, Pasadena, CA, USA, 23–26 January 1995. Available online: <https://ntrs.nasa.gov/search.jsp?R=19950027368> (accessed on 24 May 2017).
31. Craig, M.D. Minimum Volume Transforms for Remotely Sensed Data. *IEEE Trans. Geosci. Remote Sens.* **1994**, *32*, 542–552.
32. Rogge, D.; Bachmann, M.; Rivard, B.; Feng, J. Spatial Sub-Sampling using local endmembers for adapting OSP and SSEE for Large-Scale Hyperspectral Surveys. *IEEE J. Sel. Top. Appl. Earth Obs. Remote Sens.* **2011**, *5*, 183–195.
33. Clark, R.N.; Swayze, G.A.; Wise, R.; Livo, E.; Hoefen, T.; Kokaly, S.J.; Sutley, R. USGS Digital Spectral Library splib06a. U.S. Geological Survey, 2007, Digital Data Series 231. Available online: <http://speclab.cr.usgs.gov/spectral.lib06/> (accessed on 29 May 2017).
34. Kotthaus, S.; Smith, T.E.L.; Wooster, M.J.; Grimmond, C.S.B. Derivation of an urban materials spectral library through emittance and reflectance spectroscopy. *ISPRS J. Photogramm. Remote Sens.* **2014**, *94*, 194–212.
35. Herold, M.; Roberts, D.A.; Gardner, M.E.; Dennison, P.E. Spectrometry for urban area remote sensing—Development and analysis of a spectral library from 350 to 2400 nm. *Remote Sens. Environ.* **2004**, *91*, 304–319.

36. Ben-Dor, E.; Levin, N.; Saaroni, H. A spectral based recognition of the urban environment using the visible and near-infrared spectral region (0.4–1.1 μm). A case study over Tel-Aviv, Israel. *Int. J. Remote Sens.* **2001**, *22*, 2193–2218.
37. Heiden, U.; Segl, K.; Roessner, S.; Kaufmann, H. Determination of robust spectral features for identification of urban surface materials in hyperspectral remote sensing data. *Remote Sens. Environ.* **2007**, *111*, 537–552.
38. Okujeni, A.; Van der Linden, S.; Tits, L.; Somers, B.; Hostert, P. Support vector regression and synthetically mixed training data for quantifying urban land cover. *Remote Sens. Environ.* **2013**, *137*, 184–197.
39. Wetherley, E.B.; Roberts, D.A.; McFadden, J.P. Mapping spectrally similar urban materials at sub-pixel scales. *Remote Sens. Environ.* **2017**, *195*, 170–183.
40. Priem, F.; Canters, F. Synergistic Use of LiDAR and APEX Hyperspectral Data for High-Resolution Urban Land Cover Mapping. *Remote Sens.* **2016**, *8*, 787.
41. Heiden, U.; Heldens, W.; Roessner, S.; Segl, K.; Esch, T.; Mueller, A. Urban structure type characterization using hyperspectral remote sensing and height information. *Landsc. Urban Plan.* **2012**, *105*, 361–375.
42. Roessner, S.; Segl, K.; Heiden, U.; Kaufmann, H. Automated differentiation of urban surfaces based on airborne hyperspectral imagery. *IEEE Trans. Geosci. Remote Sens.* **2001**, *39*, 1525–1532.
43. Herold, M.; Roberts, D.A. Spectral characteristics of asphalt road aging and deterioration: Implications for remote-sensing applications. *Appl. Opt.* **2005**, *44*, 4327–4334.
44. Lacherade, S.; Miesch, C.; Briottet, X.; Le Men, H. Spectral variability and bidirectional reflectance behavior of urban materials at a 20 cm spatial resolution in the visible and near-infrared wavelength. A case study over Toulouse (France). *Int. J. Remote Sens.* **2005**, *26*, 3859–3866.
45. Cocks, T.; Jenssen, A.; Stewart, A.; Wilson, I.; Shields, T. The HyMap airborne hyperspectral sensor: The system, calibration and performance. In Proceedings of the 1st EARSel Workshop on Imaging Spectroscopy, Zurich, Switzerland, 6–8 October 1998; pp. 1–6.
46. Richter, R. *ATCOR 4 User Guide*; DLR-German Aerospace Centre, Remote Sensing Data Centre: Oberpfaffenhofen, Germany, 2009.
47. Mueller, R.; Lehner, M.; Reinartz, P.; Schroeder, M. Evaluation of Spaceborne and Airborne Line Scanner Images using a Generic Ortho Image Processor. In Proceedings of the 2005 ISPRS High Resolution Earth Imaging for Geospatial Information, Hannover, Germany, 17–20 May 2005; Volume XXXVI.
48. Habermeyer, M.; Marschall, U.; Roth, A. Digital elevation model database W42-A scalable system for spatial data. In Proceedings of the ISPRS Conference, International Archives of the Photogrammetry, Remote Sensing and Spatial Information Sciences, Beijing, China, 3–11 July 2008; pp. 1253–1258.
49. Rogge, D.; Rivard, B. Iterative spatial filtering for reducing intra-class spectral variability and noise. In Proceedings of the 2nd Workshop on hyperspectral image and signal processing: Evolution in remote sensing (WHISPERS), REXKJAVIK, Iceland, 14–16 June 2010.
50. Kruse, F.A.; Lefkoff, A.B.; Boardman, J.W.; Heidebrecht, K.B.; Shapiro, A.T.; Barloon, P.J.; Goetz, A.F.H. The spectral image processing system (SIPS)—Interactive visualization and analysis of imaging spectrometer Data. *Remote Sens. Environ.* **1993**, *44*, 145–163.
51. Chang, C.I. An information theoretic-based approach to spectral variability, similarity and discriminability for hyperspectral image analysis. *IEEE Trans. Inf. Theory* **2000**, *46*, 1927–1932.
52. Bajwa, S.G.; Bajcsy, P.; Groves, P.; Tian, L.F. Hyperspectral image data mining for band selection in agricultural application. *Trans. ASAE* **2004**, *43*, 895–907.

53. Van der Meer, F.; Bakker, W. CCSM: Cross correlogram spectral matching. *Int. J. Remote Sens.* **1997**, *18*, 1197–1201.
54. Padma, S.; Sanjeevi, S. Jeffries Matusita based mixed-measure for improved spectral matching in hyperspectral image analysis. *Int. J. Appl. Earth Obs. Geoinf.* **2014**, *32*, 138–151.
55. Naresh Kumar, M.; Seshasai, M.V.R.; Vara Prasad, K.S.; Kamala, V.; Ramana, K.V.; Dwivedi, R.S.; Roy, P.S. A hybrid spectral similarity measure for discrimination among *Vigna* species. *Int. J. Remote Sens.* **2011**, *32*, 4041–4053.
56. Du, Y.; Chang, C.I.; Ren, H.; Chang, C.C.; Jensen, J.O.; D'Amico, F.M. New hyperspectral discrimination measure for spectral characterization. *Opt. Eng.* **2004**, *43*, 1777–1786.
57. Van der Meer, F. The effectiveness of spectral similarity measures for analysis of hyperspectral imagery. *Int. J. Appl. Earth Obs. Geoinf.* **2006**, *8*, 3–17.
58. Ding, J.G.; Li, X.B.; Huang, L.Q. A novel method for spectral similarity measure by fusing shape and amplitude features. *J. Eng. Sci. Technol. Rev.* **2015**, *8*, 172–179.
59. Mende, A.; Heiden, U.; Bachmann, M.; Hoja, D.; Buchroithner, M. Development of a new spectral library classifier for airborne hyperspectral images on heterogeneous environments. In Proceedings of the EARSeL 7th SIG-Imaging Spectroscopy Workshop, Edinburgh, UK, 11–13 April 2011. Available online: <http://elib.dlr.de/72268/> (accessed on 23 May 2017).
60. Toffoli, T.; Margolus, N. *Cellular Automata Machines: A New Environment for Modeling*; MIT Press: Cambridge, MA, USA, 1987; ISBN 0-262-20060-0.
61. Cohen, J. A coefficient of agreement for nominal scales. *Educ. Psychol. Meas.* **1960**, *20*, 37–46.
62. Kurz, F.; Mueller, R.; Stephani, M.; Reinartz, P.; Schroeder, M. Calibration of a wide-angle digital camera system for near real time scenarios. In Proceedings of the ISPRS Hannover Workshop 2007-High Resolution Earth Imaging for Geospatial Information, Hannover, Germany, 29 May–1 June 2007; ISSN 1682-1777.
63. Jilge, M.; Heiden, U.; Habermeyer, M.; Mende, A.; Juergens, C. Identifying pure urban image spectra using a learning urban image spectral archive (LUISA). In Proceedings of the SPIE 10008, Remote Sensing Technologies and Applications in Urban Environments, 100080J, Edinburgh, UK, 26–29 September 2016.
64. Schaaf, A.N.; Dennison, P.E.; Fryer, G.K.; Roth, K.L.; Roberts, D.A. Mapping plant functional types at multiple spatial resolutions using imaging spectrometer data. *GISci. Remote Sens.* **2011**, *48*, 324–344.



© 2017 by the authors. Submitted for possible open access publication under the terms and conditions of the Creative Commons Attribution (CC BY) license (<http://creativecommons.org/licenses/by/4.0/>).

CHAPTER IV

Gradients in urban material composition: A new concept to map cities with spaceborne imaging spectroscopy data

Remote Sensing of Environment, 223(2019), 179-193

Marianne Jilge, Uta Heiden, Carsten Neumann and
Hannes Feilhauer

© 2019 The Authors. Published by Elsevier Inc. under the CC BY-NC-ND license (open access).

doi: 10.1016/j.rse.2019.01.007

Received 5 June 2018; revised 12 December 2018; accepted 8 January 2019.

Abstract

To understand processes in urban environments, such as urban energy fluxes or surface temperature patterns, it is important to map urban surface materials. Airborne imaging spectroscopy data have been successfully used to identify urban surface materials mainly based on unmixing algorithms. Upcoming spaceborne Imaging Spectrometers (IS), such as the Environmental Mapping and Analysis Program (EnMAP), will reduce the time and cost-critical limitations of airborne systems for Earth Observation (EO). However, the spatial resolution of all operated and planned IS in space will not be higher than 20 to 30 m and, thus, the detection of pure Endmember (EM) candidates in urban areas, a requirement for spectral unmixing, is very limited. Gradient analysis could be an alternative method for retrieving urban surface material compositions in pixels from spaceborne IS. The gradient concept is well known in ecology to identify plant species assemblages formed by similar environmental conditions but has never been tested for urban materials. However, urban areas also contain neighbourhoods with similar physical, compositional and structural characteristics. Based on this assumption, this study investigated (1) whether cover fractions of surface materials change gradually in urban areas and (2) whether these gradients can be adequately mapped and interpreted using imaging spectroscopy data (e.g. EnMAP) with 30 m spatial resolution.

Similarities of material compositions were analysed on the basis of 153 systematically distributed samples on a detailed surface material map using Detrended Correspondence Analysis (DCA). Determined gradient scores for the first two gradients were regressed against the corresponding mean reflectance of simulated EnMAP spectra using Partial Least Square regression models. Results show strong correlations with $R^2=0.85$ and $R^2=0.71$ and an RMSE of 0.24 and 0.21 for the first and second axis, respectively. The subsequent mapping of the first gradient reveals patterns that correspond to the transition from predominantly vegetation classes to the dominance of artificial materials. Patterns resulting from the second gradient are associated with surface material compositions that are related to finer structural differences in urban structures. The composite gradient map shows patterns of common surface material compositions that can be related to urban land use classes such as Urban Structure Types (UST). By linking the knowledge of typical material compositions with urban structures, gradient analysis seems to be a powerful tool to map characteristic material compositions in 30 m imaging spectroscopy data of urban areas.

Keywords: EnMAP, Gradient analysis, Imaging spectroscopy, Urban, Surface materials

1. Introduction

More than 54% of the world's population is currently residing in cities. This percentage will continue to increase in the future (UN, 2014), leading to an urgent and growing demand for detailed and spatially explicit information about urban areas. Chen et al. (2012) discuss the detailed information of surface materials needed for urban weather and climate modelling and specify the requirements to better describe urban canopy models. These models are based on information about the spatial configuration of urban areas and about the surface materials of urban objects that drive surface-atmosphere exchange processes (e.g. Shashua-Bar et al., 2004; Taleghani et al., 2015; Bruse and Fler, 1998). Knowledge gained from such model simulations can be used to measure and understand the impacts of climate change on urban areas. Since these impacts affect the urban population locally (Grimm et al., 2008), urban planning focuses on the transformation of cities in response to the changing climate and to develop adaptation responses in advance (Carter et al., 2015).

A wide range of airborne and spaceborne Earth Observation missions have previously been used to study details of urban structures (Voltersen et al., 2014; Cai et al., 2017), urban growth (Esch et al., 2017; Pesaresi et al., 2016; Bagan and Yamagata, 2012; Herold et al., 2003) and ecological functions of urban areas (Lakes and Kim, 2012; Alberti, 2005; Alonzo et al., 2016). With the wider availability of airborne imaging spectrometers, studies have been expanded to map and quantify surface material composition in urban areas (Roessner et al., 2001; Heiden et al., 2007; Heiden et al., 2012; Okujeni et al., 2013; Priem and Canters, 2016; Segl et al., 2003; Franke et al., 2009; Demarchi et al., 2014). The main advantage of using imaging spectroscopy data is the rich spectral information content that enables a detailed surface material inventory.

However, airborne imaging spectroscopy data have limited availability and are cost-intensive and, thus, not applicable for frequent monitoring of cities. These limitations can be overcome with spaceborne imaging spectrometers, although studies are still rare due to the limited availability of sensor data. There are a few urban studies using spaceborne imaging spectroscopy data from former and operating sensors, such as Hyperion on EO-1 (Cavalli et al., 2008; Fan and Deng, 2014; Weng and Lu, 2008; Weng et al., 2008; Xu and Gong, 2007; Zhang, 2016) and CHRIS on the PROBA platform (Demarchi et al., 2012a; Demarchi et al., 2012b; Duca and Del Frate, 2008; Licciardi and Del Frate, 2011). Data from Chinese platforms such as the HJ-1A and TG-1 (Tong et al., 2014; Guo et al., 2016)

and the Russian Resurs-P fleet (Zaichko 2014) are also promising but currently not available to the public. There are several spaceborne imaging spectrometer missions planned for the near future such as PRISMA (Guarini et al., 2017), DESIS (Mueller et al., 2017), EnMAP (Guanter et al., 2015), HypIRI (Abrams and Hook, 2013) and HISUI (Matsunaga et al., 2014). These upcoming missions could provide data on a regular and operational basis suitable for monitoring urban functionalities.

To explore the full potential of spaceborne imaging spectrometer data in urban environments, simulated imagery has been used (e.g. Roberts et al., 2012; Okujeni et al., 2015; Rosentreter et al., 2017). These studies focus on adapting and improving mapping methods, where the majority of mapping concepts and techniques has to cope with the high spectral information content and the complex spectral mixtures (Small, 2003) that occur in the image data due to diverse material compositions and structures in the urban environment. A variety of linear and non-linear Spectral Mixture Analyses (SMA) have been developed (Shimabukuro and Smith, 1991; Keshava, 2003; Adams and Gillespie, 2006), all of which estimate abundances of surface materials within a pixel, provided that all occurring surface materials, so-called Endmembers (EM) are known (Adams et al., 1986). This concept was successfully applied to airborne imaging spectroscopy data for various environments (Adams and Smith, 1986; Asner and Lobell, 2000; Okin et al., 2001; Asner and Heidebrecht, 2002; Neville et al., 2003; Roth et al., 2012; Roberts et al., 2017). However, uncertainty in abundance estimation increases with the number of EMs in a mixing model (Winter et al., 2003). Therefore, concepts such as Multiple Endmember Spectral Mixture Analysis (MESMA) (Roberts et al., 1998) have been developed, which allows the number of EMs per pixel to be varied and optimized (e.g. Dennison and Roberts, 2003). Further, mathematical and spatial constraints have been introduced (e.g. Dennison and Roberts, 2003; Roessner et al., 2001; Rogge et al., 2006; Franke et al., 2009) to reduce the number of EMs per pixel (Zare and Ho, 2013), rather than considering all EMs occurring in a scene for generating the per-pixel mixture model. The EM variability and its influence on spectral mixture analysis have been discussed in Somers et al. (2011). The applicability of spectral unmixing approaches for identifying surface materials using present and upcoming spaceborne imaging spectrometer systems is limited. The spatial resolution of most of these systems ranges between 20 m and 30 m. Consequently, the number of EMs per pixel usually increases and the complexity of spectral mixtures in urban areas can hardly be explained by models containing just a few EMs. Further, it is challenging to find spectrally pure EMs, which is a requirement for SMA. The latter

problem was tackled by a concept developed by [Okujeni et al. \(2013\)](#) that uses synthetically mixed urban spectra applied to simulated EnMAP data of Berlin ([Okujeni et al., 2015](#)) using support vector regression. Sub-pixel abundances of surface categories such as roofs, pavement, low vegetation and trees could be estimated with higher accuracies in comparison to spaceborne multispectral data ([Okujeni et al., 2015](#)). However, the majority of detailed surface material related information is lost in this generalization because the mixed spectra cannot be deconvolved at this high thematic level. Improvements in mapping the broad vegetation, imperviousness and soil classes ([Ridd, 1995](#)) or extended VIS (vegetation-impervious-soil) classes (e.g. [Weng, 2008](#); [Okujeni et al., 2015](#)) could be achieved by using spaceborne imaging spectroscopy data instead of multispectral imagery with the same spatial resolution.

By changing the perspective from Earth Observation (EO) images to the ground, it becomes obvious that even highly heterogeneous landscapes such as urban environments contain urban neighbourhoods with similar structural and compositional characteristics ([Tobler, 1970](#)). Often, these physical characteristics are a result of the specific land use. Industrial areas serve as an extreme example. They are often composed of large low-rise to mid-rise buildings and mainly impervious open surfaces. In contrast to industrial sites, residential areas such as detached housing developments are composed of small low-rise buildings, pervious surfaces such as gardens and exposed soils. This obvious link between land cover and land use is reflected in various urban classification systems such as the German Urban Structure Type (UST) classification ([Wittig et al., 1998](#), [Gilbert, 1994](#); [Maier et al., 1996](#)) that was established by urban ecologists to study urban biota. It describes urban areas as an ecosystem with biotic and abiotic components, whereby the ecosystem is formed by its history, structure and function ([Sukopp and Weiler, 1988](#); [Wittig et al., 1998](#); [Niemela, 1999](#)). The well-known Urban Atlas (UA) nomenclature ([EEA, 2017](#)) is built by merging CORINE and the GMES Urban Services to compare the development and structure of European cities. The UA classes mainly describe land use, which cannot easily be related to physical parameters such as those required by urban climatologists ([Lefebvre, 2015](#)). Therefore, [Stewart and Oke \(2012\)](#) developed the Local Climate Zone (LCZ) framework. This framework explicitly considers the physical characteristics of urban areas, such as building height and compactness, vegetation abundance, and surface material characteristics, to serve as input for urban climate models. However, this framework is also subject to land use terms, as the class LCZ 10 “Heavy

industry” shows, but it reveals the link between an area’s land use and its resulting land cover parameters.

In summary, all of these classification frameworks have in common that they postulate the existence of urban neighbourhoods with similar physical, compositional, structural or land use characteristics or a mixture of it. Urban neighbourhoods are hence also composed of specific surface material compositions and these compositions are represented by typical spectral mixtures in spaceborne imaging spectroscopy data. The existence of such neighbourhood-specific mixtures of surface materials have been investigated by statistical analyses of roofing materials and their occurrence in UST classes in Munich, Germany (Heiden et al., 2003; 2012; Heldens 2010). Bochow et al. (2007) successfully used the composition of surface materials, in addition to structural and form parameters, as a proxy for updating urban biotope maps in Dresden, Germany. Finally, Earth Observation based concepts of Vegetation-Imperviousness-Soil (VIS; Ridd, 1995) and extended VIS studies could show even at a very coarse spatial scale that there are areas dominated by high albedo surfaces such as metals and concrete instead of areas that are more mixed with vegetation. The above described logic and previous work support the assumption that neighbourhood-specific surface material compositions and, thus, typical spectral mixtures are very likely to exist. Bearing in mind the drawbacks of spectral unmixing approaches, a new methodology is required to interpret the complex spectral mixtures in spaceborne imaging spectroscopy data.

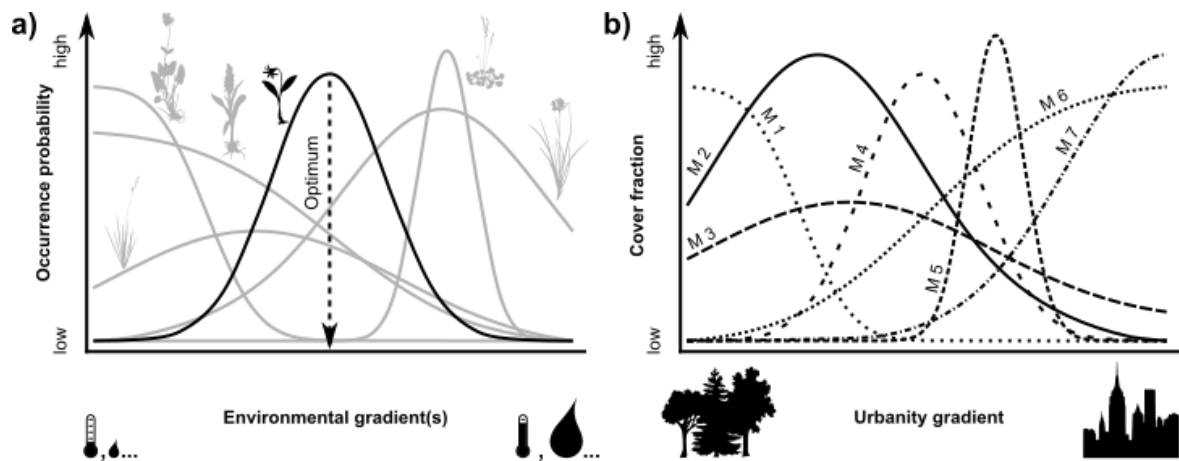


Fig. 1: a) Plant species show a maximum occurrence probability on environmental gradients (such as temperature, water, light, and nutrient availability) where the environmental conditions meet their ecological demand. However, they are able to subsist outside this optimum setting, resulting in a unimodal occurrence probability on the environmental gradient. b) Similarly, urban materials (here M1 – M7) are assumed to show a unimodal trend in their cover fractions along a non-spatial gradient in the material feature space. Co-occurrences in these distributions result in characteristic material mixtures that form gradual transitions and may be mapped with spectral data.

A possible way to interpret complex spectral mixtures is to use gradient analysis, which so far has been used to map species compositions in natural ecosystems. We can consider the mixture of urban surface materials in analogy to the species mixture in a natural vegetation stand. Species mixtures are not arbitrary but result from the ecological demands of the individual species and gradients in the prevailing environmental conditions. Each species has an optimal, multivariate set of environmental conditions that fully meets its demands. In consequence, the highest occurrence probability of the species is given for these optimal conditions (Fig. 1a). The species is also able to subsist slightly outside its environmental optimum, but with a lower occurrence probability. In unsuitable conditions, the species will not occur. As different species have different demands, the optima of their occurrence probability curves on the environmental gradients differ, while the curves of species with similar ecological demands show some overlap. This induces a gradually changing species composition along environmental gradients in mixed vegetation stands. The concept of gradual changes in species composition in the vegetation continuum, the so-called floristic gradients, was first introduced by Gleason (1926) as an alternative to classificatory

approaches. It has been successfully used in several studies for mapping vegetation as continuous fields based on remote sensing ([Schmidtleein and Sassini 2004](#); [Schmidtleein et al., 2007](#); [Feilhauer et al., 2011](#); [2014](#); [Harris et al., 2015](#); [Neumann et al., 2015, 2016](#)). In the city, gradient analysis was first used by [Gu et al. \(2015\)](#) to quantify the composition of tree species using multisensor remote sensing data. Besides the fact that the resulting gradient maps preserve the fuzziness of natural vegetation patterns and, thus, provide a more accurate generalization rather than discrete classes, the approach has a fundamental advantage: The gradient concept is based on the assumption that all pixels are mixed and no “pure” pixel exists. It is, thus, not necessary to identify EMs to apply the concept. Instead, the gradients are extracted from a representative sample of mixed species compositions ([Schmidtleein and Sassini, 2004](#)). For this purpose, a gradient analysis is performed to analyse inter-correlations in the distributions of co-occurring species. The gradient analysis is basically a dimensionality reduction of the species occurrence data, where the original n dimensions of a data set with n species is reduced to a few, independent floristic gradients. It is important to note that the extracted gradients are non-spatial and only describe gradual transitions of species occurrences in the species feature space. No information on the geographical position of the samples is considered in their extraction.

In transferring this concept to mixtures of urban surface materials, we follow the hypothesis of the existence of typical surface material compositions in urban neighbourhoods, assuming that urban surface materials form patterns of co-occurring cover fractions along a non-spatial gradient in the material feature space ([Fig. 1b](#)). Here, we can assume that each surface material has a maximum in its distribution along one or multiple, non-spatial gradients and that these gradients can be extracted in a data-driven way using the gradient analysis techniques adopted from ecology. Since the approach treats all urban areas as mixtures, it may be applicable to spaceborne imaging spectroscopy data despite their rather coarse spatial resolution with complex mixed pixels. In the present proof-of-concept-study, we test whether the gradient concept offers a feasible solution for the analysis of urban data sets with a high amount of spectral mixtures. In particular, we aim to answer three questions:

- Are there gradual transitions in the occurrence of urban surface materials so that the gradient concept can be applied?
- Can these material gradients be related to spectral mixtures and can their spatial distribution be mapped with imaging spectroscopy data with 30 m spatial resolution?
- How can these spectral patterns be used to retrieve urban material compositions?

2. Study area

An area of 4.12 km², east of the city centre of Munich, Germany, was selected as the study site (48.133045°N, 11.565026°E and 48.106969°N, 11.631842°E). The Isar River with a broad vegetated river side, mainly east of the river, crosses through the study site from the southwest to the northeast. Further north, the large and conspicuous complex of the German Museum is located on an island. West of the Isar River, the study site is dominated by buildings originating in the Wilhelminian time, mainly built in the 19th to early 20th centuries. This part of the old town is characterized by a dense perimeter block development with a large variety of different roofing materials and marginal proportions of open space (see Fig. 2). On the eastern side of the Isar River, different USTs are alternated. The residential areas can be generally divided into perimeter and regular block development, high-rise buildings, row house development and detached and semi-detached houses, according to the definition of UST classification in [Heldens \(2010\)](#). Additionally, the study site is shaped by several industrial areas with an agglomeration of differently sized halls and warehouses. The largest industrial area in the study site is located east of the railway station Ostbahnhof in the northern part. In the centre, a larger green space indicates the dimension of the eastern cemetery with a systematic combination of woody and non-woody vegetation traversed by small paths. In the southeastern part, the study site mostly consists of residential areas with detached and semi-detached houses with typically higher proportions of vegetation. For sporting and leisure purposes, several sporting fields and public parks are spread over the entire study site. In summary, USTs characterizing the study site range from residential and commercial dwellings to industrial areas, road and rail network, recreation areas such as sports fields, cemeteries, open green spaces including forested areas, and a section of the Isar River. The variety of different USTs accompanied by a wide range of predominate surface materials embedded in a relatively small-scaled

area provide almost ideal preconditions for investigating urban surface material compositions and the analysis for urban gradients. For a visual representation of USTs, refer to [Heldens \(2010\)](#) and [Heiden et al. \(2012\)](#), who illustrate the differences between the individual USTs using selected examples of high-resolution orthophotos of the city of Munich.

3. Data

3.1 Airborne imaging spectroscopy data - HyMap

Imaging spectroscopy data were used for two purposes; first, as a basis for detailed surface material mapping ([Heiden et al., 2012](#)) as a surrogate for ground truth data regarding the actual material composition, and second, for simulating EnMAP reflectance of the study site. These image data were acquired with the HyMap hyperspectral sensor ([Cocks et al., 1998](#)) during the HyEurope 2007 flight campaign on June 17th and June 25th 2007 by the German Aerospace Center (DLR) Oberpfaffenhofen, Germany. Spectroscopic measurements of the study site were recorded from a flight height of 2000 m for 128 spectral bands ranging from 450 to 2500 nm, resulting in a pixel size of 4 m \times 4 m. The pre-processing of the image data was carried out as described in [Heldens \(2010\)](#) and [Heiden et al. \(2012\)](#) and includes radiometric correction ([Cocks et al., 1998](#)), removal of three noisy bands, atmospheric correction, transformation into reflectance values, a nadir-normalization to correct the brightness gradient with ATCOR ([Richter, 2009](#)), geometric correction into WGS-84, UTM zone 32 N using the software ORTHO ([Mueller et al., 2005](#)), and orthorectification based on a digital terrain model produced from SRTM (Shuttle Radar Topography Mission) data ([Habermeyer et al., 2008](#)). [Heldens \(2010\)](#) report an average Root Mean Squared Error (RMSE) of 0.8 pixels after geometric pre-processing.

3.2 Surface material map

A detailed surface material map derived from HyMap data, with 42 initial surface material classes, served as the basis for the sampling and ordination procedure. Surface materials were identified with an automated multi-stage processing system ([Heiden et al., 2012](#)) based on the following steps: a) spectral feature-based extraction of EMs ([Segl et al., 2006](#)) using a spectral library of image spectra ([Roessner et al. 2011](#)), b) maximum

likelihood classification using the previously determined EMs to increase the number of spectrally pure pixels in the image (Roessner et al., 2000; Roessner et al., 2001), c) improvement of surface material classification based on a digital surface model (DSM) obtained from a High Resolution Stereo Camera (HRSC) (Heldens, 2010) and d) iterative linear spectral unmixing to model remaining mixed pixels while considering two EMs per pixel. At 4 m HyMap resolution, almost half of the pixels correspond to pure material spectra, while the other half is composed of dominant surface material abundances. In Heldens (2010) and Heiden et al. (2012), accuracies for the surface material map were determined with an area-based approach to identify differences between the surface material map and the validation data originating from digitized building blocks using 3K aerial orthophotos. The accuracies of surface material classes were indicated by a mean absolute error (Willmott and Matsuura, 2005) of up to 14%, with the highest underestimation of 10% occurring for the artificial material classes ‘asphalt’ and ‘concrete’ and almost 20% for the natural surface material class ‘deciduous trees’. For individual accuracies of single surface material classes please refer to Heiden et al. (2012).

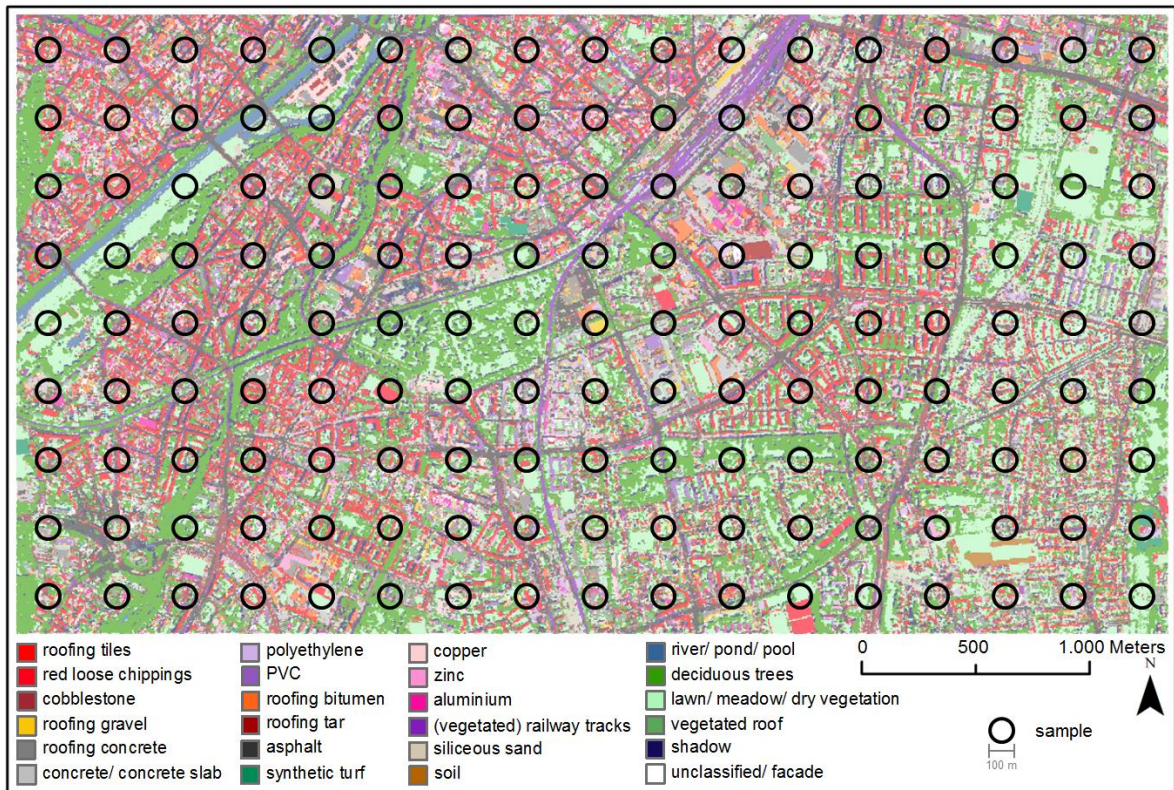


Fig. 2: Detailed urban surface material map determined from HyMap data with a systematic sampling scheme (section 5.1) in which circles represent the sample size and position in the Munich study site.

For simplicity and consistency reasons, several material classes were aggregated, after they were initially differentiated according to spectral intra-class variabilities, such as different coatings or according to aging effects. These material instances (e.g. old and new roofing tiles), were therefore aggregated to surface materials (e.g. roofing tiles). In addition, classes labelled as unknown, shadow or facades were removed from the surface material map, since only real surface materials that can be identified by remote sensing should be analysed with gradient analysis. The process of aggregation and removal of single material classes leads to a material map consisting of 27 surface material classes. This modified surface material map (Fig. 2) was used for the sampling (section 4.1 and 5.1) to analyse material compositions with gradient analysis (section 4.2). Table 1 lists the number of pixels in the surface material map (Fig. 2) for the 27 surface material classes and the fractional abundances within the samples.

Table 1: Categorisation of urban surface materials (with material abbreviations) into material groups, including total and sampled cover fractions per surface material in the Munich study site.

Material Group	Surface Material	Abbreviation	Total pixels in surface material map	Sampled Cover Fractions in [%]
Minerals	roofing tiles	rtil	66,886	9.2%
	roofing concrete	rcon	27,440	7.4%
	roofing gravel	rgra	8,206	11.1%
	concrete	fcon	42,104	10.2%
	concrete slabs	pcon	11,015	8.7%
	loose chippings	prlc	20,546	10.7%
	cobblestone	pcob	47,358	8.5%
Metals	copper	rcop	13,366	8.6%
	zinc	rzin	7,607	8.0%
	aluminium	ralu	10,466	8.5%
Hydrocarbons	PVC	rpvc	13,434	8.2%
	polyethylene	rpol	8,625	9.2%
	roofing bitumen	rbit	14,883	8.3%
	roofing tar	rtar	29,249	8.8%
	asphalt	fasp	84,854	8.1%
	synthetic turf	fkun	3,209	9.1%
	deciduous trees	vdec	172,784	8.1%
Vegetation	lawn	vlaw	16,983	8.7%
	meadow	vmea	87,525	8.9%
	dry vegetation	vdry	35,690	8.9%
	vegetated roof	rveg	18,879	8.0%
Soil and Water	siliceous sand	bsan	11,765	8.9%
	humous soil	bsoi	2,978	6.0%
	river	wriv	4,518	10.7%
	pond	wpon	4,691	8.5%
Railway tracks	railway tracks	prail	10,811	7.2%
	vegetated railway tracks	prailveg	11,546	8.1%
Total			Σ (100%) 787,418	\varnothing 8.7%

3.3 EnMAP data

The HyMap data were also used as input to simulate EnMAP reflectance values of the study site (Fig. 3) using the end-to-end simulator (Segl et al., 2012). The simulated EnMAP data are characterized by a ground sampling distance of 30 m and 242 spectral bands ranging from 423 nm to 2439 nm. Sensor specific characteristics for the prospective EnMAP mission are given in Guanter et al. (2015). In the range of the overlapping spectral bands (904 nm to 985 nm) of the two sensors (VNIR and SWIR), only the spectral bands of the SWIR sensor were used. Additional spectral bands ranging from 1358 nm to 1429 nm and 1318 nm to 1960 nm were eliminated due to atmospheric water absorption.

The samples shown in Fig. 2 (see section 4.1), are also used for the extraction of spectral signatures and their subsequent linkage to the gradients obtained from the surface material compositions. For this purpose, the mean simulated EnMAP reflectance values of all pixels whose centre coordinates lie within a sampling polygon were calculated and used for the further analysis.

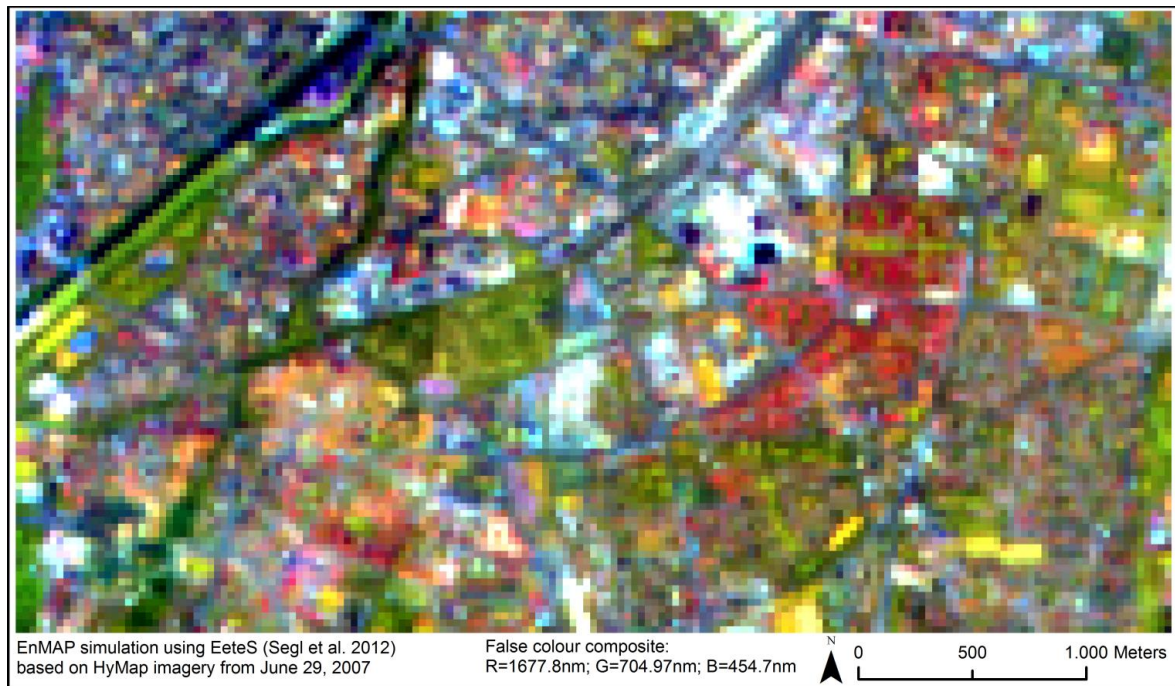


Fig. 3: Simulated EnMAP data for the Munich study site based on HyMap data.

4. Methods

The complex material compositions in the urban environment are subjected to gradient analysis in order to analyse patterns of co-occurring cover fractions. Fig. 4 provides an overview of the required input data, the main processing steps (sampling, ordination, regression and prediction) and the resulting outputs from gradient analysis.

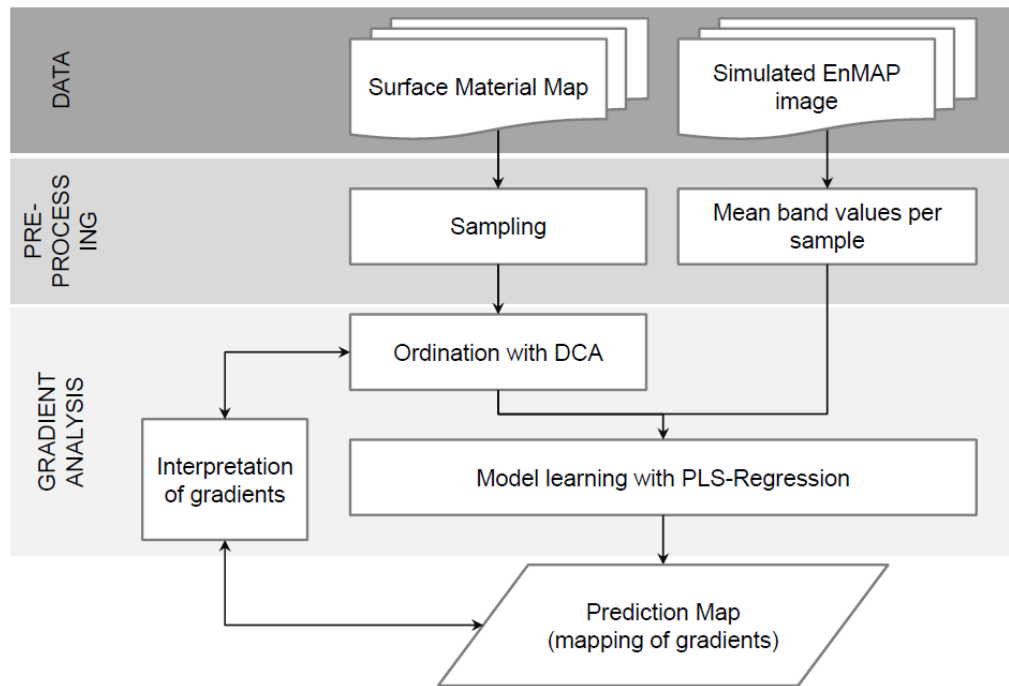


Fig.4: Flowchart of gradient analysis for analysing material compositions in urban environments.

4.1 Sampling

The intention to analyse urban material compositions in simulated EnMAP pixels with gradient analysis requires a fundamental understanding of the occurrence of surface materials with regard to material-specific gradual transitions. This information can be obtained by defining samples from the surface material map (Fig. 2) with the aim to describe all occurring surface material classes and their compositions. Material compositions in the study site were analysed by means of a systematic sampling grid consisting of 153 circular polygons, each with a diameter of 100 m, evenly distributed over the study site (Fig. 2). The polygon diameter of 100 m was chosen to ensure that mixtures of materials are present in each sample and that each polygon is covered by multiple simulated EnMAP pixels. Polygons were arranged with inter-distances of 300 m between the centre points of each polygon. A systematic sampling scheme has the advantage that

the urban space is sampled with a homogeneous spatial density; the inter-distances were used to mitigate effects of spatial autocorrelation in the data. Consequently, the sampling fully covers the diverse urban structures dominating the study site. Cover fractions of single surface material classes per sample were stored in a database (material table) that was finally used as input for the analysis of surface material compositions using the ordination method.

4.2 Ordination

The matrix of surface material cover fractions per polygon was passed on to a gradient analysis to extract the main gradients in surface material composition from the data. The gradient analysis arranges the sampling polygons according to their material composition in a multidimensional gradient space. No information on the geographic position of the sampling polygons is considered; hence, the resulting gradients are feature space gradients and not spatial gradients. Samples with similar material compositions are located nearby in the gradient space, whereas samples with very dissimilar material compositions are located on the opposing end of a gradient axis. The gradients are numbered in hierarchically decreasing order, i.e. the first gradient is the longest and most pronounced one, higher order gradients are less prominent. The position of each sample in the gradient space is indicated by a numerical score – the so-called gradient score – which is determined by the ordination in order to evaluate its similarities with respect to the composition of the material classes and their cover fractions. These gradient scores are an indicator of the surface material composition in the sample and were, therefore, used as response variables in spatial extrapolation models.

Several techniques can be used to perform a gradient analysis; here, we used detrended correspondence analysis (DCA; [Hill and Gauch, 1980](#)), since DCA is an established technique in vegetation science and has been successfully used for gradient mapping before (e.g. [Schmidtlein and Sassini, 2004](#); [Feilhauer and Schmidtlein, 2009](#); [Feilhauer et al., 2011](#)). In the present study, the selection of DCA was simply based on the authors' good experience with this technique in ecological analyses. No systematic analysis of the performance of DCA for urban gradient analysis in comparison to other techniques were conducted. In consequence, other methods for gradient analysis could have likewise been used for this pilot study. In ecology, DCA is used to model a sample distribution of varying

plant species assemblages on the basis of unimodal occurrence probabilities along environmental gradients. The underlying assumption here is that species' occurrence is maximized in optimal environmental conditions. This behaviour can be determined in species samples of cover abundances that are collected over wide ranges of external gradients. For every species, a Weighted Average (WA) over all samples of cover abundances can be calculated using Gradient Values (GV) as weights. Subsequently, the samples and species are projected into a rank-ordered $WA \times GV$ matrix. The resulting matrix represents species abundances in a diagonal structure, where dissimilarities between species and gradient responses are maximized at the endpoints of the diagonal. In DCA, the gradients are not measured a priori. They start with random values and will be iteratively re-calculated until an optimal diagonal matrix is generated. Hence, the resulting GV represents a factor variable that allows for an optimal delineation of species variance within the samples. Since one gradient often does not account for the total variance in species composition (samples with different species assemblages can be close together in a one-dimensional projection), additional axes are generated using decorrelated GVs for the iteration. The overall procedure was introduced as reciprocal averaging ([Hill, 1973](#)). In analogy to species abundances, the urban material cover can be used for the averaging cascade in order to calculate the diagonal representations of material samples within an urban gradient space. Because the gradients result from correspondence analysis, they are both unscaled and sometimes affected by artefacts. For this reason, a rescaling and detrending process was introduced in DCA. Although this correction is subject to criticism due to its mathematical inelegance ([McCune et al., 2002](#)), it is a well-performing and pragmatic technique that is frequently used in ecology. A major advantage of DCA over other algorithms for gradient analysis is the scaling of the axes in Standard Deviation (SD) units, which allows a detailed analysis of the compositional turnover in the gradient space: a distance of four SDs on a gradient indicates a full turnover, e.g. two samples with an inter-distance of four SDs have no surface materials in common ([Hill and Gauch, 1980](#)). Samples with a shorter inter-distance share at least occurrences of some materials. To mitigate an overly prominent influence of rare materials on the ordination result, we used the built-in downweighting option in our set up.

The number of gradients to be considered in the analysis is determined from the respective gradient lengths, and the percentage of total variance in the data set explained by the gradients. Short gradients that explain only a small percentage of the total variance are often very difficult to interpret, and hence, dismissed from the analysis.

4.3 Regression modelling and prediction

The gradient scores of the polygons were subsequently regressed against the averaged simulated EnMAP reflectance spectra (section 3.3) of the corresponding pixels using Partial Least Square Regression (PLSR; [Wold et al., 2001](#)). PLSR establishes a linear relationship between the reflectance values in the spectral EnMAP bands as predictor variables and the corresponding DCA scores as response variables. A separate model is built for each DCA axis. PLSR builds the regression using latent vectors in order to handle the high degree of inter-correlation of the spectral bands, to cope with the small number of samples compared to the large number of spectral bands, and to maximize the performance of the models. These latent vectors are linear combinations of the original spectral bands that contain, on the one hand, maximum spectral information and, on the other hand, are optimized towards a good representation of the response variable. The spectral information content is hierarchically decreasing from the first to the higher order latent vectors. The number of latent vectors resulting in the smallest validation error was identified and used for the final model to minimize the risk of over-fitting. This number is determined in an elaborate procedure by analysing trends in the cross-validation RMSE. Here, we used a 10-fold cross-validation for this purpose. The importance of the individual spectral bands in the model is determined by considering the variability of the regression coefficients across the cross-validation steps ([Martens and Martens, 2000](#)). A stable and high absolute value of the coefficient in all steps of the cross-validation indicates a high importance of the spectral band for the regression. This approach allows for an efficient backward selection of spectral bands and an iterative refinement of the model towards an optimized set of spectral bands that is both parsimonious and has a strong and reliable predictive power ([Schmidtlein et al., 2012](#)). The models are finally applied to the image data for a spatial prediction of the DCA scores across the study area.

5. Results

5.1 Sampling

The sampled cover fractions of the study site are relatively similar (6%-11.1%), independent of the total coverage of the respective material classes (Table 1). The similar cover fractions of individual materials in the samples show that the sampling schema considers all materials equally, independent of their actual occurrence in the study site. Cover fractions for each surface material class per sample demonstrate the heterogeneity of material compositions in urban areas, even in these small observation units of the samples. Material compositions in the samples (Fig. 2) are formed by 4-26 different surface materials. The complexity of material compositions varies depending on the size of the urban objects and the position of the samples in the study site. Therefore, highly diverse material compositions occur more frequently in densely built-up areas of smaller objects (e.g. Wilhelminian styled urban neighbourhoods) and in industrial shaped neighbourhoods, than in relatively homogeneous areas such as open green spaces. Samples with the highest number of different surface materials are represented by block developments located in the north and in the transitional area of industrial and residential neighbourhoods in the south of the test site.

5.2 Ordination

The two main gradients determined with the DCA have an axis length of 3.1 SDs for the first gradient and 2.1 SDs for the second gradient. Samples are distributed in the material-specific DCA-space according to the determined gradient scores of the samples for both gradients (Fig. 5). The material-specific DCA-spaces visualize the differences in the occurrence of individual material classes in the sampled study site (see Table 1).

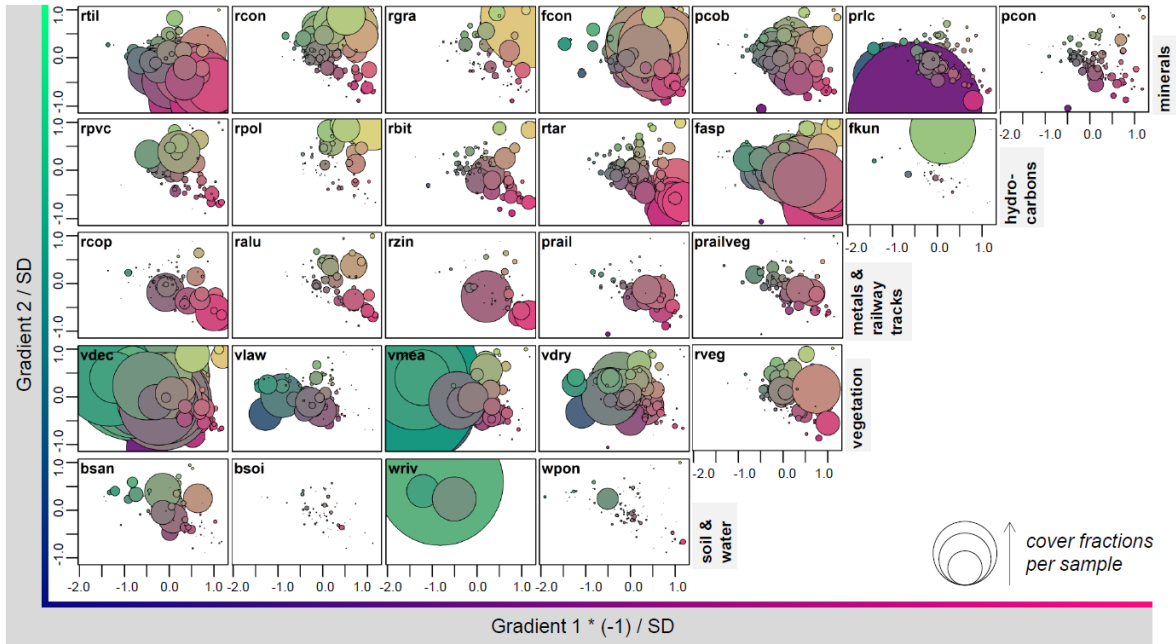


Fig. 5: Material-specific DCA-spaces facilitate the visualization of varying cover fractions in the samples to determine maximum occurrences of individual material classes. The position of a circle centre defines the position of a sample and its material composition in the DCA-space, while the circle diameter visualizes the material-specific cover fractions in each sample. The samples are coloured as a result of the transformation of the DCA-space into a colour space (see Fig. 9b). Accumulated samples indicate the maximum occurrence of this material in the gradient space.

For easier interpretation of the gradients, the samples were projected onto the corresponding axis. Most material classes show a maximum occurrence along the gradients, as indicated by the position and size of the circles (Fig. 5). The left part of gradient 1 (negative DCA scores) is covered by dominant vegetation classes such as trees and meadows. The right part of gradient 1 (positive DCA scores) is mainly dominated by roofing minerals and hydrocarbons, but also by materials typically used for roads such as concrete (fcon) and asphalt (fasp). Generally, all material classes show dominant occurrence patterns along the first gradient.

Maximum occurrences for the material classes rtil, rtar, fasp, and rcop are shown along the lower (negative) part of gradient 2, while rcon, rgra, fcon, and rpol mainly occur on the upper (positive) area. Some material classes (e.g. vdec) do not have a maximum occurrence along the second gradient but occur across the entire axis with almost even cover fractions. This is also shown by the different colour hues of the samples along the second gradient. The maximum occurrences of materials can be visualized by a biplot scaling of the samples. For this purpose, material vectors were defined on the basis of the

DCA scores, which determine an orientation of the occurrence of materials in the DCA-space (Fig. 6). These vectors, together with the material-specific DCA-spaces (Fig. 5), serve as a tool for interpreting the gradients.

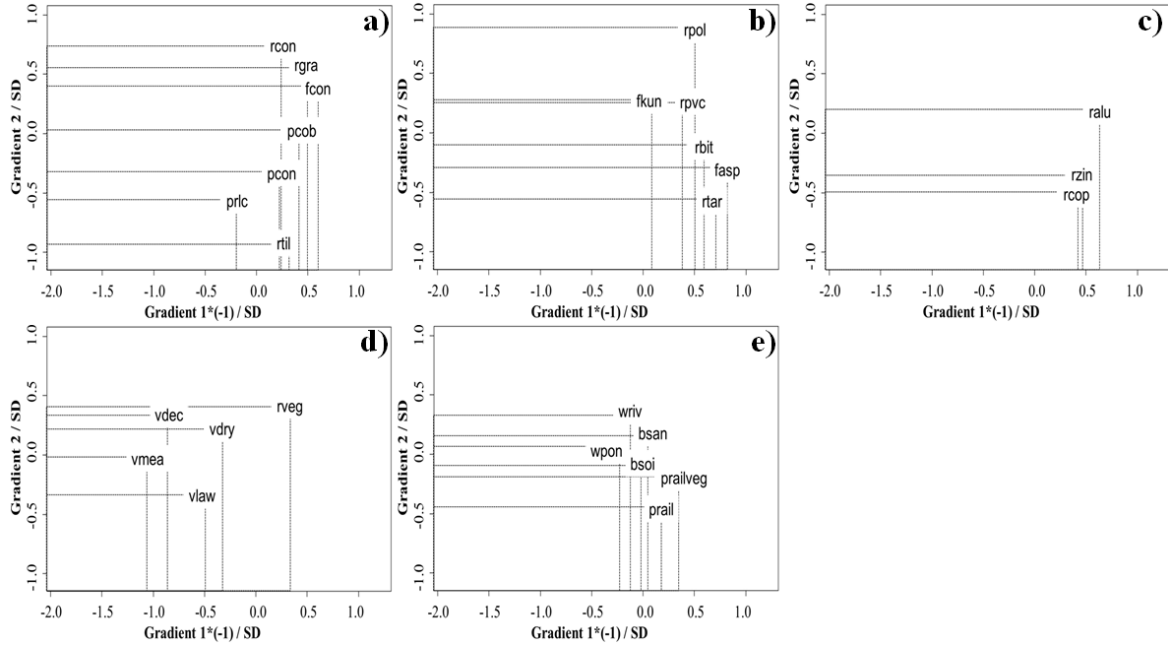


Fig. 6: Biplot scaling of the main material groups a) minerals, b) hydrocarbons, c) metals, d) vegetation, and e) the remaining material classes, composed of soil, water, and railway tracks (see Table 1), to visualize the maximum occurrences of individual material classes in the DCA-space (represented by the position of material names in the DCA-space).

5.3 Regression modelling

The best PLSR model for gradient 1 (Fig. 7a) resulted in $R^2 = 0.85$ for calibration and $R^2 = 0.84$ in 10-fold cross-validation. The final model was based on 35 spectral bands (distributed over the entire spectral range). These bands were selected because they survived the backward selection process and were then summarized to two latent vectors. The respective model error is indicated with an RMSE of 0.23 SDs for calibration and 0.24 SDs for validation. The model for the second gradient included five latent vectors based on 13 spectral bands (mainly distributed in the SWIR region) with a fit of $R^2 = 0.71$ for calibration and $R^2 = 0.67$ for validation (Fig. 7b). The respective RMSE for the calibration of gradient 2 was 0.21 SDs and 0.22 SDs for validation.

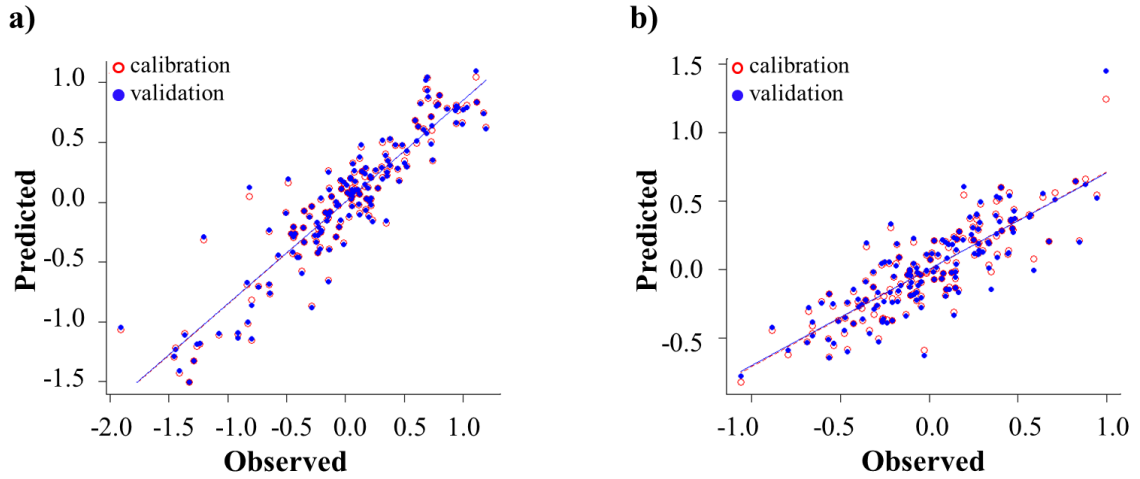


Fig. 7: Model fits of the PLS regression analysis for a) the first and b) the second gradient.

5.4 Mapping of DCA scores

The regression models for the first and second gradient have been applied to the simulated EnMAP data. Pixels with predicted DCA scores exceeding ± 0.5 compared to the minimum or maximum DCA scores determined for the samples are not taken into account (white pixels), as these ranges were not covered by the sampling. A colour bar corresponding to the gradient axis is used to visualize the predicted DCA scores for gradient 1 (Fig. 8a) and gradient 2 (Fig. 8b). Fig. 8a and b show the formation of different spatial patterns based on the specific material compositions of the respective gradient, which do not coincide and, thus, give an indication of different information represented by each gradient.

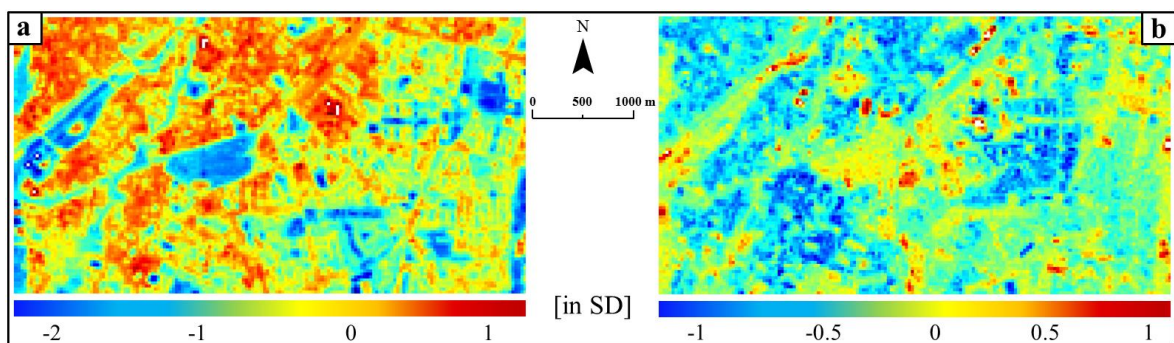


Fig. 8: Mapping of predicted DCA scores for simulated EnMAP pixels in the study site in Munich for a) the first and b) the second gradient.

The composite map in Fig. 9a combines predicted DCA scores for gradients 1 and 2, resulting in Cartesian coordinates for each pixel. The colour values of the pixels are taken from the position of the coordinates in a two-dimensional colour space (shown in Fig. 9b) that is related to the DCA-space. Accordingly, different material compositions are marked by different colour shades of the pixels in the prediction map (Fig. 9a). Similarly, coloured patterns indicate similar material compositions. Fig. 9b shows the colour scheme that is assigned to the DCA-space of both gradients with selective surface materials (written in white). The position of the surface materials in the coloured DCA-space highlights their maximum occurrence according to Fig. 6. However, similar to Fig. 9a, the colour hues need to be interpreted as surface material compositions.

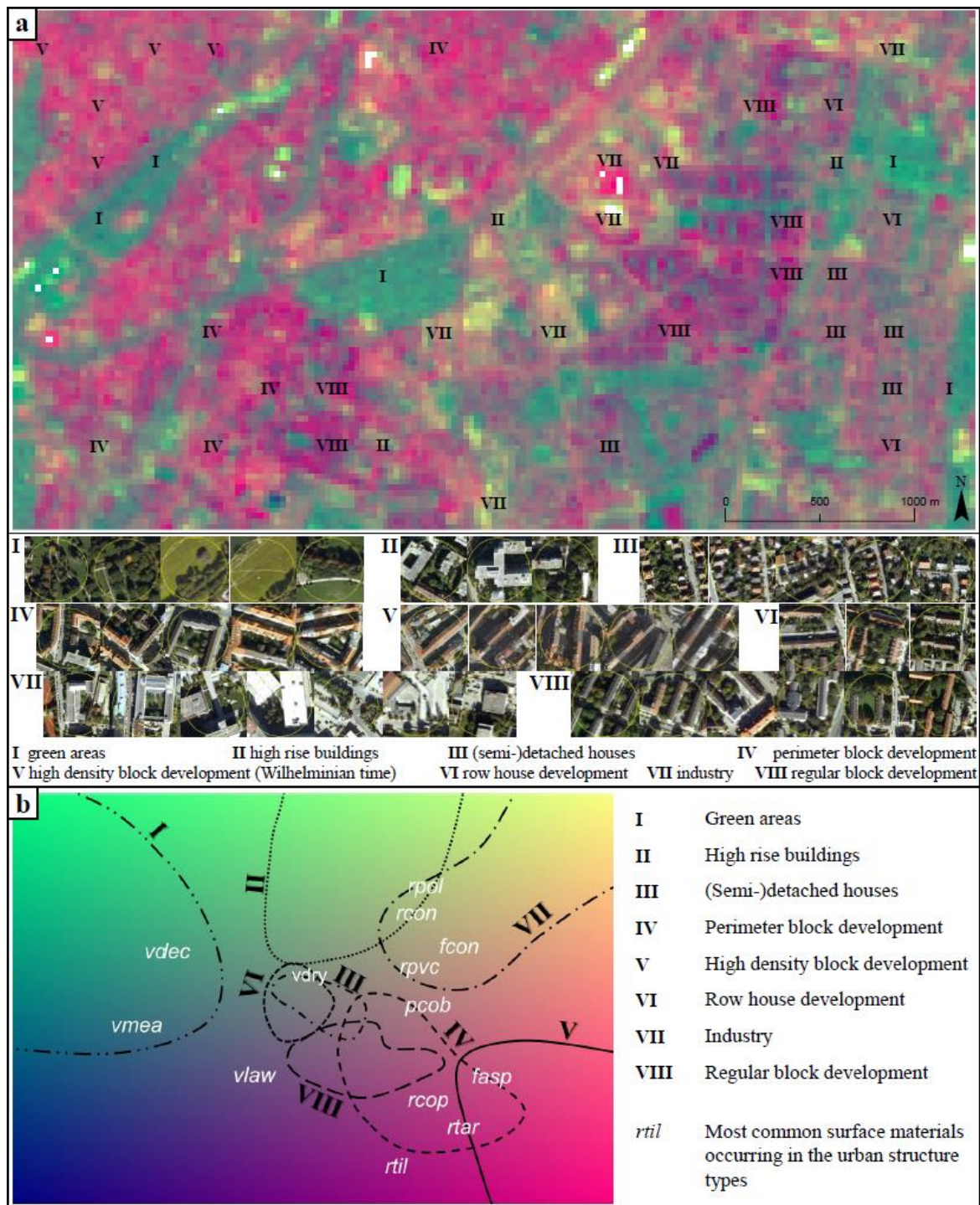


Fig. 9: a) Prediction map of DCA scores for composed gradient models for the study site in Munich, with a selection of samples from the sampling scheme (Fig. 2) that represent distinct USTs (I-VIII) - for historical high-resolution GoogleEarth® orthophotos - to support the identification of b) the colour scheme (legend) with regard to the delimitation of USTs (solid and dashed lines) based on characteristic material compositions.

The black solid and dashed boundaries in Fig. 9b results from the visual analysis and interpretation of the prediction map (Fig. 9a) that is described in detail in section 6.2. First

visual inspections indicate that the UST classification of Munich (see section 1) widely corresponds to the patterns in the prediction map (Fig. 9a). We used this correlation to interpret the colour hues with respect to a characteristic material composition. For this purpose, we (1) selected samples from Fig. 2 that are unambiguously assigned to a specific UST using corresponding historical GoogleEarth orthophotos (Fig. 9a.I-VIII). The positions of the samples are marked by Roman numerals plotted into the prediction map. Subsequently, these samples were (2) highlighted in the colour-coded DCA-space, which leads to the formation of clusters of samples with similar material compositions. (3) Further samples are integrated into these clusters, which are adjacent to the representative samples (Fig. 9a.I-VIII) in the DCA-space, until a new assignment of samples no longer alters the UST clusters. Finally, (4) the resulting clusters were used to delineate USTs in the colour-coded DCA-space (solid and dashed lines in Fig. 9b). These cluster boundaries of USTs should not be viewed as discrete class boundaries but should characterize a probability of the occurrence of material composition that is characteristic for a certain UST. The delineated boundaries support the analysis of characteristic material compositions of USTs.

5.5 Analysing characteristic material compositions

Characteristic material compositions of USTs were analysed in order to gain an advanced understanding of typical spectral mixtures of simulated EnMAP pixels in the urban scene. For this purpose, the selected samples extracted from the sampling scheme (Fig. 2), as shown in Fig. 9a.I-VIII, were analysed for the co-occurrence of individual material classes and their cover fractions. Therefore, the material classes were aggregated to the four main material groups – minerals, metals, hydrocarbons and vegetation, according to Table 1. The material classes of soil and water were not considered, as these classes do not frequently occur in the study site, nor the urban structure railway tracks, as these are not among the observed USTs (Fig. 9a.I-VIII). Abundances of individual material classes were averaged for all samples per USTs. On the basis of these observations, the USTs are described by the most co-occurring cover fractions of dominating material classes; thus, material classes with frequencies below 5% were neglected in further analysis. Based on these statistics of averaged material cover fractions, the two most

prominent material classes of each material group are displayed in Fig. 10, representing the most common surface materials for a particular UST of the study site.

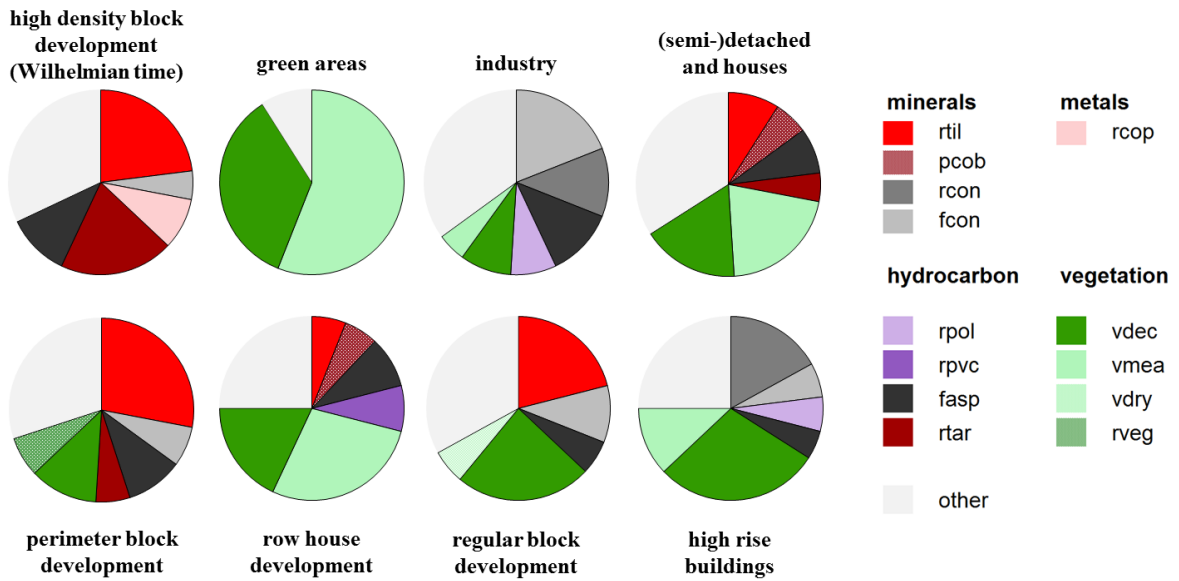


Fig. 10: Proportions (in %) of the two most commonly co-occurring material cover fractions (minimum material fraction has to be at least 5%) in the four main material groups for a selection of averaged samples per UST (Fig. 9a.I-VIII). The class 'others' comprises the remaining materials of the four main material groups as well as soil, water, and railway tracks.

6. Discussion

6.1 Do gradients exist in urban material composition?

The results in Figs. 5 and 6 demonstrate the maximum occurrence of material classes, which correspond to the theory of the probability distribution along the respective gradient axis introduced in Fig. 1. This indicates the applicability of the gradient concept for the analysis of complex material compositions in cities. The gradient interpretation is based on the analysis of dominant material distributions (determined from material-specific DCA-spaces, Fig. 5) along a corresponding gradient. On gradient 1, vegetation types mainly dominate the negative range of the DCA-space, while their cover fractions decrease towards the positive end of the axis. In contrast, artificial materials such as fasp, fcon, and rbit, which are often used for rooftops and streets of larger manmade urban objects, dominate the positive end of the gradient 1 and, thus, can be interpreted as a gradient of imperviousness. The interpretation of the second gradient, with a shorter axis length, is more difficult. Artificial material groups such as minerals and hydrocarbons dominate both

the negative and positive range of gradient 2. From the dominant occurrence of individual material classes along the gradient axis, possible conclusions can be drawn about land use and the functions of the built-up areas. For instance, materials that mainly occur in industrial areas have positive DCA scores on the second gradient (e.g. rcon, fcon, and rpol), while the negative DCA scores are dominated by roofing materials such as rtil, rtar and rcop, which are typically found in residential areas of European cities (Wittig et al., 1998). The maximum occurrences of individual surface materials in the samples are highlighted in the biplot scaling (Fig. 6).

The position of the materials in the biplot scaling is also important for the interpretation of the gradients. The further away the maximum occurrences of the material classes from the origin of the DCA-space (the longer the material vectors), the more reliable the prediction of the occurrence of materials. The vector length is also influenced by the frequency of material occurrences in the study site. For example, vdec is represented by 172784 pixels (Table 1) in the study site, showing a long material vector. In contrast, bsoi, wpon and wriv have the lowest number of pixels in the study site (2978, 4691 and 4518 pixels) expressed in short material vectors. It shows that the sampling scheme is important because it represents the material abundances in the study site. Nevertheless, the dominant material occurrences and their gradual transitions show the formation of two interpretable urban gradients analogous to the formation of floristic gradients on the basis of maximum occurrences of plant species.

The visualization of the maximum occurrences of material classes along the gradient axes (Fig. 6) also indicate co-occurrences of materials. This means, for example, that in our study site, buildings covered with roofing tar (rtar) are often located in the neighbourhood of buildings with tiled roofs (rtil) and the streets are mostly asphalted (fasp), whereas, in areas with a higher occurrence of polyethylene on roofs (rpol), roofing tiles (rtil) are rarely found. These observations also confirm the neighbouring occurrence of similarly composed samples in the DCA-space. The probability of co-occurring material classes supports the assumption of the existence of typical spectral mixtures in 30 m simulated EnMAP pixels. A drawback of the wider applicability of this method could be the necessity of immense ground truth data. Since generating ground truth information can be very time- and cost-intensive, if the samples are derived from field surveys or other non-automated approaches, a detailed surface material map derived from airborne imaging spectroscopy and height data is used in this study. This solid data base was necessary to prove the existence of material gradients in this study site, which is one of the major

requirements to proceed with investigations about the transferability of this concept. Since transferability analysis goes far beyond the scope of this paper, it should be analysed in future studies focusing on the robustness of the gradients and the regression models.

6.2 Are urban material gradients linked to complex spectral mixtures?

Results of the PLS regression analysis (Fig. 7) show strong correlations between visually recognizable patterns of the simulated EnMAP reflectance and gradual transitions of materials, especially in the first gradient. The shorter length of gradient 2 led to a slightly weaker validation fit of the model compared to gradient 1. This also explains the difficulties in interpreting the second gradient (section 6.1).

The subsequent mapping of gradient 1 on the entire simulated EnMAP image (Fig. 8a) allows the prediction of co-occurring cover fractions and their pattern formation. Fig. 8a clearly shows spatial patterns that are associated with green spaces on the one hand and built-up areas on the other hand. Based on the patterns in Fig. 8a, we observe a decrease in the proportion of vegetation coverage and, at the same time, an increase in imperviousness with increasing DCA scores. These findings are in line with the observation regarding the dominance of vegetation classes in samples with negative DCA scores on axis 1 to high cover fractions of roofing and paving materials on the opposing end of the gradient (Fig. 5). Thus, gradient 1 expresses a rural-to-urban transect (increasing urbanity from blue to red).

The prediction of gradient 2 shows new patterns (Fig. 8b) that indicate additional gradual information originating from material occurrences. It is observed that pixels with predicted very high positive DCA scores (red) for the second gradient are dominated by a composition of material classes with typically high albedos in the VNIR range (bright material classes such as rpol), while very low predicted negative DCA scores (dark blue) correspond to material compositions of rather darker artificial materials, such as rtil. However, these findings can only be observed for the very high and very low DCA scores, while material compositions of pixels that are in the middle of the gradient space do not fully correspond to this behaviour. Thus, a dominant occurrence of materials along a brightness gradient (Small and Lu, 2006) for the second gradient axis cannot be observed. Compared to the lower DCA scores (blue), the very high DCA scores displayed in reddish shades indicate a material composition that is rather unique. These pixels were mainly

composed of similar materials and characterize areas whose material composition is rarely found in the study site, such as larger sand areas or homogeneous roofs of larger storage halls. Variations in blue patterns (DCA scores ranging from -1.5 to 0) represent urban neighbourhoods with different building sizes and building orientations. Light-blue to green patterns are associated with (semi-) detached houses, while row house constructions appear in dark blue (an adjacent pattern can be observed, for example in the northeast of the study site). Mid-blue patterns are associated with perimeter block development and high-density block development (Wilhelminian time) in the southwest and northwest of the study site. Thus, the second gradient can be interpreted as a structural gradient, although no structural information was used in this study. Since the colour differences in Fig. 8 indicate different material compositions, structural differences are most probably related to a certain material composition in the simulated EnMAP pixels.

By combining the two gradients, new patterns that are associated with spectral mixtures in the simulated EnMAP data can be found. The patterns in Fig. 9a generally correspond to patterns from the surface material maps. Interpretation of the coloured patterns in terms of material compositions was carried out by visual inspections of the surface material map. As a result, patterns with a greenish shade are characterized by exceptionally high proportions of vegetation classes such as *vdec* and *vmea*. Predominantly industrially shaped regions with a significantly increased proportion of artificial materials, such as hydrocarbons, are characterized by yellowish pixels. The patterns in different shades of red characterize the various residential neighbourhoods, such as (semi-)detached houses, row houses, and block developments. Each of these is composed of a characteristic material mixture. The structural differences between the neighbourhoods described for gradient 2 (Fig. 8b) are still present in the combined prediction map. These findings are also supported by the orthophotos of different types of buildings shown in Fig. 9a.I-VIII. Therefore, we conclude that the differentiation of the structural information must indirectly result from the material compositions that determine the spectral mixtures of simulated EnMAP pixels. These findings are supported by a study of [Roberts et al. \(2017\)](#) that already showed the correlation between material fractions, determined with MESMA, with structural information regarding height differences in urban environments. In forests, relationships between canopy structure and leaf biochemistry were found in imaging spectroscopy data ([Wang et al., 2017](#); [Knyazikhin et al., 2013](#)). In summary, the patterns in the combined prediction map enable a finer differentiation of the rural-to-urban transition

formed by gradient 1 (Fig. 8a) and confirm the existence of co-occurring cover fractions of individual material classes in the simulated EnMAP pixels.

One might argue that a simple Tasseled Cap transformation (Crist and Kauth, 1986) of multispectral data results in a similar spatial pattern as displayed in the gradient maps. In particular, the first DCA axis with a gradual change in vegetation cover resembles the greenness component, while only the extremes of the second DCA axis corresponds to the brightness component; however, the interpretability of a Tasseled Cap transformed image is largely limited to increases in brightness and greenness, whereas the DCA-space enables more detailed conclusions. This includes the opportunity to draw pixelwise conclusions on the occurrence probability of specific materials based on their distributions in the DCA space (Fig. 5) and the ability to quantify the spatial turnover and functional diversity of materials along the gradients (see, e.g., Feilhauer & Schmidtlein, 2009 and Rocchini et al., 2018 for similar analyses targeting vegetation patterns). Neither of this is possible with a Tasseled Cap transformed multispectral image. We thus consider the additional effort required by the application of the gradient concept as justified by the additional information provided.

6.3 Do spectral patterns correspond to characteristic material compositions?

The interpretation of gradients discussed above and the patterns in the prediction map of DCA scores (Fig. 9a) for the composed gradient models (section 6.2) can be related to the patterns of the main USTs classification of the study site based on their material compositions. The selected samples of USTs (Fig. 9a.I-VIII) were analysed in regard to their dominating material cover fractions in order to specify their characteristic material compositions. Fig. 10 shows that material compositions are distinctive for all of the selected samples.

Even in visually similar USTs such as row houses and (semi-) detached houses, the characteristic material compositions vary, especially in the occurrence of different types of hydrocarbons. The findings are in line with the formation of patterns in the mapping of the second gradient (Fig. 8b). The patterns visualize the structural differences of the USTs resulting from the different material compositions (Roberts et al., 2017) and, thus, enable their differentiation. In contrast, the USTs high-rise buildings and industry manifest the composition of the same co-occurring materials, but with varying cover fractions of material classes and also different proportions of remaining material classes. The similar

material composition of the most commonly co-occurring material classes is also observable by the narrow positions of the two USTs in the legend (Fig. 9b) and verifies the difficulties in the discrimination of these two types in the prediction map. This may also be due to the fact that high-rise buildings are rather underrepresented in the study site (only three samples were available). The discrimination of the two USTs could be tackled by using additional information on the building heights, which can be derived from a digital surface model. In addition, it was observed that the samples of unambiguously assignable USTs consist of at least 2/3 co-occurring cover fractions of characteristic material classes. Through its capability of linking the knowledge of typical material compositions with urban structures, gradient analyses is a powerful tool to map characteristic material compositions in 30 m imaging spectroscopy data of urban areas.

Further testing is required to answer the question whether the urban gradient space can similarly be mapped with multispectral data or whether such detailed information can only be retrieved from IS data. A first hint is given by the regression coefficients of the PLSR model for the second gradient. These coefficients (not shown here) indicate the high explanatory power of narrow wavelength regions in the SWIR for this gradient. In particular man-made materials such as metals and hydrocarbons as well as minerals show specific absorption features in these wavelength regions. Since the second gradient largely describes variation in these materials, the regression coefficients are in line with the pattern to be expected. Multispectral sensors provide only a few broad bands in the SWIR region; we thus expect that multispectral data are less suitable for modelling the second gradient.

7. Conclusion and outlook

According to our best knowledge, this is the first study that retrieves surface material compositions from simulated spaceborne imaging spectroscopy data with a spatial resolution of 30 m. A concept developed for mapping floristic gradients in natural environments was applied to an urban test site in Munich, Germany, to explore the capability of this method to retrieve surface material compositions from 30 m simulated EnMAP data. It has been demonstrated that there are gradual changes in material compositions in urban areas and that these gradients can be related to patterns of surface reflectance of simulated EnMAP data. The predicted gradient scores for the simulated EnMAP data results in patterns of material compositions that are related to a rural-to-urban

transect (gradient 1) and allow the differentiation of structural subtleties associated with urban structures (gradient 2). The first gradient ranges from fully pervious materials, such as different vegetated surfaces, water bodies and open soils, to fully impervious materials such as roofing materials, concrete and asphalt pavements and metals. Although the second gradient is not as pronounced as the first gradient, it contains information about material related structural subtleties that can be linked to the use and function of built-up areas. A brightness gradient as, for example, described in [Small and Lu \(2006\)](#) could not be clearly observed in both gradients.

It is, however, important to note that DCA and, thus, also the gradient approach used in this study are data-driven and the extracted gradients are not simply transferable to other urban environments. The gradient analysis only considers materials that are included in the training dataset. Due to this fundamental constraint, the DCA-space only describes gradual transitions in the material composition of Munich. Any other urban environment may comprise new materials that are not represented by the Munich dataset. The Munich gradients are most likely not fully suitable to describe these environments, and customized gradients have to be determined from a local training dataset. However, this opens up the potential for further investigations. Since the underlying approach is data-driven, the robustness of the identified gradients needs to be tested. The consideration of a larger area of Munich, including more and possibly different urban materials, would be the first step to analyse the robustness of the gradient interpretation. Special emphasis should be placed on previously underrepresented material compositions of common urban structures (e.g. high-rise buildings) and neighbourhoods with similar material compositions such as “industry” and “high-rise buildings”.

In addition, the influence of sample size and sample distribution should be further analysed. If the polygon area is large enough to contain a mixture of different materials, the gradient analysis will always come to a result, even if the material composition does not change gradually. However, in this case, the dimensionality reduction will be rather weak and result in many short gradients that are hardly interpretable. On the other hand, if the polygon area is too small, the gradient analysis will fail to extract the gradients since the co-occurrences of materials are not adequately represented in the sampled data. In our study, the gradient analysis resulted in two long gradients that could easily be interpreted. This indicates that the polygon diameter of 100 m was sufficient for the purpose of this study. The quantity and size of the samples (Fig. 2) result in a sampling coverage of 8.6% of the total area, with the proportion of 6-11% (Table 1) for each material class regardless

of its occurrence in the study area. Accordingly, natural over- or under-representations of material classes are taken into account and also confirm the suitability of the selected sampling scheme for Munich. Further research is needed to investigate the effects of the sampling scale and design on the ordination outcome. This is an important aspect to investigate the transferability of the approach to other cities.

The study presented in this paper reveals the potential for determining urban surface material compositions from data of upcoming spaceborne imaging spectroscopy missions such as EnMAP, PRISMA or HISUI. Although the pixel size of this data ($30\text{ m} \times 30\text{ m}$) is too coarse to resolve most of the urban objects, the gradient analysis seems to be a suitable method to investigate the resulting complex spectral mixtures. The advantage of using the gradient analysis is that 1) no pure EMs are required and 2) material compositions and material co-occurrences can be retrieved that go beyond VIS or extended VIS categories. Thus, spaceborne imaging spectroscopy data could be a valuable and complementary data source for urban studies where surface material information are essential such as for urban climate modelling, urban physical modelling and for sustainable urban planning. The design of the presented study and the achieved insights build an important fundament for future analyses that will explore the extent and conditions to which the gradient concept can be transferred to unknown urban areas.

Acknowledgements: The authors would like to thank the German Aerospace Center e.V. (DLR) – Space Administration, Germany, and the Ministry of Economics and Technology (BMWi), Germany, for funding the EnFusionMAP project (50 EE 1343). We would also like to thank Dr. Karl Segl from Deutsches GeoForschungsZentrum (GFZ) in Potsdam, Germany, for simulating the EnMAP data and Dr. Wieke Heldens for providing the surface material map of Munich. Furthermore we would like to thank Dr. Nicole Pinnel for final proof reading and four anonymous reviewers for their constructive comments that helped to improve the manuscript.

References

- Abrams, M.J., & Hook, S. J. (2013). NASA's hyperspectral infrared imager (HyspIRI). In Kuenzer, C., S. Dech, S. (Eds.), *Thermal Infrared Remote Sensing*, Springer, New York, NY, USA, pp. 117–130.
- Adams, J. B., Smith, M. O., & Johnson, P. E. (1986). Spectral mixture modeling: a new analysis of rock and soil types at the Viking Lander 1 site. *Journal of Geophysical Research*, 91 8098 - 8112.
- Adams, J. B., & Smith, M. O. (1986): Spectral mixture modeling: A new analysis of rock and soil types at the Viking Lander 1 site. *Journal of Geophysical Research*, 91(B8), 8098–8112.
- Adams, J. B., & Gillespie, A. R. (2006). *Remote sensing of landscapes with spectral images: A physical modeling approach*. Cambridge University Press, Cambridge, UK.
- Alberti, M. (2005). The effects of urban patterns on ecosystem function. *International Regional Science Review*, 28, 168–192.
- Alonzo, M., McFadden, J.P., Nowak, D.J., & Roberts, D.A. (2016). Mapping urban forest structure and function using hyperspectral imagery and lidar data. *Urban Forestry & Urban Greening*, 17, 135–147.
- Asner, G. P., & Heidebrecht, K. B. (2002). Spectral unmixing of vegetation, soil and dry carbon cover in arid regions: comparing multispectral and hyperspectral observations. *International Journal of Remote Sensing*, 23(19), 3939–3958.
- Asner, G. P., & Lobell, D. B. (2000). A Biogeophysical approach for automated SWIR unmixing of soils and vegetation. *Remote Sensing of Environment*, 74, 99–112.
- Bagan, H., & Yamagata, Y. (2012). Landsat analysis of urban growth: How Tokyo became the world's largest megacity during the last 40years. *Remote Sensing of Environment*, 127, 210-222.
- Bochow, M., Segl, K., & Kaufmann, H. (2007). An Update System for Urban Biotope Maps Based on Hyperspectral Remote Sensing Data. *Proceedings of 5th EARSeL Workshop on Imaging Spectroscopy*, Bruges, Belgium, April 23-25.
- Bruse, M., & Fleer, H. (1998). Simulating surface-plant-air interactions inside urban environments with a three dimensional numerical model. *Environmental Modelling and Software*, 13(3–4), 373–384.
- Cai, J., Huang, B., & Song, Y. (2017). Using multi-source geospatial big data to identify the structure of polycentric cities. *Remote Sensing of Environment*, 202, 210-221.
- Carter, J.G., Cavan, G., Connelly, A., Guy, S., Handley, J., & Kazmierczak, A. (2015). Climate change and the city: Building capacity for urban adaptation. *Progress in Planning*, 95, 1-66.
- Cavalli, R.M., Fusilli, L., Pascucci, S., Pignatti, S., & Santini, F. (2008). Hyperspectral sensor data capability for retrieving complex urban land cover in comparison with multispectral data: Venice City case study (Italy). *Sensors* 2008, 8(5), 3299–3320.
- Chen, F., Bornstein, R., Grimmond, S., Li, J., Liang, X., Martilli, A., Miao, S., Voogt, J., & Wang, Y. (2012). Research priorities in observing and modeling urban weather and climate. *Bull. American Meteorological Society*, 93, 1725-1728.
- Cocks, T., Jenssen, A., Stewart, A., Wilson, I., & Shields, T. (1998). The HyMap airborne hyperspectral sensor: The system, calibration and performance. *Proceedings of the 1st EARSeL Workshop on Imaging Spectroscopy*, Zurich, Switzerland, October 6–8, pp. 1–6.
- Crist, E.P., & Kauth, R.J. (1986). The Tasseled Cap de-mystified. *Photogrammetric Engineering and Remote Sensing*, 52(1), 81-86.
- Demarchi, L., Canters, F., Cariou, C., Licciardi, G., & Chan, J.C.-W. (2014). Assessing the performance of two unsupervised dimensionality reduction techniques on hyperspectral APEX data for high resolution urban land-cover mapping. *ISPRS Journal of Photogrammetry and Remote Sensing*, 87, 166–179.

- Demarchi, L., Canters, F., Chan, J.C.-W., & Van de Voorde, T. (2012a). Multiple endmember unmixing of CHRIS/Proba imagery for mapping impervious surfaces in urban and suburban environments. *IEEE Transactions on Geoscience and Remote Sensing*, 50(9), 3409–3424.
- Demarchi, L., Chan, J.C.-W., Ma, J., & Canters, F., (2012b). Mapping impervious surfaces from superresolution enhanced CHRIS/Proba imagery using multiple endmember unmixing. *ISPRS Journal of Photogrammetry and Remote Sensing*, 72, 99–112.
- Dennison, P. E., & Roberts, D. A. (2003). endmember selection for mapping chaparral species and fraction using Multiple endmember Spectral Mixture Analysis. *Remote Sensing of Environment*, 41, 123–135.
- Duca, R., Del Frate, F. (2008). Hyperspectral and multiangle CHRIS-PROBA images for the generation of land cover maps. *IEEE Transactions on Geoscience and Remote Sensing*, 46(10), 2857-2866.
- EEA (2017). Copernicus Land Monitoring Service – Local Component: Urban Atlas. (Online: <https://land.copernicus.eu/user-corner/publications/ua-flyer/view> (accessed September 17, 2018)).
- Esch, T., Heldens, W., Hirner, A., Keil, M., Marconcini, M., Roth, A., Zeidler, J., Dech, S., & Strano, E. (2017). Breaking new ground in mapping human settlements from space - The Global Urban Footprint. *ISPRS Journal of Photogrammetry and Remote Sensing*, 134, 30-42.
- Fan, F., & Deng, Y. (2014). Enhancing endmember selection in multiple endmember spectral mixture analysis (MESMA) for urban impervious surface area mapping using spectral angle and spectral distance parameters. *International Journal of Applied Earth Observation and Geoinformation*, 33, 290-301.
- Feilhauer, H., Dahlke, C., Doktor, D., Lausch, A., Schmidtlein, S., Schulz, G., & Stenzel, S. (2014). Mapping the local variability of Natura 2000 habitats with remote sensing. *Applied Vegetation Science*, 17, 765–779.
- Feilhauer, H., Faude, U., & Schmidtlein, S. (2011). Combining Isomap ordination and imaging spectroscopy to map continuous floristic gradients in a heterogeneous landscape. *Remote Sensing of Environment*, 115, 2513–2524.
- Feilhauer, H., & Schmidtlein, S. (2009). Mapping continuous fields of forest alpha and beta diversity. *Applied Vegetation Science*, 12, 429-439.
- Franke, J., Roberts, D.A., Halligan, K., & Menz, G. (2009). Hierarchical Multiple Endmember Spectral Mixture Analysis (MESMA) of hyperspectral imagery for urban environments. *Remote Sensing of Environment*, 113(8), 1712-1723.
- Gilbert, O.L. (1994). *Städtische Ökosysteme*. Neumann Verlag, Radebeul, Germany.
- Guanter, L., Kaufmann, H., Segl, K., Foerster, S., Rogass, C., Chabrillat, S., Kuester, T., Hollstein, A., Rossner, G., Chlebek, C., Straif, C., Fischer, S., Schrader, S., Storch, T., Heiden, U., Mueller, A., Bachmann, M., Muehl, H., Mueller, R., Habermeyer, M., Ohndorf, A., Hill, J., Buddenbaum, H., Hostert, P., Van der Linden, S., Leitão, P.J., Rabe, A., Doerffer, R., Krasemann, H., Xi, H., Mauser, W., Hank, T., Locherer, M., Rast, M., Staenz, K., & Sang, B. (2015). The EnMAP Spaceborne Imaging Spectroscopy Mission for Earth Observation. *Remote Sensing*, 7, 8830-8857.
- Grimm, N. B., Faeth, S. H., Golubiewski, N. E., Redman, C. L., Wu, J., Bai, X., & Briggs, J. M. (2008). Global change and the ecology of cities. *Science*, 319(5864), 756-760.
- Gu, H., Singh, A., & Townsend, P. (2015). Detection of gradients of forest composition in an urban area using imaging spectroscopy. *Remote Sensing of Environment*, 167, 168-180.
- Guarini, R., Loizzo, R., Longo, F., Mari, S., Scopa, T., & Varacalli, G. (2017). Overview of the prisma space and ground segment and its hyperspectral products. *IEEE International Geoscience and Remote Sensing Symposium (IGARSS)*, Fort Worth, TX, USA, July 23-28.
- Guo, H., Dou, C., Zhang, X., Han, C., & Yue, X. (2016). Earth observation from the manned low Earth orbit platforms. *ISPRS Journal of Photogrammetry and Remote Sensing*, 115, 103-118.

- Habermeyer, M., Marschalk, U., & Roth, A. (2008). Digital elevation model database W42-A scalable system for spatial data. *Proceedings of the ISPRS Conference, International Archives of the Photogrammetry, Remote Sensing and Spatial Information Sciences*, Beijing, China, July 3-11. pp. 1253–1258.
- Harris, A., Charnock, R., & Lucas, R.M. (2015). Hyperspectral remote sensing of peatland floristic gradients. *Remote Sensing of Environment*, 162 (1), 99–111.
- Heiden, U., Segl, K., Roessner, S., & Kaufmann, H. (2003). Ecological evaluation of urban biotope types using airborne hyperspectral HyMap data. *Proceedings of the 2nd GRSS/ISPRS Joint Workshop on Remote Sensing and Data Fusion over Urban Areas*, Berlin, Germany, May 22-23.
- Heiden, U., Segl, K., Roessner, S., & Kaufmann, H. (2007). Determination of robust spectral features for identification of urban surface materials in hyperspectral remote sensing data. *Remote Sensing of Environment*, 111, 537-552.
- Heiden, U., Heldens, W., Roessner, S., Segl, K., Esch, T., & Mueller, A., (2012). Urban structure type characterization using hyperspectral remote sensing and height information. *Landscape and Urban Planning*, 105(4), 361-375.
- Heldens, W. (2010). Use of airborne hyperspectral data and height information to support urban micro climate characterisation. PhD thesis. University Würzburg, Germany. (Online: <https://opus.bibliothek.uni-wuerzburg.de/opus4-wuerzburg/frontdoor/index/index/docId/4060> (accessed March 9, 2018)).
- Herold, M., Goldstein, N.C., & Clarke, K.C. (2003). The spatiotemporal form of urban growth: measurement, analysis and modeling. *Remote Sensing of Environment*, 86(3), 286-302.
- Hill, M.O. (1973). Reciprocal averaging: an eigenvector method of ordination. *Journal of Ecology*, 61, 237-249.
- Hill, M.O., & Gauch, H.G. (1980). Detrended Correspondence Analysis: an improved ordination technique. *Vegetatio*, 42, 47-58.
- Keshava, N. (2003). A Survey of Spectral Unmixing Algorithms. *Lincoln Laboratory Journal*, 14(1), 55–78.
- Knyazikhin, Y., Schull, M.A., Stenberg, P., Mottus, M., Rautiainen, M., Yang, Y., Marshak, A., Latorre Carmona, P., Kaufmann, R.K., Lewis, P., Disney, M.I., Vanderbilt, V., Davis, A.B., Baret, F., Jacquemoud, S., Lyapustin, A., & Myneni, R.B.(2013). Hyperspectral remote sensing of foliar nitrogen content. *Proceedings of the National Academy of Sciences of the United States of America*, 110 (3), E185-E192.
- Lakes, T., & Kim, H.-O. (2012). The urban environmental indicator “Biotope Area Ratio” - An enhanced approach to assess and manage the urban ecosystem services using high resolution remote-sensing. *Ecological Indicators*, 13(1), 93-103.
- Lefebvre, A. (2015): Feasibility study about the mapping and monitoring of green linear features based on VHR satellites imagery - EEA/MDI/14/006. Final Report, SIRS, Villeneuve-d'Ascq, France, (Online: <http://land.copernicus.eu/user-corner/technical-library/study-lead-by-sirs> (accessed September 05, 2018)).
- Licciardi, G.A., & Del Frate, F. (2011). Pixel Unmixing in Hyperspectral Data by Means of Neural Networks. *IEEE Transactions on Geoscience and Remote Sensing*, 49(11), 4163–4172.
- Maier, R., Punz, W., Dörflinger, A.N., Hietz, P., Brandlhofer, M., & Fussenegger, K. (1996). Ökosystem Wien - Die Subsysteme und deren Vegetationsstruktur. *Verhandlungen der Zoologisch-Botanischen Gesellschaft in Wien. Zoologisch-Botanische Gesellschaft in Wien*, 133, 1-26. (Online: https://www.zobodat.at/pdf/VZBG_133_0001-0026.pdf (accessed September 05, 2018)).

- Martens, H., & Martens, M. (2000). Modified Jack-knife estimation of parameter uncertainty in bilinear modelling by partial least squares regression (PLSR). *Food Quality and Preference*, 11, 5–16.
- Matsunaga, T., Iwasaki, A., Tsuchida, S., Tanii, J., Kashimura, O., Nakamura, R., Yamamoto, H., Tachikawa, T., & Rokugawa, S. (2014). Current status of Hyperspectral Imager Suite (HISUI). *IEEE International Geoscience and Remote Sensing Symposium (IGARSS)*, Québec, Canada, July 13–18.
- McCune, B., Grace, J.B., & Urban, D.L. (2002). *Analysis of ecological communities*. MjM Software Design, Gleneden Beach, OR, USA.
- Mueller, R., Cerra, D., Carmona, E., Alonso, K., Bachmann, M., Gerasch B., & Krawczyk, H. (2017). The Hyperspectral Sensor DESIS on MUSES: Processing and Applications. *International Symposium on Remote Sensing of Environment (ISRSE)*, Tshwane, South Africa, May 8-12.
- Mueller, R., Lehner, M., Reinartz, P., & Schroeder, M. (2005). Evaluation of Spaceborne and Airborne Line Scanner Images using a Generic Ortho Image Processor. *Proceedings of the 2005 ISPRS High Resolution Earth Imaging for Geospatial Information*, Hannover, Germany, May 17–20, Volume XXXVI.
- Neumann, C., Itzerott, S., Weiss, G., Kleinschmit, B., & Schmidtlein, S. (2016). Mapping multiple plant species abundance patterns - A multiobjective optimization procedure for combining reflectance spectroscopy and species ordination. *Ecological Informatics*, 36, 61-76.
- Neumann, C., Weiss, G., Schmidtlein, S., Itzerott, S., Lausch, A., Doktor, D., & Brell, M. (2015). Gradient-Based Assessment of Habitat Quality for Spectral Ecosystem Monitoring. *Remote Sensing*, 7(3), 2871-2898.
- Neville, R. A., Lévesque, J., Staenz, K., Nadeau, C., Hauff, P., & Borstad, G. A. (2003). Spectral unmixing of hyperspectral imagery for mineral exploration: comparison of results from SFSI and AVIRIS. *Canadian Journal of Remote Sensing*, 29(1), 99–110.
- Niemela, J. (1999). Ecology and urban planning. *Biodiversity and Conservation*, 8(1), 119-131.
- Okin, G. S., Roberts, D. A., Murray, B., & Okin, W. J. (2001). Practical limits on hyperspectral vegetation discrimination in arid and semiarid environments. *Remote Sensing of Environment*, 77, 212–225.
- Okujeni, A., Van der Linden, S., Tits, L., Somers, B., & Hostert, P. (2013). Support vector regression and synthetically mixed training data for quantifying urban land cover. *Remote Sensing of Environment*, 137, 184-197.
- Okujeni, A., Van der Linden, S., & Hostert, P. (2015). Extending the vegetation–impervious–soil model using simulated EnMAP data and machine learning. *Remote Sensing of Environment*, 158, 69-80.
- Pesaresi, M., Ehrlich, D., Ferri, S., Florczyk, A.J., Freire, S., Halkia, M., Julea, A., Kemper, T., Soille, P., & Syrris, V. (2016). Operating Procedure for the Production of the Global Human Settlement Layer from Landsat Data of the Epochs 1975, 1990, 2000, and 2014. Publications Office of the European Union, EUR 27741 EN, JRC Technical Report.
- Priem, F., & Canters, F. (2016). Synergistic Use of LiDAR and APEX Hyperspectral Data for High Resolution Urban Land Cover Mapping. *Remote Sensing*, 8(10), 787.
- Richter, R. (2009). *ATCOR 4 User Guide*. DLR-German Aerospace Centre, Remote Sensing Data Centre, Oberpfaffenhofen, Germany.
- Ridd, M.K. (1995). Exploring a V-I-S (Vegetation-Impervious Surface-Soil) Model for Urban Ecosystem Analysis through Remote-Sensing - Comparative Anatomy for Cities. *International Journal of Remote Sensing*, 16(12), 2165-2185.
- Roberts, D.A., Gardner, M., Church, R., Ustin, S., Scheer, G., & Green, R.O. (1998). Mapping Chaparral in the Santa Monica Mountains Using Multiple Endmember Spectral Mixture Models. *Remote Sensing of Environment*, 65, 267–279.

- Roberts, D.A., Quattrochi, D.A., Hulley, G.C., Hook, S.J., & Green, R.O. (2012). Synergies between VSWIR and TIR data for the urban environment: An evaluation of the potential for the Hyperspectral Infrared Imager (HyspIRI) Decadal Survey mission. *Remote Sensing of Environment*, 117, 83-101.
- Roberts, D. A., Alonzo, M., Wetherley, E., Dudley, K., & Dennison, P. (2017). Multiscale analysis of urban areas using mixing models. In Quattrochi, D. A., Wentz, E., Lam, N. S., Emerson, C. W. (Eds.), *Integrating Scale in Remote Sensing and GIS*, CRC press, New York, NY, USA, pp. 247-282.
- Rocchini, D., Luque, S., Pettorelli, N., Bastin, L., Doktor, D., Faedi, N., Feilhauer, H., Féret, J.B., Foody, G.M., Gavish, Y., Godinho, S., Kunin, W.E., Lausch, A., Leitão, P.J., Marcantonio, M., Neteler, M., Ricotta, C., Schmidtlein, S., Vihervaara, P., Wegmann, M., Nagendra, H. (2018). Measuring β -diversity by remote sensing: a challenge for biodiversity monitoring. *Methods in Ecology and Evolution*, 9, 1787-1798.
- Roessner, S., Segl, K., & Heiden, U. (2000). Comparison of automated methods for identification of urban surfaces using airborne hyperspectral data of reflective and thermal wavelength ranges. 2nd EARSeL workshop on imaging spectroscopy, Enschede, The Netherlands, July 11-13.
- Roessner, S., Segl, K., Heiden, U., & Kaufmann, H. (2001). Automated differentiation of urban surfaces based on airborne hyperspectral imagery. *IEEE Transactions on Geoscience and Remote Sensing*, 39(7), 1525–1532.
- Roessner, S., Segl, K., Bochow, M., Heiden, U., Heldens, W., & Kaufmann, H. (2011). Potential of hyperspectral remote sensing for analyzing the urban environment. In Yang, X. (Ed.), *Urban remote sensing: Monitoring, synthesis and modeling in the urban environment*, John Wiley and Sons Ltd., Oxford, UK, pp. 49–62.
- Rogge, D.M., Rivard, B., Zhang, J., & Feng, J. (2006). Iterative spectral unmixing for optimizing per-pixel endmember sets. *IEEE Transactions on Geoscience and Remote Sensing*, 44(12), 3725-3736.
- Rosentreter, J., Hagensieker, R., Okujeni, A., Roscher, R., Wagner, P.D., & Waske, B. (2017). Subpixel Mapping of Urban Areas Using EnMAP Data and Multioutput Support Vector Regression. *IEEE Journal of Selected Topics in Applied Earth Observations and Remote Sensing*, 10(5), 1938-1948.
- Roth, K. L., Dennison, P. E., & Roberts, D. A. (2012). Comparing endmember selection techniques for accurate mapping of plant species and land cover using imaging spectrometer data. *Remote Sensing of Environment*, 127, 139–152.
- Schmidtlein, S., Feilhauer, H., & Bruehlheide, H. (2012). Mapping plant strategy types using remote sensing. *Journal of Vegetation Science*, 23, 395–405.
- Schmidtlein, S., & Sassini, J. (2004). Mapping continuous floristic gradients in grasslands using hyperspectral imagery. *Remote Sensing of Environment*, 92, 126-138.
- Schmidtlein, S., Zimmermann, P., Schüpferling, R., & Weiß, C. (2007). Mapping the floristic continuum: Ordination space position estimated from imaging spectroscopy. *Journal of Vegetation Science*, 18, 131-140.
- Segl, K., Roessner, S., Heiden, U., & Kaufmann, H. (2003). Fusion of spectral and shape features for identification of urban surface cover types using reflective and thermal data. *ISPRS Journal of Photogrammetry and Remote Sensing*, 58(1-2), 99-112.
- Segl, K., Bochow, M., Roessner, S., Kaufmann, H., & Heiden, U. (2006). Feature-based identification of urban endmember spectra using hyperspectral HyMap data. *Proceedings of the 1st EARSeL Workshop of the SIG Urban Remote Sensing*, Berlin, Germany, March 2-3.
- Segl, K., Guanter, L., Rogass, C., Kuester, T., Roessner, S., Kaufmann, H., Sang, B., Mogulsky, V., & Hofer, S. (2012). EeteS - The EnMAP end-to-end simulation tool. *IEEE Journal of Selected Topics in Applied Earth Observations and Remote Sensing*, 5(2), 522–530.

- Shashua-Bar, L., Tzmir, Y., & Hoffman, M.E. (2004). Thermal effects of building geometry and spacing on the urban canopy layer microclimate in a hot-humid climate in summer. *International Journal of Climatology*, 24(13), 1729–1742.
- Shimabukuro, Y.E., & Smith, J.A. (1991). The least-square mixing model to generate fraction images from remote sensing multispectral data. *IEEE Transactions on Geoscience and Remote Sensing*, 29(1), 16–20.
- Small, C. (2003). High spatial resolution spectral mixture analysis of urban reflectance. *Remote Sensing of Environment*, 88(1–2), 170–186.
- Small, C., & Lu, J.W.T. (2006). Estimation and vicarious validation of urban vegetation abundance by spectral mixture analysis. *Remote Sensing of Environment*, 100(4), 441–456.
- Somers, B., Asner, G.P., Tits, L., & Coppin, P. (2011). Endmember variability in Spectral Mixture Analysis: A review. *Remote Sensing of Environment*, 115(7), 1603–1616.
- Stewart, I.D., & Oke, T.R. (2012). Local climate zones for urban temperature studies. *Bull. American Meteorological Society*, 93(12), 1879–1900.
- Sukopp, H., & Weiler, S. (1988). Biotope mapping and nature conservation strategies in urban areas of the Federal Republic of Germany. *Landscape and Urban Planning*, 15(1–2), 39–58.
- Taleghani, M., Kleerekoper, L., Tenpierik, M., & van den Dobbelsteen, A.A.J.F. (2015). Outdoor thermal comfort within five different urban forms in the Netherlands. *Building and Environment*, 83, 65–78.
- Tobler, W.R. (1970). A computer movie simulating urban growth in the Detroit region. *Economic Geography*, 46, 234–240.
- Tong, Q., Xue, Y., & Zhang, L. (2014). Progress in Hyperspectral Remote Sensing Science and Technology in China Over the Past Three Decades. *IEEE Journal of Selected Topics in Applied Earth Observations and Remote Sensing*, 7(1), 70–91.
- UN (2014). *World Urbanization Prospects: The 2014 Revision*, United Nations, New York, NY, USA, (Online: <https://esa.un.org/unpd/wup/Publications/Files/WUP2014-Report.pdf> (accessed March 16, 2018)).
- Voltersen, M., Berger, C., Hese, S., & Schmullius, C. (2014). Object-based land cover mapping and comprehensive feature calculation for an automated derivation of urban structure types at block level. *Remote Sensing of Environment*, 154, 192–201.
- Wang, Z., Skidmore, A.K., Wang, T., Darvishzadeh, R., Heiden, U., Heurich, M., Latifi, H., & Hearne, J. (2017). Canopy foliar nitrogen retrieved from airborne hyperspectral imagery by correcting for canopy structure effects. *International Journal of Applied Earth Observation and Geoinformation*, 54, 84–94.
- Weng, Q., Hu, X., & Lu, D. (2008). Extracting impervious surfaces from medium spatial resolution multispectral and hyperspectral imagery: A comparison. *International Journal of Remote Sensing*, 29, 3209–3232.
- Weng, Q., & Lu, D. (2008). A sub-pixel analysis of urbanization effect on land surface temperature and its interplay with impervious surface and vegetation cover in Indianapolis, United States. *International Journal of Applied Earth Observation*, 10, 68 – 83.
- Willmott, C.J., & Matsuura, K. (2005). Advantages of the mean absolute error (MAE) over the root mean square error (RMSE) in assessing average model performance. *Climate Research*, 30, 79–82.
- Winter, M.E., Lucey, P.G., & Steutel, D. (2003). Examining Hyperspectral Unmixing Error Reduction due to Stepwise Unmixing. In: Shen, S.S., Lewis, P.E. (Eds.) *Proceedings of SPIE(5093), AeroSense 2003, Algorithms and Technologies for Multispectral, Hyperspectral, and Ultraspectral Imager IX*, Orlando, FL, USA, April 21–25, pp. 380–389.
- Wittig, R., Sukopp, H., & Klausnitzer, B. (1998). Die ökologische Gliederung der Stadt. In: Sukopp H. and Wittig R. (Eds.) *Stadtökologie*, Gustav Fischer Verlag, Stuttgart, Germany, pp. 316–372.

- Wold, S., Sjöström, M., & Eriksson, L. (2001). PLS-regression: A basic tool of chemometrics. *Chemometrics and Intelligent Laboratory Systems*, 58, 109–130.
- Xu, B., & Gong, P. (2007). Land-use/Land-cover classification with multispectral and hyperspectral EO-1 data. *Photogrammetric Engineering and Remote Sensing*, 73, 955–965.
- Zaichko, V. (2014). Current Status and Plans for the Development of the Russian Space Systems for Earth Remote Sensing. 28th CEOS Plenary, Tromso, Norway, October 29-30.
- Zare, A., & Ho, K.C. (2014). Endmember Variability in Hyperspectral Analysis: Addressing Spectral Variability During Spectral Unmixing. *IEEE Signal Processing Magazine*, 31(1), 95-104.
- Zhang, C. (2016). Multiscale quantification of urban composition from EO-1/Hyperion data using object-based spectral unmixing. *International Journal of Applied Earth Observation and Geoinformation*, 47, 153-162.

CHAPTER V

Synthesis

This thesis focuses on mapping of urban surface materials with imaging spectroscopy data on different spatial scales. In particular, it deals with the automated extraction and identification of spectrally pure pixels from airborne imaging spectroscopy data, taking into account the limitations of using an urban image spectral library in terms of transferability. In addition, it deals with the analysis of complex urban spectral mixtures that result from simulated spaceborne imaging spectroscopy data based on a spatial resolution of 30 m. In the following sections, the results that have been achieved are discussed (section 5.1) with regard to the research objectives and in the broader context of this thesis and finally a main conclusion and an outlook (section 5.2) on further research directions is given.

5.1 Overall discussion

This section aims to, summarize the most general discussion aspects, which are mainly addressed in detail in each of the stand-alone manuscripts presented in chapter II, III and IV, to answer the three main research questions outlined in section 1.4.

a) Can an initial urban spectral library be used to automatically extract and identify sensor- and site-independent, scene-based endmembers from high spatial resolution imaging spectroscopy data that are required for further mapping techniques?

In chapter II a framework of a learning urban image spectral archive – called LUISA, was developed. LUISA is a two modular concept for the automatic determination and identification of spectrally pure pixels using high spatial resolution airborne imaging spectroscopy data from urban environments. The modules comprise an initial spectral archive (LUISA-A) for data storage and organization, and a toolbox (LUISA-T) consisting of methods for the determination and identification of scene-based spectrally pure pixels. Spectral resampling and adaptation of reference spectra in the initial spectral library onto the spectral characteristics of the used image data facilitates a sensor independent application. Spectrally pure pixels are determined by an iterative pixel-by-pixel thresholding approach of spectral similarities based on the user-defined choice of an implemented spectral similarity measure. A hierarchically organized structure of reference spectra in the initial spectral library allows a posterior implementation of new scene-based

pure material spectra. Thus, the initial spectral library can be expanded to overcome the lack of potentially missing spectral inter- and intra-class variabilities for the application of the LUISA framework in a new study area. Based on a dissimilarity analysis - presented and verified in detail in chapter III – unknown spectrally pure pixels can be detected as well to improve the subsequent mapping of urban surface materials. This development demonstrate the potentials of using an incomplete urban spectral library (i.e. missing reference spectra of certain material classes and incomplete representation of spectral variability of urban surface materials)

The LUISA framework was applied on a new study site for which no pure material spectra were available in the initial spectral library. For this study site spectrally pure pixels were determined by the LUISA framework and used as training data for a supervised classification to map urban surface materials in detail. Results of the classification showed a promising overall accuracy of 79.8% and a kappa of 0.76 for the known material classes. Errors result from confusions of material classes due to spectral similarities such as asphalt, dark bitumen and concrete as well as between red loose chippings and red roofing tiles. Asphalt and concrete spectra are known for spectral confusions (Heiden et al., 2007) due to a similar spectral shape and the almost missing spectral features in their spectral signature. These materials are known to be discriminable by their albedo differences (Heiden et al., 2007). Consequently, the used similarity measure SID-SCA (hybrid measure of Spectral Information Divergence and Spectral Correlation Angle; Naresh Kumar et al., 2011) does not seem to sufficiently consider the albedo differences of the spectra in order to assign determined spectrally pure pixels to the responsible surface material class. Thus, further research is needed to analyse differences in the classification accuracies while using different similarity measures for urban areas. Confusion of red loose chippings and red roofing tiles also results from rather minor spectral differences which are caused by the variations of texture of these surface materials. Their differentiation only by spectral characteristics is therefore very difficult. Knowledge about the general occurrence of specific surface materials to be used on certain types of urban objects (e.g. roofing or paving) could be used to improve the identification by means of auxiliary information such as a building mask, the consideration of rule-based identification or height information.

However, the quality of the subsequent mapping results proved the usability of a spectral library on a new test site to determine a sufficient number of spectrally pure pixels for mapping urban surface materials. Due to the similarity conditions, the presented approach

only allows the extraction of spectrally similar pixels, which take to a certain degree the spectral variability of surface materials into account. This means, that the spectral library can be transferred to new study areas and does not lead to an incorrect extraction of mixed pixels. The application of this method only has to take into account the difficulties in the automated identification of the previously determined spectrally pure pixels.

The possibility to implement new reference spectra in LUISA-A might also enhance the applicability for a new area by improving the spectral diversity of urban surface materials of the reference spectra. However, it is essential to ensure that spectra are carefully analysed in order to verify that these spectra are really new pure reference spectra, which would strongly affect the result in further studies. In addition, it has to be defined which of the scene-based known pure pixels are to be integrated, as they would extensively increase the intra-class variability and simultaneously the computation time for the pixel-by-pixel comparison of reference spectra with the pixels. It is therefore necessary to find a balance between the required intra-class variability and the number of reference spectra. Spectral library pruning techniques (e.g. [Degerickx et al., 2016](#)) could be helpful to avoid a user-dependent decision for or against the integration of new spectra in LUISA-A and simultaneously avoid redundant reference spectra. Spectral library pruning would also control the essential inter- and intra-class variability of the reference spectra.

The developed LUISA-framework was just tested in one unknown study area, which is assumed to be spectrally similar to the available reference spectra in the initial spectral library. An application of LUISA to a completely different geographical region (e.g. US American cities) acquired by a sensor other than HyMap is required in order to extensively analyse possible common problems in the entire determination of scene-based, sensor- and site-independent spectrally pure pixels. However, the very promising results from the presented study reveal the great potentials for the sensor- and site-independent use of a spectral library to determine spectrally pure pixels in urban areas. This opens up new possibilities for the development of generic urban spectral library.

The most important research developments for the use of LUISA can be summarised as follows:

- Automated determination of scene-based spectrally pure pixels using spectral similarity analysis
- Automated identification of spectrally pure pixels
- Applicability of an initial spectral library to a new study area without prior implementation of scene-, site-, and sensor-based reference spectra.

- High accuracies were obtained for a subsequent mapping of urban surface materials
- Framework does not require spectral expert knowledge
- Possibility for implementation of new reference spectra to enhance spectral variabilities of surface materials and for missing material classes

The limitations require further research and are related to:

- Confusions in the automated identification of spectrally similar surface materials
- Quality checks are not yet available for optional implementation of new reference spectra concerning redundancies
- Albedo differences of spectrally similar material classes are not (fully) considered by common similarity measures

b) Can an image-based spectral library be used to determine spectrally pure pixels in urban areas despite a potential incompleteness of the spectral library, so that it can be transferred to an unknown urban area?

Chapter III focuses on analysing the determination of unknown pure urban surface material spectra using a basic spectral library. This research is based on the development of the LUISA framework for airborne imaging spectroscopy data (chapter II) to overcome the limitations of an incomplete spectral library when applied to a new test site. Unknown spectrally pure urban pixels are determined based on a dissimilarity analysis using a basic spectral library. Spectral similarities of pixels to reference spectra from the basic spectral library are determined on a user-defined similarity measure (see above). A defined percentage of pixels (dissimilarity threshold) with a low similarity to the reference spectra are extracted for further analysis to determine unknown pure pixels. It is assumed that these pixels are not only represent spectral mixtures, but also the spectral signatures of pure unknown urban surface materials, which are missing in the basic spectral library due to their application to a new study site. However, to avoid a fixed threshold for the extraction of these potentially unknown pure pixels, the number of dissimilar pixels is automatically extended. For this purpose, a second similarity analysis is performed using the extracted dissimilar pixels as reference spectra. Pixels that are more similar to the extracted dissimilar pixels are integrated to the analysis to distinguish mixed pixels from unknown pure pixels. For this analysis, neighbourhood relations are considered, since it is assumed that pure materials exist mainly on larger objects consisting of an agglomeration of pixels with similar spectra. Potentially pure unknown pixels are categorised into

unknown material classes based on spectral inter- and intra-class-variabilities of spatial clusters (objects). This step allows spectral variabilities per unknown material class based on a spectral homogeneity criterion. The homogeneity criterion is based on a user-defined threshold using SAM (Spectral Angle Mapper; [Kruse et al., 1993](#)) as a well-known, commonly used, and easy to interpret similarity measure. A subsequent post-processing step removes the remaining mixed pixels based on neighbourhood relations and the number of pixels per unknown material class.

The dissimilarity analysis was applied to four test sites using different incomplete spectral libraries. In addition, the dissimilarity threshold was extensively analysed concerning its influence on the number and quality of the determined potentially unknown pure pixels. In general, the study presents that previously removed material classes for the simulation of incomplete spectral libraries could be recognized again in almost all experimental settings with dissimilarity analysis. For the simulation of incompleteness, reference spectra of roofing tiles were eliminated from the basic spectral library. The findings, in all test sites and all variations of the dissimilarity threshold, showed that only pixels of dark roof tiles could be recognized as unknown pure surface materials. This results from the spectral similarity of red roof tiles and red loose chippings, so that pixels from red roofing tiles were not extracted as potentially unknown pure pixels. Even an adjusted dissimilarity threshold does not lead to a consideration of these pixels as potentially unknown surface materials. An increasing dissimilarity threshold was found to mainly increase the number of spectral mixtures which are commonly aggregated into spatial clusters and thus failed in the steps to eliminate mixed pixels. At the same time, the number of pixels per unknown material class and thus the spectral intra-class variability was reduced.

Findings demonstrate only some misclassifications, e.g. due to the known issue of confusion with spectrally similar material classes when using an established spectral similarity measures (same issue as described above). Therefore, it can be assumed that the results could be improved by using an advanced similarity measure which also takes albedo differences into account (e.g. FusingSAF; [Ding et al., 2015](#)). It further shows that the more incomplete a spectral library is, the lower the number of re-detected pure pixels per material class and the higher the probability that they will not be re-detected.

A higher dissimilarity threshold was found to be more appropriate for this case. However, this observation relies on the investigation of only two missing material classes in the spectral library. It leads to the assumption that some prior knowledge about the completeness of the spectral library is preferable to specify the dissimilarity threshold.

Principally it can be stated that the more complete the basic spectral library, the more accurate the determination of unknown pure pixels using the dissimilarity analysis. However, even with a more incomplete spectral library, the dissimilarity analysis allows the transferability and use of an incomplete urban spectral library to extract unknown spectrally pure pixels from urban airborne imaging spectroscopy data.

The most important research developments can be summarised as follows:

- Applicability of an incomplete urban spectral library
- Determination of unknown spectrally pure pixels (due to incompleteness)
- Pre-categorization of determined unknown pure pixels to support identification
- Enhance library completeness by implementation of new reference spectra
- Spectral variability is considered in determined unknown material classes

The limitations of dissimilarity analysis require further research and are related to:

- Only spectrally dissimilar pure pixels can be determined as unknown material classes
- Requires manual labelling of determined and pre-categorized unknown material classes

c) Do complex urban spectral mixtures of spaceborne imaging spectroscopy data with a spatial resolution of 30 m form gradual material transitions and can they be mapped and analysed?

In chapter IV compositions of urban surface materials in spaceborne imaging spectroscopy data were analysed. This analysis is based on the adaptation of gradient analysis originally developed to map floristic gradients in natural environments. Results show that the occurrence of urban surface materials behaves similarly to vegetation species and forms interpretable urban material gradients. It turned out that the occurrence probability of urban surface materials is directly related to structural, historical and functional characteristics of the city and result in typical material compositions.

The adapted gradient analysis involves the investigation of transitions from urban surface materials, relation of urban material gradients with spectral mixtures of simulated spaceborne imaging spectroscopy data, and the analysis of typical compositions of urban surface materials for a test site in Munich. Therefore, regularly distributed samples (covering almost similar material proportions of 6% - 11% per material class) from a

detailed urban surface material map (determined from airborne imaging spectroscopy data) were used to analyse material compositions and occurrences in the test site, using the ordination method DCA (Detrended Correspondence Analysis; [Hill and Gauch, 1980](#)). Gradual material transitions in the gradient space resulting from the material occurrences obviously represent a gradient of imperviousness. The interpretation of a second gradient was found to be associated to structural differences in land use and function. The relation of gradients with the respective surface reflectance from simulated EnMAP data shows the formation of spectral patterns indicating similar material compositions.

Respective partial least square regression (PLSR; [Wold et al., 2001](#)) modelling, using 10-fold cross-validation, results for the first gradient model in $R^2 = 0.85$ and RMSE of 0.23 SD for calibration and $R^2 = 0.84$ with RMSE of 0.24 SD for validation, and for the second gradient model in $R^2 = 0.71$ with RMSE of 0.21 SD for calibration and $R^2 = 0.67$ with RMSE of 0.22 SD for validation. Spectral patterns resulting from similar material compositions interestingly correspond to the urban structure type (UST; [Wittig et al., 1998](#); [Gilbert, 1994](#); [Maier et al., 1996](#)) classification. A detailed analysis of the material compositions per UST shows typical compositions of consistent surface materials for at least 2/3 of the cover fractions. Surprisingly, these 2/3 cover fractions per sample are formed from a maximum of six different surface materials, although samples in built-up areas were found to consist of up to 24 different surface materials. However, the analysis of typical material compositions also shows that in structurally very different UST, such as high-rise buildings and industry, the typical material composition for this test site is identical and differs only in the cover fractions per material.

Material compositions in the second gradient are dependent on structural differences although detailed information such as height information are specifically not taken into account. In the mapping of gradient models, the spectral patterns of these areas are therefore difficult to distinguish. This may be due to the fact that the gradient analysis is a data-driven approach and only considers the composition of the materials in the respective samples. In addition, the number of samples that are used to analyse the characteristic material composition of an UST is also decisive, especially if only a small area of the study site with a very specific material composition belongs to an UST. A consideration of further samples which represent these initially similarly composed UST would prove or disprove their typical material compositions. Also the additional use of height information would support the differentiation. Presented as a proof-of-concept study and as a data-driven approach, further analyses regarding the effects of the implemented ordination and

regression methods are required. Also the impact of the determined samples (sampling scheme, size, number of samples) needs to be further analysed to give an impression of the transferability and stability of the methods in different urban areas.

However, the study has already shown the applicability of gradient analysis for the investigation of urban material compositions in spaceborne imaging spectroscopy data. The analysis go far beyond the categorisation of broader groups of materials and demonstrate the great potential to map urban surface materials with spaceborne imaging spectroscopy data. It is also an advantage that no prior knowledge of EMs or spectrally pure pixels from the study area is required.

The most important findings can be summarised as follows:

- More detailed analysis of material compositions that goes beyond the mapping of broader categories of aggregated materials groups
- Existence of typical material compositions dependent on structural, functional, and historical patterns in the city
- Formation and interpretation of urban material gradients
- Potentials towards an area-wide mapping of urban surface materials

The method ist limited due to:

- Data-driven approach
- Requires detailed information about surface material occurrences (e.g. detailed surface material map)

5.2 Main conclusion and prospects for urban surface material mapping with imaging spectroscopy

Effects caused by the occurrence of urban surface materials (section 1.3.1) have led to the need for detailed mapping of urban surface materials. The use of narrow band imaging spectrometers mounted on airborne or spaceborne platforms allows for a very fine differentiation of urban surface materials for larger areas (section 1.3.2). In addition to the spectral resolution, the spatial resolution is of fundamental importance (sections 1.2 and 1.3.2) for the methodology development of mapping urban surface materials.

Thus, this thesis focused on the development, application, and evaluation of methods for retrieving information on urban surface materials using imaging spectroscopy data with different spatial resolutions. The general requirements for the method's applicability were taken into account when analysing the characteristically high spatial and spectral conditions of the city, which are also subject to the fast processes of urbanisation (section 1.1). This includes, on the one hand, the reduction of limitations in the use of urban image spectral libraries with high spatial resolution data and on the other hand a more detailed analysis of material compositions from mixed pixels resulting from coarser spatial resolution.

Specifically a concept for overcoming the limitations while transferring urban spectral libraries using high spatial resolution airborne imaging spectroscopy data is introduced to derive scene-based spectrally pure pixels. Spectral libraries are still a major component in imaging spectroscopy and serve as data container to store and organize EMs or spectrally pure pixels for further image analysis. The developed LUISA concept is based on a spectral library consisting of spectrally pure pixels determined from a couple of urban training test sites. This includes the complete representation of the spectral intra- and inter-class variability of urban surface materials for the used training test sites that is required for a detailed mapping of urban surface materials. However, the applicability of a spectral library to a new urban area is associated with a lack of reference spectra of new materials as well as a lack of inter- and intra-class variabilities due to variations in illumination, degradation, sensor properties, and chemical and physical compositions (section 1.3.1). Missing spectral references of a new test site result in ignoring these newly occurring urban surface materials or spectral variabilities when using this spectral library to map

urban surface materials. These limitations in the transferability of a spectral library have been addressed by the methods based on spectral similarity and dissimilarity analysis to determine scene-based spectrally pure pixels for the subsequent mapping of urban surface materials. In general, this means that known and unknown spectrally pure pixels including the scene-based spectral variability of urban surface materials can be determined with the LUISA framework.

The development of LUISA represents a major progress in the determination of spectrally pure pixels from spatially and spectrally highly complex urban landscapes. This includes the automated determination and identification of scene-based spectrally pure pixels from an urban spectral library, which does not have to be complete and does not require any prior knowledge on the investigation site or spectral expertise. Thus, it overcomes the limitations of the transferability of an urban spectral library and shows new possibilities regarding the development of a generic urban spectral library. The results of the subsequent mapping of urban surface materials show the functionality of LUISA for a unknown test site.

However, it also reveals the limitations of the automated identification of certain urban surface materials by means of common similarity measures and confirms the importance of considering albedo (amplitude) differences in the determination of urban surface materials (Heiden et al., 2007). The similarity measures implemented in LUISA are those that are commonly used in the community, but all of them have been found not to take sufficient account of the amplitude to distinguish between spectrally similar urban surface materials. An adaption of a more sophisticated similarity measure (e.g. FusingSAF; Ding et al., 2015) would potentially further improve the results. Although confusion occurs in the identification of urban surface materials, the determined pixels are so far scene-based spectrally pure. A further critical point is the determination of unknown spectrally pure pixels which is limited to those that are to a certain degree dissimilar to existing reference spectra from the used spectral library. The responsible dissimilarity threshold is adjustable, but is also related to the incorrect implementation of mixed pixels the more similarity is tolerated in the analysis. A fine adjustment is therefore proposed.

Future research work for the development of a generic urban spectral library needs to comprehensively analyse the advantages and limitations of the developed LUISA framework. It has to be focus on quality assessments of newly implemented reference spectra to increase the completeness of the used spectral library. A constantly growing spectral library is also critical with regard to computation time, redundant spectra,

exaggerated inter- and intra-class variability and would be someday no longer be usable. Library pruning techniques (e.g. [Degerickx et al., 2016](#)) should control the quality and usability of such large spectral libraries. Prospective research recommendations for the development of a generic urban spectral library would improve the mapping of urban surface materials without the need for spectral expert knowledge.

The demand for regular area-wide monitoring of urban environment due to dynamic changes in land cover and land use (sections [1.1](#) and [1.3](#)) entailed the use of imaging spectrometers from space. Current restrictions due to data availability (section [1.2](#)) and the general applicability issues of former state of the art methods for mapping urban surface materials using a medium spatial resolution lead to a marginal number of research studies in this domain. The monitoring of urban areas with spaceborne imaging spectrometers result in almost only very complex spectral mixtures at this spatial scale.

With gradient analysis (chapter [IV](#)), information on the occurrence of urban surface materials in these complex spectral mixtures were determined for the first time. The adaptation of the method derived from vegetation ecology is based on the theory of structural divisions of cities, which forms the context for this research. Used as proof of concept for an urban test area, site-specific typical material compositions of spectral mixtures could be determined and analysed in a continuous field.

In particular, the ordination results from a sampled surface material map (similar as the one introduced in chapter [I](#)) showed a similar and explainable behaviour of typical compositions of urban surface materials versus the jointly occurrence of vegetation species in ecological habitats. Resulting formations of urban surface material gradients lead to logically interpretable transitions of urban surface materials with respect to imperviousness and structural compositions. The mapping of surface material compositions due to the relation of material gradients with spectral reflectance from simulated spaceborne imaging spectroscopy data demonstrate a typical composition of urban surface materials per administration unit.

The results show great potentials for mapping urban surface materials from spaceborne imaging spectroscopy data and open up a new field of research. First results of material gradients and characteristic material compositions needs to be analysed for stability and transferability of the method as it is a data driven approach. In addition to the analysis and selection of the most suitable gradient analysis methods (i.e. ordination, regression), this also includes the analysis of the selected sampling with regard to its impacts on the final

result, as well as the influence of the test site concerning a general statement on urban material gradients and the formation of typical material compositions. The great advantage for using gradient analysis is that no prior determination of EMs or spectrally pure pixels is needed, the spectral mixtures themselves remain as source of information. Detailed surface material maps required e.g. for an entire city, could be supported by the automated determination of spectrally pure pixels with LUISA to generate detailed surface material information.

Imaging spectroscopy data from airborne or spaceborne platforms are associated with different spatial resolutions, which still pose a challenge for mapping urban surface materials. The spatial resolution of imaging sensor systems is certainly decisive for the level of detail in mapping urban surfaces. However, also the temporal resolution and the possibility for an area wide mapping is still important when analysing urban areas. The ideal sensor system, which combines high spatial, spectral, and temporal resolution as well as the possibility of larger data coverage to enable a regular area-wide mapping of urban surface materials at subpixel level, will not be available in the near future.

In general, the importance of using hyperspectral data of different spatial scales for the mapping of surface materials has been confirmed. The information content of the spectral domain is superior to that of the spatial domain and also urban surface materials can even be acquired and analysed in 30 m imaging spectroscopy data. The obtained results show the enormous potential especially for analysing urban surface material occurrences on a larger scale, such as for an entire city, which is of great importance for studying the numerous urban processes e.g. urban climate modelling.

With the launch of the new spaceborne sensor systems, temporal high-resolution data will be available very soon and will allow an area wide spectral mapping of our highly dynamic cities. Due to the coarser spatial resolution of these sensors, compared to airborne systems, the use of airborne sensors will still remain of great importance for spatially very detailed analyses. Recent developments in the fusion of spatial imaging spectroscopy data with multispectral data (e.g. [Yokoya et al., 2012](#); [Selva et al., 2015](#); [Yokoya et al., 2017](#)) to combine high spectral resolution with high spatial resolution appear to be very promising and may overcome the limitations of sensor properties when using data from a single sensor system. Such fused data sets could meet the requirements of remote sensing for the very detailed analysis of the occurrence of urban surface materials to provide this basic source of information for the investigation of urban processes and impacts.

References

The references from section II, III, and IV are given at the end of each section, as these sections are structured as stand-alone manuscripts.

Abrams, M.J., Hook, S.J., (2013). NASA's hyperspectral infrared imager (HyspIRI). In: Kuenzer, C., Dech, S. (Eds.), *Thermal Infrared Remote Sensing*. Springer, New York, NY, USA, pp. 117–130.

Adams, J.B., Smith, M.O., (1986). Spectral mixture modeling: a new analysis of rock and soil types at the Viking Lander 1 site. *J. Geophys. Res.* 91 (B8), 8098–8112

Adams, J.B., Smith, M.O., Gillespie, A.R., (1993). Imaging spectrometry: Interpretation based on spectral mixture analysis. In *Remote geochemical analysis: Elemental and mineralogical composition* (eds. C.M. Pieters and P. Englert). pp. 145–166. New York, NY: Cambridge University Press.

Adams, J.B., Gillespie, A.R., (2006). *Remote Sensing of Landscapes with Spectral Images: A Physical Modeling Approach*. Cambridge University Press, Cambridge, UK.

Adeline, K.R.M., Chen, M., Briottet, X., Pang, S.K., Paparoditis, N., (2013) Shadow detection in very high spatial resolution aerial images: a comparative study. *ISPRS J Photogramm Remote Sens* 80:21–38.

Alberti, M., Booth, D., Hill, K., Coburn, B., Avolio, C., Coe, S., Spirandelli, D., (2007). The impact of urban patterns on aquatic ecosystems: an empirical analysis in Puget lowland sub-basins. *Landscape and urban planning*, 80, 345-361.

Albertz, J., (2009). *Einführung in die Fernerkundung – Grundlagen der Interpretation von Luft- und Satellitenbildern*. 4. Auflag, Wissenschaftliche Buchgesellschaft, Darmstadt, Germany.

Ampe, E.M., Vanhamel, I., Salvatore, E., Dams, J., Bashir, I., Demarchi, L., Chan, J.C.-W., Sahli, H., Canters, F., Batelaan, O., (2012). Impact of Urban Land-Cover Classification on Groundwater Recharge Uncertainty. *IEEE J. Sel.Top. Appl. Earth Obs. Remote Sens.*, 5(6), 1859-1867.

Arnfield, A.J., (2003). Two decades of urban climate research: a review of turbulence, exchanges of energy and water, and the urban heat island. *International Journal of Climatology*, 23, 1–26.

Asner, G.P., Lobell, D.B., (2000). A biogeophysical approach for automated SWIR unmixing of soils and vegetation. *Remote Sens. Environ.* 74, 99–112.

Asner, G.P., Heidebrecht, K.B., (2002). Spectral unmixing of vegetation, soil and dry carbon cover in arid regions: comparing multispectral and hyperspectral observations. *Int. J. Remote Sens.* 23 (19), 3939–3958.

Bateson, C.A.; Asner, G.P.; Wessman, C.A., (2000). Endmember bundles: A new approach to incorporating endmember variability into spectral mixture analysis. *IEEE Trans. Geosci. Remote Sens.*, 38, 1083–1094.

Bell, S., Alves, S., Silveirinha de Oliveira, E., Zuin, A., (2010). Migration and Land Use Change in Europe: A Review. *Living Reviews in landscape research*, 4(2), 1-49.

Ben-Dor, E., (2001). Imaging spectrometry for urban applications. In F. D. Van der Meer and S.M. DeJong (Eds.), *Imaging spectrometry. Basic principles and prospective applications*. Dordrecht: Kluwer Academic Publisher.

Ben-Dor, E., Levin, N., Saaroni, H., (2001). A spectral based recognition of the urban environment using the visible and near-infrared spectral region (0.4–1.1 μ m). A case study over Tel-Aviv, Israel. *Int. J. Remote Sens.* 22, 2193–2218.

Benediktsson, J. A., Palmason, J. A., Sveinsson, J. R., (2005). Classification of hyperspectral data from urban areas based on extended morphological profiles. *IEEE Transactions on Geoscience and Remote Sensing*, 43, 480-491.

Boardman, J.W.; Kruse, F.A.; Green, R.O., (1995). Mapping target signatures via partial unmixing of AVIRIS data. In *Proceedings of the Fifth JPL Airborne Earth Science Workshop*, Pasadena, CA, USA, 23–26 January 1995; Available online: <https://ntrs.nasa.gov/search.jsp?R=19950027368> (accessed on 24 May 2017).

Bochow, M., Segl, K., Kaufmann, H., (2007). An update system for urban biotope maps based on hyperspectral remote sensing data. In: *Proceedings of 5th EARSeL Workshop on Imaging Spectroscopy*, Bruges, Belgium, April 23-25.

Carle, M.V., Halpin, P.N., Stow, C.A., (2005). Patterns of watershed urbanization and impacts on water quality. *Journal of the American Water Resources Association (JAWRA)*, 41(3), 693-708.

Carlson, T., Arthur, S.T., (2000). The impact of land use – land cover changes due to urbanization on surface microclimate and hydrology: a satellite perspective. *Global and planetary change*, 25(1), 49-65.

Cavalli, R.M., Fusilli, L., Pascucci, S., Pignatti, S., Santini, F., (2008). Hyperspectral sensor data capability for retrieving complex urban land cover in comparison with multispectral data: Venice City case study (Italy). *Sensors* 8 (5), 3299–3320.

Clark, R.N., Swayze, G.A., Livo, K.E., Kokaly, R.F., Sutley, S.J., Dalton, J.B., McDougal, R.R., Gent, C.A., (2003). Imaging spectroscopy: Earth and planetary remote sensing with the USGS Tetracorder and expert systems. *J. Geophys. Res. Planets* 2003, 108.

- Clark, R.N., Swayze, G.A., Wise, R., Livo, E., Hoefen, T., Kokaly, R., Sutley, S.J., (2007). USGS Digital Spectral Library splib06a. U.S. Geological Survey: Reston, VA, USA; Digital Data Series 231; Available online: <http://speclab.cr.usgs.gov/spectral.lib06/> (accessed on 29 May 2017).
- Cocks, T., Jenssen, A., Stewart, A., Wilson, I., Shields, T., (1998). The HyMap airborne hyperspectral sensor: the system, calibration and performance. In: Proceedings of the 1st EARSeL Workshop on Imaging Spectroscopy, Zurich, Switzerland, October 6–8, pp. 1–6.
- Cuo, L., Lettenmaier, D.P., Mattheussen, B.V., Storck, P., Wiley, M., (2008). Hydrologic prediction for urban watersheds with the distributed hydrology—Soil-Vegetation Model. *Hydrological Processes*, 22, 4205–4213.
- Degerickx, J., Okujeni, A., Iordache, M.D., Hermy, M., van der Linden, S., Somers, B. (2016). A novel spectral library pruning technique for spectral unmixing of urban land cover. *Remote Sensing*, 9(565), 1-24.
- Degerickx, J., Roberts, D.A., Somers, B., (2019). Enhancing the performance of Multiple Endmember Spectral Mixture Analysis (MESMA) for urban land cover mapping using airborne lidar data and band selection. *Remote Sensing of Environment*, 221, 260-273.
- Demarchi, L., Canters, F., Chan, J.C.-W., Van de Voorde, T., (2012a). Multiple endmember unmixing of CHRIS/Proba imagery for mapping impervious surfaces in urban and suburban environments. *IEEE Trans. Geosci. Remote Sens.* 50 (9), 3409–3424.
- Demarchi, L., Chan, J.C.-W., Ma, J., Canters, F., (2012b). Mapping impervious surfaces from superresolution enhanced CHRIS/Proba imagery using multiple endmember unmixing. *ISPRS J. Photogramm. Remote Sens.* 72, 99–112.
- Demarchi, L., Canters, F., Cariou, C., Licciardi, G., Chan, J.C.-W., (2014). Assessing the performance of two unsupervised dimensionality reduction techniques on hyperspectral APEX data for high resolution urban land-cover mapping. *ISPRS J. Photogramm. Remote Sens.* 87, 166–179.
- Dennison, P.E., Roberts, D.A., (2003). Endmember selection for mapping chaparral species and fraction using multiple endmember spectral mixture analysis. *Remote Sens. Environ.* 41, 123–135.
- Dennison, P. E., Charoensiri, K., Roberts, D. A., Peterson, S. H., Green, R. O. (2006). Wildfire temperature and land cover modeling using hyperspectral data. *Remote Sensing of Environment*, 100, 212-222.
- Ding, J.G., Li, X.B., Huang, L.Q., (2015). A novel method for spectral similarity measure by fusing shape and amplitude features. *J. Eng. Sci. Technol. Rev.*, 8, 172–179.
- Dong, Y., Forster, B., Ticehurst, C., (1997). Radar backscatter analysis for urban environments. *International Journal of Remote Sensing*, 18(6),1351–1364.

- Duca, R., Del Frate, F., (2008). Hyperspectral and multiangle CHRIS-PROBA images for the generation of land cover maps. *IEEE Trans. Geosci. Remote Sens.* 46 (10), 2857–2866.
- Dudley, K.L., Dennison, P.E., Roth, K.L., Roberts, D.A., Coates, A.R., (2015). A multi-temporal spectral library approach for mapping vegetation species across spatial and temporal phenological gradients. *Remote Sensing of Environment*, 167, 121–134.
- Eckmann, T.C., Roberts, D.A., Still, C.J., (2008). Using multiple endmember spectral mixture analysis to retrieve subpixel fire properties from MODIS. *Remote sensing of environment*, 112, 3773–3783.
- Fan, F., Deng, Y., (2014). Enhancing endmember selection in multiple endmember spectral mixture analysis (MESMA) for urban impervious surface area mapping using spectral angle and spectral distance parameters. *Int. J. Appl. Earth Obs. Geoinf.* 33, 290–301.
- Franke, J., Roberts, D.A., Halligan, K., Menz, G., (2009). Hierarchical Multiple Endmember Spectral Mixture Analysis (MESMA) of hyperspectral imagery for urban environments. *Remote Sens. Environ.* 113 (8), 1712–1723.
- Gamba, P., and Dell'Acqua, F., (2006). Spectral resolution in the context of very high resolution urban remote sensing. In Q. Weng, & D. Quattrochi (Eds.), *Urban remote sensing* (pp. 377–391). Boca Raton: CRC Press.
- Gamba, P., and Dell'Acqua, F., (2007). Spectral resolution in the context of very high resolution urban remote sensing. In Weng, Q. & Quattrochi, D. (Eds.), *Urban Remote Sensing* (pp. 377–391). Boca Raton: CRC Press.
- Gamba, P., Dell'Acqua, F., Lisini, G., Trianni, G., (2007). Improved VHR urban area mapping exploiting object boundaries. *IEEE Transactions on Geoscience and Remote Sensing*, 45, 2676–2682.
- GEO [Group on Earth Observations] (2019). What is earth observation? Online: https://www.earthobservations.org/g_faq.html (accessed date 04 March 2019).
- Gilbert, O.L., (1994). *Städtische Ökosysteme*. Neumann Verlag, Radebeul, Germany.
- Gill, S., Handley, J., Ennos, A., Pauleit, S., (2007). Adapting cities for climate change: The role of the green infrastructure. *Built Environment*, 33(1), 115–133.
- Green, R.O., Eastwood, M.L., Sarture, C.M., Chrien, T.G., Aronsson, M., Chippendale, B.J., Faust, J.A., Pavri, B.E., Chovit, C.J., Solis, M.S., Olah, M.R., & Williams, O. (1998). Imaging spectroscopy and the Airborne Visible Infrared Imaging Spectrometer (AVIRIS). *Remote Sensing of Environment*, 65, 227–248.
- Grimm, N.B., Foster, D., Groffman, P., Grove, J.M., Hopkinson, C.S., Nadelhoffer, K.J., Pataki, D.E., Peters, D.P.C., (2008). The changing landscape: ecosystem responses to urbanization and pollution across climatic and societal gradients. *Frontiers in Ecology and the Environment*, 6(5), 264–272.

Grimmond, S., (2007). Urbanization and global environmental change: local effects of urban warming. *Geogr. Journal*, 173, 83–88.

Guanter, L., Kaufmann, H., Segl, K., Foerster, S., Rogass, C., Chabrillat, S., Kuester, T., Hollstein, A., Rossner, G., Chlebek, C., Straif, C., Fischer, S., Schrader, S., Storch, T., Heiden, U., Mueller, A., Bachmann, M., Muehl, H., Mueller, R., Habermeyer, M., Ohndorf, A., Hill, J., Buddenbaum, H., Hostert, P., Van der Linden, S., Leitão, P.J., Rabe, A., Doerffer, R., Krasemann, H., Xi, H., Mauser, W., Hank, T., Locherer, M., Rast, M., Staenz, K., Sang, B., (2015). The EnMAP spaceborne imaging spectroscopy mission for earth observation. *Remote Sens.* 7, 8830–8857.

Guarini, R., Loizzo, R., Longo, F., Mari, S., Scopa, T., Varacalli, G., (2017). Overview of the prisma space and ground segment and its hyperspectral products. In: *IEEE International Geoscience and Remote Sensing Symposium (IGARSS)*, Fort Worth, TX, USA, July 23–28.

Heiden, U., Segl, K., Roessner, S., Kaufmann, H., (2003). Ecological evaluation of urban biotope types using airborne hyperspectral HyMap data. In: *Proceedings of the 2nd GRSS/ISPRS Joint Workshop on Remote Sensing and Data Fusion over Urban Areas*, Berlin, Germany, May 22-23.

Heiden, U., Segl, K., Roessner, S. and Kaufmann, H., (2007). Determination of robust spectral features for identification of urban surface materials in hyperspectral remote sensing data. *Remote Sensing of Environment*, 111, 537-552.

Heiden, U., Heldens, W., Roessner, S., Segl, K., Esch, T., Mueller, A., (2012). Urban structure type characterization using hyperspectral remote sensing and height information. *Landsc. Urban Plan.* 105 (4), 361–375.

Heldens, W., (2010). Use of Airborne Hyperspectral Data and Height Information to Support Urban Micro Climate Characterisation (PhD thesis). University Würzburg, Germany Online. <https://opus.bibliothek.uni-wuerzburg.de/opus4-wuerzburg/frontdoor/index/index/docId/4060>, Accessed date: 9 March 2018.

Heldens, W., Heiden, U., Esch, T., Stein, E., Mueller, A., (2011). Can the Future EnMAP Mission Contribute to Urban Applications? A Literature Survey. *Remote Sensing*, 3, 1817-1846.

Heldens, W., Heiden, U., Esch, T., Müller, A., Dech, S., (2017). Integration of remote sensing based surface information into a three-dimensional microclimate model. *ISPRS Photogrammetry and Remote sensing*, 125, 106-124.

Herold, M., Gardner, M.E., Roberts, D.A., (2003). Spectral resolution requirements for mapping urban areas., *IEEE Transactions on Geoscience and remote sensing*, 41(9), 1907-1919.

Herold, M., Roberts, D.A., Gardner, M.E., Dennison, P.E., (2004). Spectrometry for urban area remote sensing - Development and analysis of a spectral library from 350 to 2400 nm. *Remote Sensing of Environment*, 91, 304-319.

- Hildebrandt, G., (1996). Fernerkundung und Luftbildmessung: Für Forstwirtschaft, Vegetationskartierung und Landschaftsökologie. Wichmann, Heidelberg, Germany.
- Hill, M.O., Gauch, H.G., (1980). Detrended correspondence analysis: an improved ordination technique. *Vegetatio* 42, 47–58.
- Hoek, G., Beelen, R., de Hoogh, K., Vienneau, D., Gulliver, J., Fischer, P., Briggs, D.J., (2008). A review of land-use regression models to assess spatial variation of outdoor air pollution. *Atmospheric Environment* 42(33), 7561–7578.
- Howard, L., (1833). The climate of London deduced from meteorological observations, made in the metropolis and at various places around it. Vol. 1, (Online: http://urban-climate.com/wp3/wp-content/uploads/2011/04/LukeHoward_Climate-of-London-V1.pdf (accessed November 3, 2018).
- Hoyano, A., Iino, A., Ono, M., Taniguchi, S., (1999). Analysis of the influence of urban form and materials on sensible heat flux—A case study of Japan's largest housing development 'Tama New Town'. *Atmospheric Environment*, 33 (24), 3931–3939.
- Iordache, M.D., Okujeni, A., van der Linden, S., Bioucas-Dias, J.M, Plaza, A., Somers, B., (2014). A multi-measurement vector approach for endmember extraction in urban environments. In: *Proceedings of ESA-EUSC-JRC 2014 - Image Information Mining Conference: The Sentinels Era*, Bucharest Romania, March 5-7.
- Jehle, M., Schaepman, M., Hueni, A., Damm, A., D'Odorico, P., Weyermann, J., Kneubühler, M., Meuleman, K., (2010). APEX – current status, performance and validation concept. In: *Sensors*, 2010 IEEE (pp. 533–537). Waikoloa, HI, USA: IEEE Sensors.
- Jensen, J.R. and Cowen, D.C. (1999). Remote sensing of urban/suburban infrastructure and socioeconomic attributes. *Photogrammetric Engineering and Remote Sensing*, 65(9), 611–622.
- Kennedy, C., Steinberger, J., Gasson, B., Hansen, Y., Hillman, T., Havránek, M., Pataki, D., Phdungsilp, A., Ramaswami, A., Mendez, G.V., (2009). Greenhouse gas emission from global cities. *Environmental Science & Technology*, 43(19), 7297-7302.
- Keshava, N. and Mustard, J.F., (2002). Spectral unmixing. *IEEE Signal Process. Mag.* 19:44–57.
- Keshava, N., (2003). A survey of spectral Unmixing algorithms. *Lincoln Lab. J.* 14 (1), 55–78.
- Kotthaus, S., Smith, T.E.L., Wooster, M.J., Grimmond, C.S.B., (2014). Derivation of an urban materials spectral library through emittance and reflectance spectroscopy. *ISPRS J. Photogramm. Remote Sensing*, 94, 194–212.

- Kruse, F.A., Lefkoff, A.B., Boardman, J.W., Heidebrecht, K.B., Shapiro, A.T., Barloon, P.J., Goetz, A.F.H., (1993). The spectral image processing system (SIPS)—Interactive visualization and analysis of imaging spectrometer Data. *Remote Sens. Environ.*, 44, 145–163.
- Lacherade, S., Miesch, C., Briottet, X., Le Men, H., (2005). Spectral variability and bidirectional reflectance behaviour of urban materials at a 20 cm spatial resolution in the visible and near-infrared wavelengths. A case study over Toulouse (France). *International Journal of Remote Sensing*, 26 (17), 3859–3866.
- Leopold, L.B., (1968). Hydrology for urban land planning—A guidebook on the hydrologic effects of urban land use. US Geological Survey, Geological Survey Circular, 554(18).
- Licciardi, G.A., Del Frate, F., (2011). Pixel unmixing in hyperspectral data by means of neural networks. *IEEE Trans. Geosci. Remote Sens.* 49 (11), 4163–4172.
- Lillesan, T.M., Kiefer, R. (2000). *Remote Sensing and Image Interpretation*, 4th Ed., John Wiley & Sons, Inc.
- Lucht, W., Schaaf, C.B., Strahler, A.H., (2000). An algorithm for the retrieval of albedo from space using semiempirical BRDF models. *IEEE Transactions on Geoscience and Remote Sensing*, 38, 977-998.
- Maier, R., Punz, W., Dörflinger, A.N., Hietz, P., Brandlhofer, M., Fussenegger, K., (1996). Ökosystem Wien - Die Subsysteme und deren Vegetationsstruktur. *Verhandlungen der Zoologisch-Botanischen Gesellschaft in Wien*. Zoologisch-Botanische Gesellschaft in Wien, 133, 1-26. Online. https://www.zobodat.at/pdf/VZBG_133_0001-0026.pdf, (Accessed date: 5 September 2018).
- Malheiros, J.M. and Vala, F. (2004). Immigration and city change: the Lisbon metropolis at the turn of the twentieth century. *Journal of Ethnic and Migration Studies*, 30(6), 1065–1086
- Martínez, P.J., Pérez, R.M., Plaza, A., Aguilar, P.L., Cantero, M.C., Plaza, J., (2006). Endmember extraction algorithms from hyperspectral images. *Annals of Geophysics*, 49(1), 93-101.
- Mather, P.M.. (2004). *Computer Processing of Remotely-Sensed Images. An Introduction*. 3rd Ed., John Wiley.
- Matsunaga, T., Iwasaki, A., Tsuchida, S., Tanii, J., Kashimura, O., Nakamura, R., Yamamoto, H., Tachikawa, T., Rokugawa, S., (2014). Current status of Hyperspectral Imager Suite (HISUI). In: *IEEE International Geoscience and Remote Sensing Symposium (IGARSS)*, Québec, Canada, July 13–18.
- Middel, A., Hab, K.I., Brazel, A.J., Martin, C.A., Guhathakurta, S., (2014). Impact of urban form and design on mid-afternoon microclimate in Phoenix Local Climate Zones. *Landscape and Urban Planning*, 122, 16–28.

- Mueller, R., Cerra, D., Carmona, E., Alonso, K., Bachmann, M., Gerasch, B., Krawczyk, H., (2017). The hyperspectral sensor DESIS on MUSES: processing and applications. In: International Symposium on Remote Sensing of Environment (ISRSE), Tshwane, South Africa, May 8-12. International Geoscience and Remote Sensing Symposium (IGARSS), Fort Worth, TX, USA, July 23–28.
- Naresh Kumar, M., Seshasai, M.V.R., Vara Prasad, K.S., Kamala, V., Ramana, K.V., Dwivedi, R.S., Roy, P.S., (2011). A hybrid spectral similarity measure for discrimination among Vigna species. *Int. J. Remote Sens.*, 32,4041–4053.
- National Research Council, (2007). *Earth Science and Applications from Space: National Imperatives for the Next Decade and Beyond*. Washington DC: The National Academies Press.
- NEO, (1995). HySpex main specifications. Online: https://www.hyspex.no/products/all_specs.php (accessed date: 4 March 2019).
- Neville, R.A., Lévesque, J., Staenz, K., Nadeau, C., Hauff, P., Borstad, G.A., (2003). Spectral unmixing of hyperspectral imagery for mineral exploration: comparison of results from SFSI and AVIRIS. *Can. J. Remote. Sens.* 29 (1), 99–110.
- Niemela, J., (1999). Ecology and urban planning. *Biodivers. Conserv.* 8 (1), 119–131.
- Oke, T. R., (1973). *City size and the urban heat island*. Atmospheric Environment Pergamon Press, 7, 769-779.
- Okin, G.S., Roberts, D.A., Murray, B., Okin, W.J., (2001). Practical limits on hyperspectral vegetation discrimination in arid and semiarid environments. *Remote Sens. Environ.* 77, 212–225.
- Okujeni, A., Van der Linden, S., Tits, L., Somers, B., Hostert, P., (2013). Support vector regression and synthetically mixed training data for quantifying urban land cover. *Remote Sensing of Environment*, 137, 184–197.
- Okujeni, A., Van der Linden, S., Hostert, P., (2015). Extending the vegetation–impervious–soil model using simulated EnMAP data and machine learning. *Remote Sens. Environ.* 158, 69–80.
- Okujeni, A., van der Linden, S., Suess, S., Hostert, P., (2017). Ensemble Learning From Synthetically Mixed Training Data for Quantifying Urban Land Cover With Support Vector Regression. *IEEE Journal of Selected Topics in Applied Earth Observations and Remote Sensing*, 10, 1640-1650.
- Pearlman, J.S., Barry, P.S., Segal, C.C., Shepanski, J., Beiso, D., Carman, S.L., (2003). Hyperion, a space-based imaging spectrometer. *IEEE Transactions on Geoscience and Remote Sensing*, 41(6), 1160-1173.

Plaza, A., Martínez, P., Perez, R., Plaza, J., (2002). Spatial/spectral endmember extraction by multidimensional morphological operations. *IEEE Transactions on Geoscience and Remote Sensing*, 40, 2025-2041.

Plaza, A., Martínez, P., Pérez, R., Plaza, J., (2004). A quantitative and comparative analysis of endmember extraction algorithms from hyperspectral data. *IEEE Trans. Geosci. Remote Sens.*, 42, 650–663.

Plaza, A., Benediktsson, J.A., Boardman, J.W., Brazile, J., Bruzzone, L., Camps-Valls, G., Chanussot, J., Fauvel, M., Gamba, P., Gualtieri, A.; et al., (2009). Recent advances in techniques for hyperspectral image processing. *Remote Sens. Environ.*, 113, S110–S122.

Priem, F., Canters, F., (2016). Synergistic use of LiDAR and APEX hyperspectral data for high resolution urban land cover mapping. *Remote Sens.* 8 (10), 787.

Ravetz, J., Fertner, C., Nielsen, T.S., (2013). The dynamics of peri-urbanization. In: Nilsson, K., Pauleit, S., Bell, S., Aalbers, C., Sick Nielsen, Th.A. (Eds.) *Peri-urban futures: Scenarios and models for land use change in Europe*, Springer-Verlag, Berlin Heidelberg, Germany, pp. 13-44.

Richards, J.A., Jia, X., (1999). *Remote Sensing Digital Analysis – An introduction*. 3rd Ed., Springer, Berlin, Germany.

Ridd, M.K., (1995). Exploring a V-I-S (vegetation-impervious surface-soil) model for urban ecosystem analysis through remote-sensing - comparative anatomy for cities. *Int. J. Remote Sens.* 16 (12), 2165–2185.

Roberts, D. A., Smith, M. O., Adams, J. B., (1993). Green vegetation, nonphotosynthetic vegetation, and soils in AVIRIS data. *Remote Sensing of Environment*, 44, 255-269.

Roberts, D.A., Gardner, M., Church, R., Ustin, S., Scheer, G., Green, R.O., (1998). Mapping chaparral in the Santa Monica Mountains using multiple endmember spectral mixture models. *Remote Sens. Environ.* 65, 267–279.

Roberts, D.A. and Herold, M., (2004). Imaging spectrometry of urban materials. In King, P., Ramsey, M.S., Swayze, G. (Eds.) *Infrared Spectroscopy in Geochemistry, Exploration and Remote Sensing*. Mineral Association of Canada: Ottawa, ON, Canada, pp. 155-181.

Roberts, D. A., Ustin, S. L., Ogunjemiyo, S., Greenberg, J., Dobrowski, S. Z., Chen, J., Hinckley, T. M., (2004). Spectral and structural measures of northwest forest vegetation at leaf to landscape scales. *Ecosystems*, 7, 545-562.

Roberts, D.A., Quattrochi, D.A., Hulley, G.C., Hook, S.J., Green, R.O., (2012). Synergies between VSWIR and TIR data for the urban environment: an evaluation of the potential for the hyperspectral infrared imager (HyspIRI) decadal survey mission. *Remote Sens. Environ.* 117, 83–101.

- Roberts, D.A., Alonzo, M., Wetherley, E., Dudley, K., Dennison, P., (2017). Multiscale analysis of urban areas using mixing models. In: Quattrochi, D.A., Wentz, E., Lam, N.S., Emerson, C.W. (Eds.), Integrating Scale in Remote Sensing and GIS. CRC press, New York, NY, USA, pp. 247–282.
- Roessner, S., Segl, K., Heiden, U., Kaufmann, H., (2001). Automated differentiation of urban surfaces based on airborne hyperspectral imagery. *IEEE Transactions on Geoscience and Remote Sensing*, 39 (7), 1525–1532.
- Rosentreter, J., Hagensieker, R., Okujeni, A., Roscher, R., Wagner, P.D., Waske, B., (2017). Subpixel mapping of urban areas using EnMAP data and multioutput support vector regression. *IEEE Journal of selected topics in applied earth observation and remote sensing*, 10(5), 1938-1948.
- Roth, K.L., Dennison, P.E., Roberts, D.A., (2012). Comparing endmember selection techniques for accurate mapping of plant species and land cover using imaging spectrometer data. *Remote Sens. Environ.* 127, 139–152
- Sánchez-Rodríguez, R., Seto, K.C., Simon, D., Solecki, W.D., Kraas, F., Laumann, G. (2005). Science Plan. Urbanization and Global Environmental Change, IHDP Report Series. Bonn: International Human Dimensions Programm on Global Environmental Change.
- Schaepman-Strub, G., Schaepman, M.E., Painter, T.H., Dangel, S., Martonchik, J.V., (2006). Reflectance quantities in optical remote sensing - definitions and case studies. *Remote Sensing of Environment*, 103, 27–42.
- Schaepman, M.E., Ustin, S.L., Plaza, A.J., Painter, T.H., Verrelst, J., Liang, S., (2009). Earth system science related imaging spectroscopy – an assessment. *Remote Sensing of Environment*, 113(1), 123-137.
- Schott, J.R., (1997). *Remote Sensing, the Image Chain Approach*, Oxford University Press, NY, 394.
- Schowengerdt, R., (1997). *Remote Sensing – Models and methods for image processing*. 2nd Ed., Academic Press, San Diego, USA.
- Segl, K., Roessner, S., Heiden, U., Kaufmann, H., (2003). Fusion of spectral and shape features for identification of urban surface cover types using reflective and thermal data. *ISPRS J. Photogramm. Remote Sens.* 58 (1–2), 99–112.
- Selva, M., Aiazzi, B., Butera, F., Chiarantini, L., Baronti, S., (2015). Hyper-Sharpening: a first approach on SIM-GA Data. *IEEE Journal of selected topics in applied earth observations and remote sensing*, 8(6), 3008-3024.
- Seto, K.C., Sanchez-Rodriguez, R., Fragkias, M., (2010). The new geography of contemporary urbanization and the environment. *Annual Review of Environment and Resources*, 35, 167-194.

- Settle, J.J. and Drake, N.A., (1993). Linear mixing and the estimation of ground cover proportions. *International Journal of Remote Sensing*, 14(6), 1159-1177.
- Shimabukuro, Y.E. and Smith, J.A., (1991). The least-square mixing model to generate fraction images from remote sensing multispectral data. *IEEE Trans. Geosci. Remote Sens.* 29(1), 16–20.
- Small, C., (2005). A global analysis of urban reflectance. *International Journal of Remote Sensing*, 26, 661-681.
- Small, C., (2001). Spectral dimensionality and scale of urban radiance AVIRIS Workshop Proceedings, Pasadena, CA, USA.
- Small, C., (2003). High spatial resolution spectral mixture analysis of urban reflectance. *Remote Sensing of Environment*, 88 (1–2), 170–186.
- Small, C. and Lu, J.W., (2006). Estimation and vicarious validation of urban vegetation abundance by spectral mixture analysis. *Remote Sensing of Environment*, 100, 441–456.
- Smith, M. O., Adams, J. B., Sabol, D. E., (1994). Spectral mixture analysis – new strategies for the analysis of multispectral data. In J. Hill & J. Megier (Eds.), *Imaging Spectrometry - a Tool for Environmental Observations*, ECSC, EEC (pp. 125-143). Brussels and Luxembourg: EAEC.
- Soergel, U., (2010), *Radar Remote Sensing of Urban Areas*. *Remote Sensing and Digital Image Processing*, 15, Springer Science + Business Media, Dordrecht, the Netherlands.
- Somers, B., Asner, G.P., Tits, L., Coppin, P., (2011). Endmember variability in spectral mixture analysis: a review. *Remote Sens. Environ.* 115 (7), 1603–1616.
- Somers, B., Tits, L., Roberts, D.A., Wetherley, E.B., (2016). Endmember library approaches to resolve spectral mixing problems in remotely sensed data: potential, challenges, and applications. *Data Handling in Science and Technology*, Elsevier. Amsterdam, The Netherlands.
- Sonnentag, O., Chen, J.M., Roberts, D.A., Talbot, J., Halligan, K.Q., Govind, A., (2007). Mapping tree and shrub leaf area indices in an ombrotrophic peatland through multiple endmember spectral unmixing. *Remote Sensing of Environment* 109: 342–360.
- Sukopp, H. and Weiler, S., (1998). Biotope mapping and nature conservation strategies in urban areas of the Federal Republic of Germany. *Landsc. Urban Plan.* 15 (1–2), 39–58.
- The World Bank (2018). Population growth (annual %), (Online: <https://data.worldbank.org/indicator/SP.POP.GROW> (accessed November 14, 2018)).
- United Nations, (2018a). *World Urbanization Prospects 2018*, (Online: <https://population.un.org/wup/Download/> (accessed November 15, 2018)).

- United Nations, (2018b). World Urbanization Prospects: The 2018 Revision, (Online: <https://population.un.org/wup/Publications/Files/WUP2018-KeyFacts.pdf> (accessed November 14, 2018).
- United Nations, (2017). World Urbanization Prospects 2017, (Online: <https://population.un.org/wpp/Download/Probabilistic/Population/> (accessed November 16, 2018).
- van der Linden, S., Janz, A., Waske, B., Eiden, M., Hostert, P., (2007). Classifying segmented hyperspectral data from a heterogeneous urban environment using support vector machines. *Journal of Applied Remote Sensing*, 1(1), 013543.
- van der Linden, S. and Hostert, P., (2009) The influence of urban structures on impervious surface maps from airborne hyperspectral data. *Remote Sens Environ* 113:2298–2305.
- van der Linden, S., Okujeni, A., Canters, F., Degerickx, J., Heiden, U., Hostert, P., Priem, F., Somers, B., Thiel, F., (2018). Imaging Spectroscopy of urban environments. *Surveys in Geophysics*, 1-18.
- Weng, Q., (2001). Modeling urban growth effects on surface runoff with the integration of remote sensing and GIS. *Environ. Manag.*, 28, 737–748.
- Weng, Q., Hu, X., Lu, D., (2008). Extracting impervious surfaces from medium spatial resolution multispectral and hyperspectral imagery: a comparison. *International Journal of Remote Sensing*, 29, 3209-3232.
- Wetherley, E.B., Roberts, D.A., McFadden, J., (2017). Mapping spectrally similar urban materials at sub-pixel scales. *Remote Sensing of Environment*, 195, 170–183.
- Wilby, R.L., (2003). Past and projected trends in London’s urban heat island. *Weather*, 58(7), 251–260.
- Wilby, R.L., (2007). A review of climate change impacts on the built environment. *Built Environment*, 33, 31–45.
- Winter, M.E., (1999). N-FINDR: an algorithm for fast autonomous spectral end-member determination in hyperspectral data, *SPIE Proc.*, 3753, 266-275.
- Winter, M.E., Lucey, P.G., Steutel, D., (2003). Examining hyperspectral unmixing error reduction due to stepwise unmixing. In: Shen, S.S., Lewis, P.E. (Eds.), *Proceedings of SPIE(5093), AeroSense 2003, Algorithms and Technologies for Multispectral, Hyperspectral, and Ultraspectral Imager IX*, Orlando, FL, USA, April 21-25, pp. 380–389.
- Wirion, C., Bauwens, W., Verbeiren, B., (2017). High resolution modeling of the urban hydrological response. In *Proceedings of the 2017 Joint Urban Remote Sensing Event (JURSE)*, Dubai, UAE, 6–8 March 2017.

- Wittig, R., Sukopp, H., Klausnitzer, B., (1998). In: Sukopp, H., Wittig, R. (Eds.), *Die ökologische Gliederung der Stadt. Stadtökologie*, Gustav Fischer Verlag, Stuttgart, Germany, pp. 316–372.
- Wold, S., Sjöström, M., Eriksson, L., (2001). PLS-regression: a basic tool of chemometrics. *Chemom. Intell. Lab. Syst.* 58, 109–130.
- Xu, B. and Gong, P., (2007). Land-use/land-cover classification with multispectral and hyperspectral EO-1 data. *Photogramm. Eng. Remote. Sens.* 73, 955–965.
- Yang, L., Huang, C., Homer, C.G., Wylie, B.K., Coan, M.J., (2003). An approach for mapping large-area impervious surfaces: Synergistic use of Landsat-7 ETM+ and high spatial resolution imagery. *Can. J. Remote Sens.*, 29, 230–240.
- Yang, J., He, Y., Caspersen, J., (2015). Fully constrained linear spectral unmixing based global shadow compensation for high resolution satellite imagery of urban areas. *Int. J. Appl. Earth Observ. Geoinf.* 38, 88–98.
- Yokoya, N., Yairi, T., Iwasaki, A., (2012). Coupled nonnegative matrix factorization unmixing for hyperspectral and multispectral data fusion. *IEEE Transactions on Geoscience and Remote Sensing*, 50(2), 528–537.
- Yokoya, N., Grohnfeldt, C., Chanussot, J., (2017). Hyperspectral and multispectral data fusion: a comparative review. *IEEE Geoscience and Remote Sensing Magazine*, 5(2), 29–56.
- Zare, A. and Ho, K.C. (2014). Endmember variability in hyperspectral analysis: addressing spectral variability during spectral unmixing. *IEEE Signal Process. Mag.* 31 (1),95–104.
- Zhang, J., Rivard, B., Sanchez-Azofeifa, A., & Castro-Esau, K. (2006). Intra- and inter-class spectral variability of tropical tree species at La Selva, Costa Rica: Implications for species identification using HYDICE imagery. *Remote Sensing of Environment*, 105, 129–141.
- Zhang, C., (2016). Multiscale quantification of urban composition from EO-1/Hyperion data using object-based spectral unmixing. *Int. J. Appl. Earth Obs. Geoinf.* 47, 153–162.

